Proceeding
Of
19th International Conference on Instrumentation, Electrical and Electronics Engineering (ICIEEE 2016)
&
19th International Conference on Production, Mechanical and Automobile Engineering (ICPMAE-2016)

Date: 12th June, 2016
Hyderabad

Editor-in-Chief

Dr. G.SURESH BABU

EEE, Dept. CBIT ,Hyderabad

Organized by:

TECHNICAL RESEARCH ORGANISATION INDIA

Website: www.troindia.in

ISBN: 978-93-85225-66-6

About Conference

Technical Research Organisation India (TROI) is pleased to organize the 19th International Conference on Instrumentation, Electrical and Electronics Engineering (ICIEEE 2016) & 19th International Conference on Production, Mechanical and Automobile Engineering (ICPMAE-2016).

ICIEEE is a comprehensive conference covering the various topics of Engineering & Technology such as Instrumentation, Electrical and Electronics Engineering. The aim of the conference is to gather scholars from all over the world to present advances in the aforementioned fields and to foster an environment conducive to exchanging ideas and information. This conference will also provide a golden opportunity to develop new collaborations and meet experts on the fundamentals, applications, and products of Computer Science and Information Technology. We believe inclusive and wide-ranging conferences such as ICIEEE can have significant impacts by bringing together experts from the different and often separated fields of Electrical and Electronics Engineering. It creating unique opportunities for collaborations and shaping new ideas for experts and researchers. This conference provide an opportunity for delegates to exchange new ideas and application experiences, we also publish their research achievements. ICPMAE shall provide a plat form to present the strong methodological approach and application focus on Production, Mechanical And Automobile Engineering Engineering that will concentrate on various techniques and applications. The ICPMAE conference cover all new theoretical and experimental findings in the fields of Production, Mechanical And Automobile Engineering or any closely related fields.

Topics of interest for submission include, but are not limited to:
Electrical Engineering
Electronics Engineering
3D Semiconductor Device Technology
Advanced Electromagnetics
Adaptive Signal Processing
Analysis of Power Quality and System Stability
Analog Circuits and Digital Circuits
Antenna and Propagation
Circuits and Electronics
Power Systems
Evolutionary Algorithm application to Power System
Power Quality
Distributed Generation
Power Electronics
Converter/Inverter Topologies
Automotive applications
Power Factor Improvements
Mechanical Engineering
Automobile Engineering
Production Engineering
Design and Manufacturing
Fluid Dynamics
3D Semiconductor Device Technology
Mechatronics and many more and many more

Organizing Committee

Editor-in-Chief:
Dr. G.SURESH BABU
EEE, Dept. CBIT, Hyderabad

Programme Committee Members:

Dr. Dariusz Jakóbczak
C.S.M, Dept., Technical university of Koszalin, Poland

Dr. A. Lakshmi Devi
Professor, Dept. of EEE
SVU college of Engineering, Sri Venkateswara university,
Tirupati

Prof O. V. Krishnaiah Chetty
Dean, Mechanical Engineering
Sri Venkateswara College of Engineering and Technology
Chittoor- Tirupati

Dr. Rajeev Agrawal
Assistant Professor,
Department of Production Engineering
Birla Institute of Technology
Ranchi, Jharkhand

Dr. Bhasker Gupta
Assistant Professor. Jaypee University of Information Technology, Himachal Pradesh

Prof. Surjan Balwinder Singh
Associate Professor in the Electrical Engineering Department,
PEC University of Technology, Chandigarh.

Dr. Shilpa Jindal ,
PEC University of Technology (Deemed University), Chandigarh
ji_shilpa@yahoo.co.in

Prof. S. V. Viraktamath
Dept. of E&CE S.D.M. College of Engg. & Technology Dhavalagiri, Dharwad

Dr. G.Suresh Babu
Professor,Dept. of EEE,CBIT, Hyderabad

Prof .Ramesh
Associate Professor in Mechanical Engineering,
St.Joseph's Institute of Technology

TABLE OF CONTENTS

Editorial

The conference is designed to stimulate the young minds including Research Scholars, Academicians, and Practitioners to contribute their ideas, thoughts and nobility in these two integrated disciplines. Even a fraction of active participation deeply influences the magnanimity of this international event. I must acknowledge your response to this conference. I ought to convey that this conference is only a little step towards knowledge, network and relationship.

The conference is first of its kind and gets granted with lot of blessings. I wish all success to the paper presenters.

I congratulate the participants for getting selected at this conference. I extend heart full thanks to members of faculty from different institutions, research scholars, delegates, TROI Family members, members of the technical and organizing committee. Above all I note the salutation towards the almighty.

Editor-in-Chief:
Dr. G.SURESH BABU
EEE, Dept. CBIT, Hyderabad

AUTOMATIC SHIP CONTROLLER USING FUZZY LOGIC

Seema Singh[1], Pooja M[2], Pavithra K[3], Nandini V[4], Sahana D V[5]
[1]Associate Prof., Dept. of Electronics and Comm., BMS Institute of Technology and Management
[2,3,4,5]Students, Dept. of Electronics and Comm., BMS Institute of Technology and Management
Email:seemasingh@bmsit.in[1], poojamohanraj26@gmail.com[2], pavithrakomargowda@gmail.com[3], nandiniv00@gmail.com[4], sahanaraj8@gmail.com[5]

Abstract

An autonomous navigation algorithm for marine vehicles is proposed in this paper using fuzzy logic. Therefore we use a multi variable fuzzy logic control system for safer automatic navigation. Although alternative approaches such as genetic algorithms and neural networks can perform just as well as fuzzy logic in many cases, fuzzy logic has the advantage that the solution to the problem can be cast in terms of that human operators can understand, so that their experience can be used in the design of the controller. An automatic ship controller using fuzzy logic is proposed here which controls the path of the ship with collision avoidance system, keeping track of the movement of ship. Fuzzy logic based controller is shown to be better than PID Controller.

Keywords: Collision avoidance, marine vehicles, fuzzy logic, moving obstacles.

I. INTRODUCTION

To design an autopilot for a ship is always a challenging problem. A ship dynamics is influenced by unpredictable environmental disturbances such as waves, winds, currents, change of depth under keel, etc. as well as ship sailing conditions such as speed, loading condition, trim, etc. To design an autopilot capable of taking into account all these factors is nowadays possible by proven adaptive or robust control design methods. The proposed adaptive fuzzy autopilot emerges as a viable practical alternative for coastal sailing where the track keeping is of vital importance in all circumstances.

There are several technique used for ship tracking, namely PID, adaptive and predictive controllers .For ship navigation task, the PID controller coefficients need to be changed due to several reasons like environmental changes (wind, waves, and currents), random disturbances, internal errors etc. To accommodate these changes PID controller coefficients Kp, Ki, Kd, must be tuned accordingly, which demands the support of other controllers (fuzzy, genetic etc.), which in turn increases the complexity of the system. Hence PID controllers are not suitable for Navigation applications.

II. RELATED WORK

At present, ship modeling and control is an issue of high interest in research areas. For the ship modeling, there many ships mathematical models namely nomoto's, bech, and norbin and yang model [1]. The control problems are challenging due to the fact that the motion of ships possess six degrees of freedom to be controlled. Usually, the ship has: large time lag, large inertia, nonlinearity and under actuated characteristics; and its motion is strongly influenced by the model parameter perturbations (wind, wave and current flow).So the design of the motion controllers with high performance is always difficult [5].

These ship models are developed such that they can be controlled by any controller by giving command signal. We used Bech's nonlinear model, which supports 6 degree of freedom and larger rudder angle turns of ship, is used to simulate ship dynamics.

There are some wave mathematical models namely Bretschnieder spectrum, Pierson-Markowitz(P-M) spectrum, Modified Pierson-Markowitz, and JONSWAP spectrum. Inorder to consider Sea disturbances, modified Pierson-Markowitz Spectrum (P-M) is used which will take into account of both high and low tides.

In such situation, the researchers call the intelligent control theories and try to achieve better results of control. In this paper, we attempt to use the fuzzy control approach for navigating the ship automatically by considering the sea parameters.

Fuzzy Logic control is a practical alternative for a variety of challenging control applications since it provides a convenient method for constructing nonlinear controllers via the use of appropriate information [8]. So, optimal control laws can be implemented based on ship path following. Fuzzy controllers have been successfully used in many fields and shown extraordinary advantages over traditional control technology, such as nonlinearities, and robustness [9].

Collision avoidance approach: The primary control command in marine vehicle navigation is the heading angle, which is affected via the rudder as shown in Fig. 3. In the figure, {*X*0 ,*Y*0} and {*X* ,*Y*} are the global and the body-fixed coordinate systems, respectively; (*x*, *y*) is the location of the
center of gravity of the marine vehicle with respect to the global coordinate system; *u* , *v* , and *r* are the longitudinal, transverse, and angular velocities, respectively;δ is the rudder angle and ψ *d* is the desired heading angle.Control of marine vehicles is usually carried out via a combination of inner and outer loops as illustrated in Fig. 4. The inner, course-keeping controller attempts to follow the heading angle command while the outer, track-keeping controller determines the desired heading in relation to the desired track. The approach proposed here, however, is inspired by the VFF method whose direct application is depicted in Fig. 5. As shown in the figure, the vehicle is assumed to beunder the influence of two forces at any given point in time: *Fa* which acts to pull the vehicle towards the next waypoint, and *Fr*, a force directed away from the given obstacle. Evidently, a simple application of VFF does not provide track-keeping in its true sense. Moreover, in the case of a moving obstacle, a single forcing function *Fr* is insufficient to address the situation adequately, particularly when the vehicle is within the proximity of multiple obstacles.

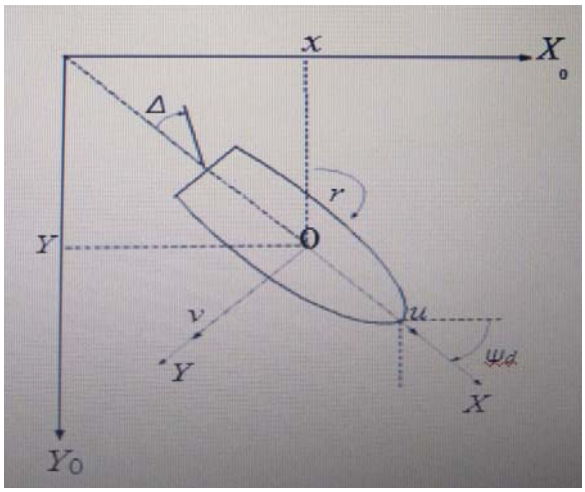

Fig. 1 The concept of track keeping mode

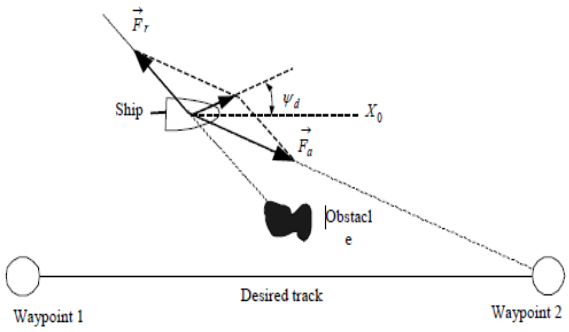

Fig. 2 Track keeping

By considering above models in this paper an attempt is made to implement the simulations obtained for the path following and for the collision avoidance in a hardware model for the marine parameters.

III. PROPOSED METHOD

There are several technique used for ship tracking, namely PID, adaptive and predictive controllers .For ship navigation task, the PID controller coefficients need to be changed due to several reasons like environmental changes (wind, waves, and currents), random disturbances, internal errors etc. To accommodate these changes PID controller coefficients Kp, Ki, Kd, must be tuned accordingly, which demands the support of other controllers (fuzzy, genetic etc.), which in turn increases the complexity of the system.
Fuzzy Controller is nothing but a fuzzy code designed to control something, usually mechanical. They can be in software or hardware and can be used in anything from small circuits to large mainframes.

To analyze PID Controller performance, the dc motor control is attained for the considered parameters and compared with the simulations obtained for the fuzzy logic.

Controller using fuzzy logic is developed for the ship as it is more robust. The algorithm for the proposed ship controller is embedded in Aurdino board.

Algorithm steps for simulation are given below:

1. Ship parameter declaration i.e. length, speed and non linear parameters of the ship.
2. Ship transfer function declaration.
3. Latitude Longitude array initialization.
4. Conversion of coordinates to angles.
5. Reference angles are given to fuzzy controller.
6. Based on the error the fuzzy controller generates the rudder angle for ship based on fuzzy rules.
7. Then rudder angle is fed to ship in presence of wave disturbance.
8. The process is continued for continuous monitoring

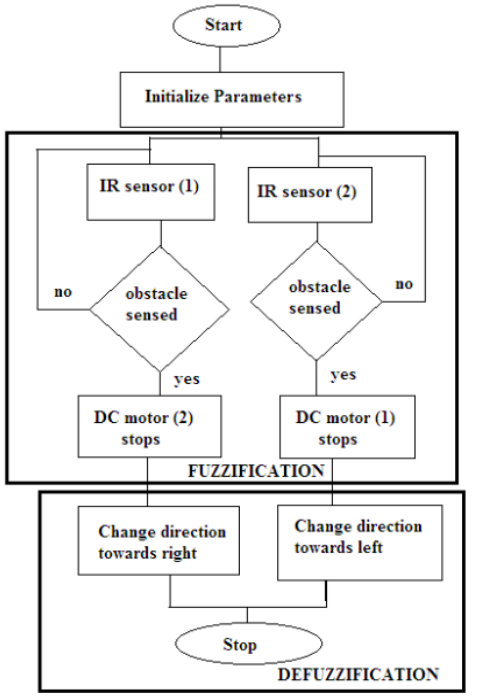

Fig. 3: Flowchart

Based on the above simulations the embedded code was formulated in fuzzy logic using the two processes of fuzzification and defuzzification and implemented on a aurdino board.

Components Used:

- Arduino nano pro board
- LCD display(16X2)
- GPS tracker
- GSM
- IR sensor
- DC Motors

In this implementation the initial parameters are loaded into the controller like obstacle distance to be sensed and the speed with which the motor should run initially. Based on the distance of the object sensed the direction to be taken is updated in the controller where actually fuzzification is done .Later the defuzzification part is carried out.

Fuzzification: For each input and output variable selected, we define two or more membership functions (MF). Qualitative category for each one of them need to be defined for example: low, normal or high.

Rule base (decision matrix) definition: Once the input and output variables and MF are defined, we have to design the rule-base (or decision matrix of the fuzzy knowledge-base) composed of expert IF <antecedents> THEN

<conclusions> rules. These rules transform the input variables to an output that will tell us the risk of operational problems (this output variable, risk of a problem, also have to be defined with MF, usually low, normal and high risk). Depending on the number of MF for the input and output variables, we will be able to define more or less potential rules. The easier case is a rule base concerning only one input and one output variable.

Example: or a given variable x involved in the development of a problem, we could have this kind of "theoretical" rule: IF x is normal THEN risk of problem is normal. The more variables we have, the more rules we have to define in order to make the inference reliable.

IF x is low THEN risk of problem is low.

IF x is normal THEN risk of problem is normal.

IF x is high THEN risk of problem is high.

		Input Y			
		LOW	NORMAL	HIGH	VERY HIGH
Input X	LOW	Low	High	High	High
	NORMAL	Low	Low	Medium	Medium
	HIGH	Low	Low	Low	Low
	VERY HIGH	Low	Low	Low	Low

Fig. 4: Rule table

Defuzzyfication: The MFs of the output have always the same shape and configuration in our risk model: the risk

of any problem has the same ranks for the MFs of the output: low, normal and high, and always without overlapping. Figure 6 shows the shape of each MF of the output variable (risk on any problem considered in the risk model).

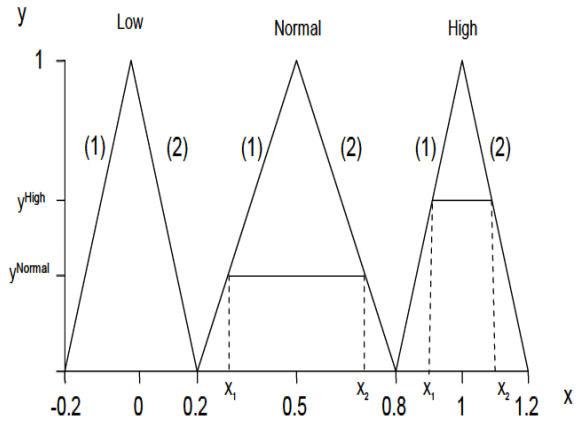

Fig. 5 Shape of MF

IV. DISCUSSION OF RESULTS

The DC motor controlling using PID in MATLAB was attained for the considered parameters and compared with the simulations obtained for the fuzzy logic. MATLAB simulation results of both PID and Fuzzy are compared and the plots of the same are as shown

Red color indicates the Reference trajectory, black color indicates the obtained PID trajectory, and blue color indicate the obtained Fuzzy Logic trajectory. From the plot it is clear that, Fuzzy Logic controller results are closer to reference trajectory (91-96%), and PID based controller has more deviation from reference trajectory (75-85%). So performance of the Adaptive (Fuzzy Logic) controller is better than PID controllers.

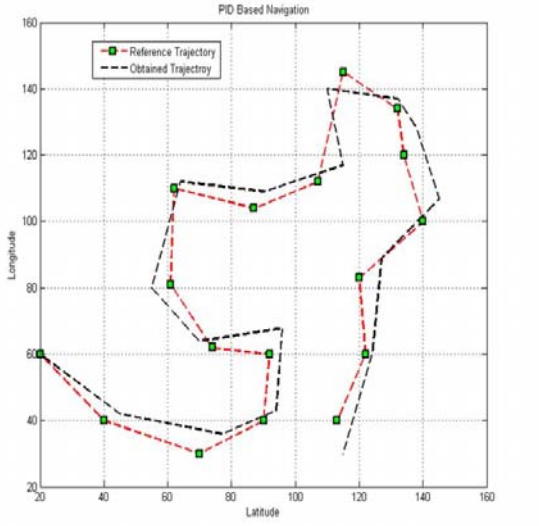

Fig. 6: Comparison of Fuzzy

Logic-PID based navigation

Hardware implementation

The aurdino board is used to interface with various sensors o receive the input for the logic and for dumping the source code into it. Here only two parameters are considered for input so as to reduce the system complexity the number of inputs can be increased in future. The IR sensor value is taken as one input and other inputs are from the temperature or wind sensor to the network. The fuzzification is done to these values which produce certain defuzzified output which is again used to control the DC motor's direction for monitoring the ship navigation. The block diagram is shown in Fig. 7.

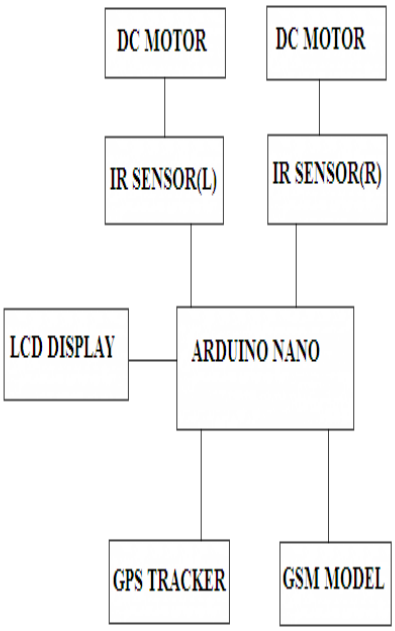

Fig. 7: Block Diagram

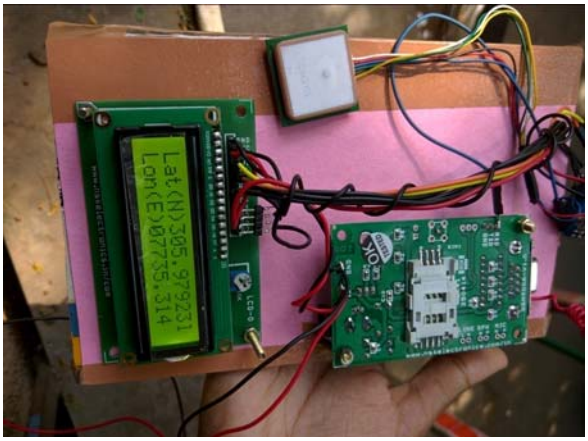

Fig. 8: Hardware implementation of Location using GPS

GPS, GSM, LCD Display, IR Sensor module are shown in Fig, 8, 9, 10, 11 respectively. The latitude and longitude position of the ship was displayed on the LCD using GPRS. GSM module was used to send the information as a message to the user. IR sensors were used for controlling the direction of DC motor based on the obstacle sensed. This model senses any obstacle in its path and changes direction accordingly and sends a message to the user when any obstacle is sensed by it. The complete hardware set-up of the controller for automatic navigation of the ship is shown in Fig. 12.

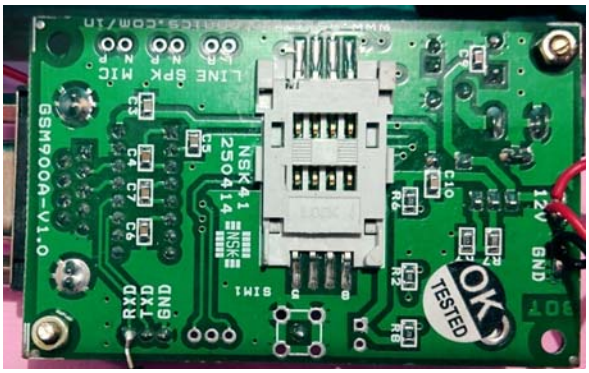

Fig 9: GSM Model

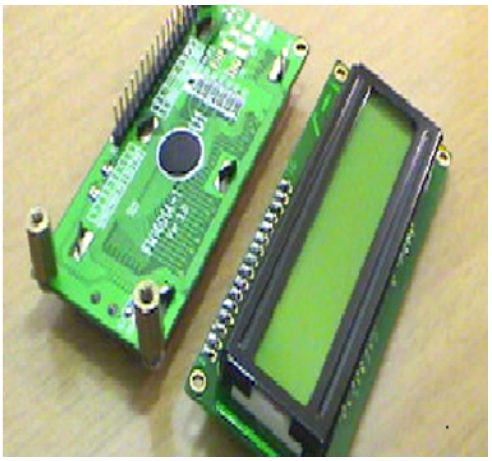

Fig. 10: LCD Display module

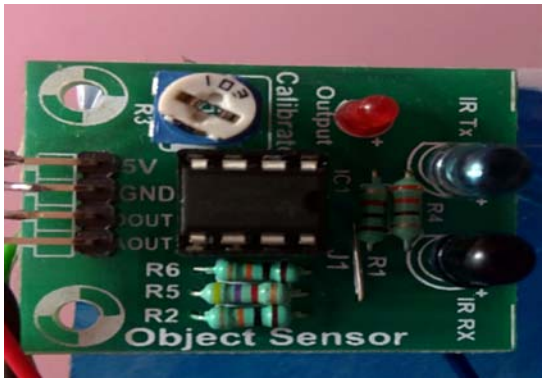

Fig. 11: IR Sensor module

ISBN: 978-93-85225-66-6, 12th June, 2016, Hyderabad

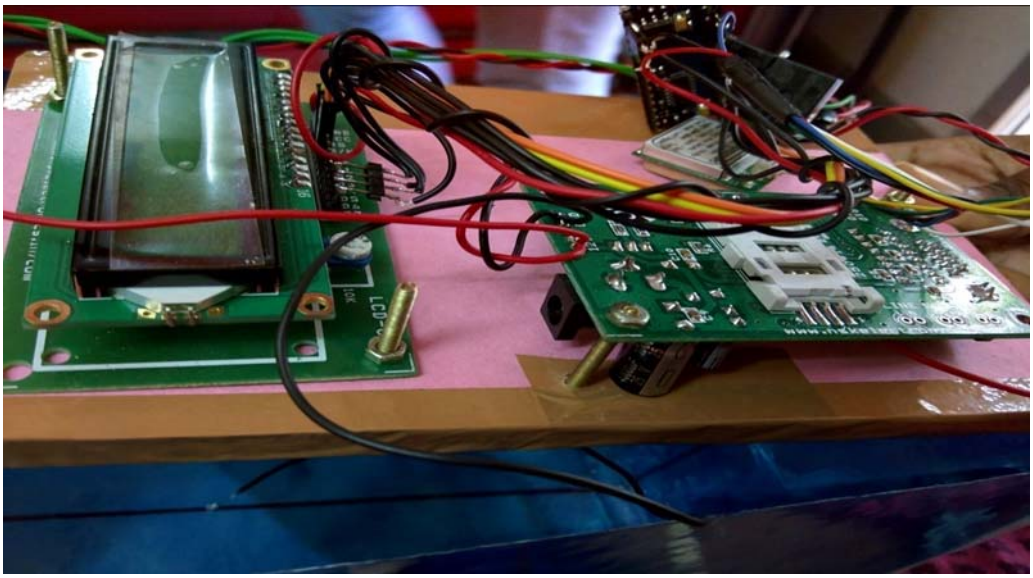

Fig. 12: Complete hardware set-up

V. CONCLUSION

The main objective of the proposed work is to overcome the limitations of traditional Navigation system, to design a efficient control system for the automatic navigation system using fuzzy logic and to inform the port offices about its location in case of missing.

Initially the simulation was carried out to develop the model for collision avoidance using PID and FUZZY. As Fuzzy was proved to be better, the further simulations were developed using fuzzy logic. Hardware implementation for fuzzy logic controller is done for the ship navigation system. The latitude and longitude position of the ship was displayed on the LCD using GPRS. GSM module was used to send the information as a message to the user. A DC motor was programmed using fuzzy logic to control its speed and direction. IR sensors were used for controlling the direction of DC motor based on the obstacle sensed.

Now this model senses any obstacle in its path and changes direction accordingly and sends a message to the user when any obstacle is sensed by it. By this an automatic navigation of the ship has been achieved.

REFERENCES

[1] Fossen Thor, "Guidance and Control of Ocean Vehicles", John Wiley and Sons Ltd., 1994

[2] A S White, "Control of Ship Capsize in Stern Quartering Seas", International Journal of Simulation, Vol. 8 No 2, ISSN 1473-8041 2007

[3] F.Camacho and Carlos Bordons, "Model predictive controller",springer, Berlin, 1999, ISBN 3540762418.

[4] Yaoua Hu, Suwu Xu "Generalized Predictive Controller Design for Ship Track Keeping" IJCSNS VOL.9 No.5, May 2009

[5] JiuhongRuan, Zuowei Li, "ADRC based Ship Tracking Controller Design and Simulations", International Conference on automation and Logistics, Qindao, China, 2008

[6] Jin Cheng, Jianqiang Yi, and Dongbin Zhao, "A New Fuzzy Autopilot for Way-point Tracking Control of Ships", 2006 IEEE International Conference on Fuzzy Systems,July 16-21, 2006, pp. 451-456.

[7] Ramzi FRAGA, Liu Sheng "Double Fuzzy Logic Control for the Ship Path Following",2nd International conference on intelligent control and information processing, July 25-28, 2011, pp. 92-96

[8] K. M. Passino, S. Yurkovich, Fuzzy Control. Tsinghua University Press, Addision-Wesley, 2001

DETECTION AND DIAGNOSIS OF BRAIN TUMOR

Seema Singh[1], Navaneeth P S[2], Rahul Ramachandra M[3], Rohith K[4], Srikar C H[5]
[1]Associate Professor, Dept. of Electronics and Comm., BMS Institute of Technology and Management, Bangalore, INDIA
[2,3,4,5]Students, Dept. of Electronics and Comm., BMS Institute of Technology and Management, Bangalore, INDIA
Email: seemasingh@bmsit.in[1], navaneethps1995@gmail.com[2], rahulm.ramchandra@gmail.com[3], rohith2205@gmail.com[4], srikarsr@gmail.com[5]

Abstract

Brain Tumor is mass or growth of abnormal cells in or around brain. The chances of survival can be increased if the tumor is detected correctly at its early stage. Conventional methods used manual analysis or segmentation which could lead to wrong classification due to human errors. Due to complexity, automated systems that perform classification with high accuracy are desired. Over the last decade, many algorithms are used which uses techniques of image processing but it is increasingly moving towards machine learning concepts. Here we propose a method that uses support vector machines. The proposed system is designed to identify the tumor region, extract features, perform classification and determine if the tumor is benign or malignant. The proposed method was found to give 98% accuracy of classification.

Index Terms: Brain Tumor, Image segmentation, Feature Extraction, Support vector machine

I. INTRODUCTION

Brain tumor is the growth of abnormal cells in or around brain. Normal cells in the body age and die and are replaced by new cells. But cancer and other tumors disrupt this cycle. Tumor cells grow even though the body doesn't need them and unlike normal old cells they don't die. Thus the tumor continues to grow.

Since brain is a closed area, as the tumor grows, they cause pressure inside the skull which will cause inflammation and swelling which damages the brain. Tumors are of two types: primary and secondary tumors. Primary tumors originate in brain, emerge from various cells that are constituents of brain and central nervous system. They can be benign or malignant. Benign tumors rarely invade other tissues and have clearly defined borders. Most common type in adults is Meningiomas which is benign, astrocytomas. In children, its Medulloblastoma. Secondary tumors are also called as Metastatic tumors. They are malignant tumors which spreads from some other part of body usually lungs. They grow rapidly and invade the healthy tissues. The tumors are graded according to how aggressive they are, with lower-grade tumors often being benign and higher-grade tumors being malignant.

MRI is an imaging technique that produces high quality images of anatomical structures of brain. Image intensity in MRI depends upon four parameters. One is proton density (PD) which is determined by the relative concentration of water molecules. Other

three parameters are T1, T2, and T2* relaxation, which reflect different features of the local environment of individual protons. In MRI, boundary of the tumor image is highly asymmetrical and irregular, so image segmentation is a great challenge to analyze the tumor. A key problem in medical imaging is automatically segmenting an image into its constituent heterogeneous processes. Automatic segmentation has the potential to positively impact clinical medicine by freeing physicians from the burden of manual labeling and by providing robust, quantitative measurements to aid in diagnosis and disease modeling.

Manual and Automated tumor segmentation:

The classification of Brain tumor segmentation methods can be made depending on the degree of human interaction as Manual segmentation, Semi-automatic segmentation and Fully automatic segmentation.

Manual segmentation involves delineation of the boundaries of tumor manually and representing region of anatomic structures with various labels. Manual segmentation requires software tools for the ease of drawing regions of interest (ROI), is a tedious and exhausting task. MRI scanners produce multiple 2-D slices and the human expert has to mark tumor regions carefully, otherwise it will generate jaggy images that lead to poor segmentation results.

Semi-automatic segmentation involves human interaction as least as possible. According to Olabarriaga et al [1], the semi-automatic or interactive brain tumor segmentation components consist of computational part, interactive part and the user interface. Since it involves both computer and human's expertise, result depends on both the combination. Efficient segmentation of brain tumor is possible through this strategy but it is also subjected to variations between expert users and within same user.

Fully automatic segmentation does not require intervention of human and segmentation of tumor is determined with the help of computer. It involves the human intelligence and is developed with soft computing techniques, which is a difficult task. Brain tumor segmentation has various properties which reduce the advantage of humans over machines.

These methods are likely to be used for large batch of images in research environment. However; these methods have not gained popularity for clinical practice, due to lack of transparency and interpretability.

II. RELATED WORK

Supervised and Unsupervised Segmentation Image segmentation objective is to segregate the image into mutually exclusive regions, which are similar with respect to pre-defined subsets. This objective can be accomplished using two methods of segmentation methods- Supervised and Unsupervised methods.

Unsupervised segmentation: If for training input vectors, target output is unknown, training method adopted is unsupervised learning. In the previous years, various unsupervised learning methods such as K-means and fuzzy clustering have gained popularity for brain tumor segmentation. The main aim of this type of segmentation is to segment the image into areas that have similar intensity and has well defined anatomic properties. Unsupervised segmentation of brain tumor achieve its anatomic goal by segmenting the image into at least two anatomically regions, one is tumor and other is edema. The advantage of this type is that it can handle very difficult tasks such as brain tumor segmentation; it produces an accurate segmentation of different regions present in heterogeneous tumor. Disadvantages of this segmentation are: number of regions is to be known before; tumors may not be specified clearly. This disadvantage can be avoided using skull stripping. Skull stripping is a pre-processing step to wipe out non-cerebral tissue such as fat, muscle, skin, skull which are not desired region of interest.

Supervised segmentation: In supervised learning, the network is provided with series of sample inputs and output is compared with expected response. It involves both training phase that uses labelled data that maps features to labels and testing phase is used to map labels to unlabeled data. The advantage of this type is that training set can be changed; it can reduce the manual task by providing labelled data. Irrespective of its advantages, it suffers from disadvantages that it requires patient specific

training for brain tumor supervised segmentation and also human variability is also a concern.

Segmentation methods: In the segmentation process, accurate delineation of the tumor is responsible for early tumor diagnosis in clinical practice. Manifold approaches for brain tumor segmentation has been proposed. But no standard segmentation technique can produce satisfactory results for all imaging applications. In general, various segmentation techniques are as follows:

Threshold-based methods: It is the convenient and basic technique of image segmentation. It convert gray scale images into binary images.If we consider g(x,y) as the segmented image, we will get two outputs for the corresponding input image f(x,y). According to this technique, g(x,y)=1; if f(x,y) >= T and g(x,y)=0;if f(x,y) nodes. Clarke [2] was the first researcher to propose a supervised classification using an ANN approach for brain tumor segmentation in MR images. Executing ANN for brain tumor segmentation entangle problems of complexity ,the size of network becomes very large, time consuming process and large number of images are required for training the network.

A particular case of ANN is the self-organizing map (SOM). SOM is an unsupervised competitive learning algorithm. SOM automatically organizes itself according to the input data using a similarity factor like Euclidean distance. The brain cortex is organized in such a manner that closer neurons will give answers to the same kind of stimulus; this is one of the reason because of which SOM technique is used in visual pattern recognition.

Fuzzy C means (FCM) FCM is based on clustering which segments one class of data into two or more clusters. It works by casting each data point matching to each cluster center on the basis of distance between the cluster and the data point. The advantages of FCM algorithm are:

a) It gives best result for overlapped data set.

b) It produces comparatively better result than k- algorithm.

c) The application of FCM to MRI data has shown satisfactory results.

FCM is gaining popularity in the research area of brain tumor segmentation. This algorithm produces segmentation images that are clinically neuroanatomic tissue contrast from raw MRI data. A knowledge-based fuzzy clustering approach was proposed and implemented for the segmentation of the MRI images of brain tumor followed by 3-D connected components to build the tumor shape. To improve the accurate detection of stage and size of tumor, a combined method of the k-means and fuzzy c-means algorithms was proposed to deal with the segmentation of brain tumor. However the disadvantages of this method are that it takes more computational time and it is more sensitive to noise.

III. PROPOSED ALGORITHM

The proposed method consists of three steps:

Step 1: Pre-processing (including feature extraction and feature reduction);

Step 2: Training the kernel SVM

Step 3: Submit new MRI brains to the trained kernel SVM, and output the prediction.

Image pre-processing consists of Otsu binarization, K-means clustering and 2D DWT, after which thirteen features are extracted for training and classification of MRI images. Further a GUI is developed to ease the usage.

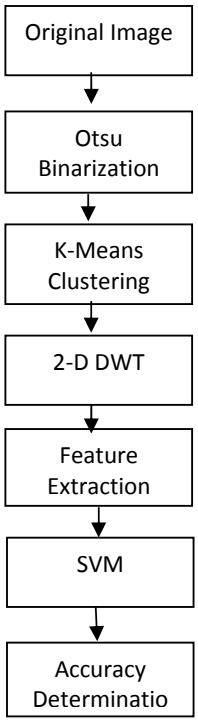

Fig1: Steps involved in brain tumor detection

Image Pre Processing Steps:

A) Otsu Binarization

In Otsu's method we exhaustively search for the threshold that minimizes the intra-class variance (the variance within the class), defined as a weighted sum of variances of the two classes:

$$\sigma_w^2(t) = \omega_0(t)\sigma_0^2(t) + \omega_1(t)\sigma_1^2(t)$$

Weights $\omega_{0,1}$ are the probabilities of the two classes separated by a threshold t and $\sigma_{0,1}^2$ are variances of these two classes.

B) K Means Algorithm

Clustering is the process of partitioning a group of data points into a small number of clusters. In general, we have n data points xi,i=1...n that have to be partitioned in k clusters. The goal is to assign a cluster to each data point. K-means is a clustering method that aims to find the positions μi,i=1...k of the clusters that minimize the square of the distance from the data points to the cluster. K-means clustering solves

$$\text{argmin}c\sum_{i=1}^{k}\sum_{x\in ci} d(x,\mu i)2 = \text{argmin}c\sum_{i=1}^{k}\sum_{x\in ci}\|x-\mu i\|22$$

where ci is the set of points that belong to cluster i.

C) 2-D Discrete Wavelet Transform

In case of 2D images, the DWT is applied to each dimension separately. There are 4 sub-band (LL, LH, HH, and HL) images at each scale. The sub-band LL is used for next 2D DWT. The LL sub band can be regarded as the approximation component of the image; while the LH, HL, and HH sub bands can be regarded as the detailed components of the image. As the level of decomposition increased, compacter but coarser approximation component was obtained.

D) Feature Reduction using Principal Component Analysis

Excessive features increase computation times and storage memory. Furthermore, they sometimes make classification more complicated, which is called the curse of dimensionality. It is required to reduce the number of features. PCA is an efficient tool to reduce the dimension of a data set consisting of a large number of interrelated variables while retaining most of the variations. It is achieved by transforming the data set to a new set of ordered variables according to their variances or importance. This technique has three effects: it orthogonalizes the components of the input vectors so that uncorrelated with each other, it orders the resulting orthogonal components so that those with the largest variation come first, and eliminates those components contributing the least to the variation in the data set.

Feature Extraction:

Following features are extracted using MATLAB simulation software.

- *Mean*
- *Standard Deviation*
- *Variance*
- *Contrast*
- *Correlation*
- *Energy*
- *Entropy*
- *Homogeneity*
- *RMS*
- *Smothness*
- *Skewness*
- *Kurtosis*
- *Inverse Differnce Method*

SVM Classification

In machine learning, support vector machines are supervised learning models with associated learning algorithms that analyze data and recognize patterns, used for classification and regression problems. Given a set of training examples, each marked for belonging to one of two categories, an SVM training algorithm builds a model that assigns new examples into one category or the other, making it a non-probabilistic binary linear classifier.

In addition to performing linear classification, SVMs can efficiently perform a nonlinear classification using what is called the kernel trick, implicitly mapping their inputs into high dimensional feature spaces.

K-Fold Stratified Organization

Since the classifier is trained by a given dataset, so it may achieve high classification accuracy only for this training dataset not yet other independent datasets. To avoid this over fitting,

we need to integrate cross validation into our method. Cross validation will not increase the final classification accuracy, but it will make the classifier reliable and can be generalized to other independent datasets.

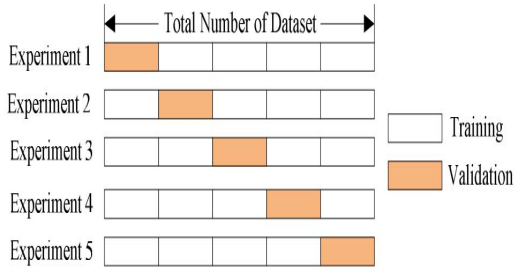

Fig 2: 5- Fold Cross Validation

Cross validation methods consist of three types: Random subsampling, K-fold cross validation, and leave-one-out validation. The K-fold cross validation is applied due to its properties as simple, easy, and using all data for training and validation. The mechanism is to create a K-fold partition of the whole dataset, repeat K times to use K − 1 folds for training and a left fold for validation, and finally average the error rates of K experiments. The schematic diagram of 5-fold cross validation is shown in Fig. The K folds can be purely randomly partitioned, however, some folds may have a quite different distributions from other folds. Therefore, stratified K-fold cross validation was employed, where every fold has nearly the same class distributions. Another challenge is to determine the number of folds. If K is set too large, the bias of the true error rate estimator will be small, but the variance of the estimator will be large and the computation will be time-consuming.

Alternatively, if K is set too small, the computation time will decrease, the variance of the estimator will be small, but the bias of the estimator will be large SVM by each value. Finally we select the optimal K value corresponding to the highest classification accuracy.

IV. RESULTS

The input MRI image of brain tumor is shown in Fig. 3. Image pre-processing steps are shown in Fig. 4 and Fig. 5. Features are extracted and the numerical values of thirteen features are displayed in GUI as shown in Fig. 6 and 7. One case of Malignant and one case of Benign tumor is shown. Similarly various MRI images were tested and their accuracy statistics are displayed in GUI. The proposed method's classification accuracy is 98 %.

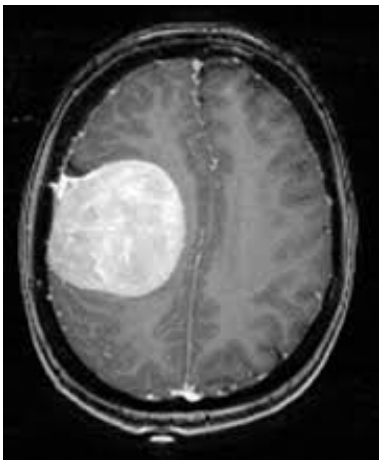

Fig 3: Input brain tumor image

Fig 4: Otsu thresholded image

Fig 5: Segmented Tumor

Graphical user interface was developed for better user experience. The user has to select the brain tumor image. Based on the feature extracted values the image is classified into benign or malignant.

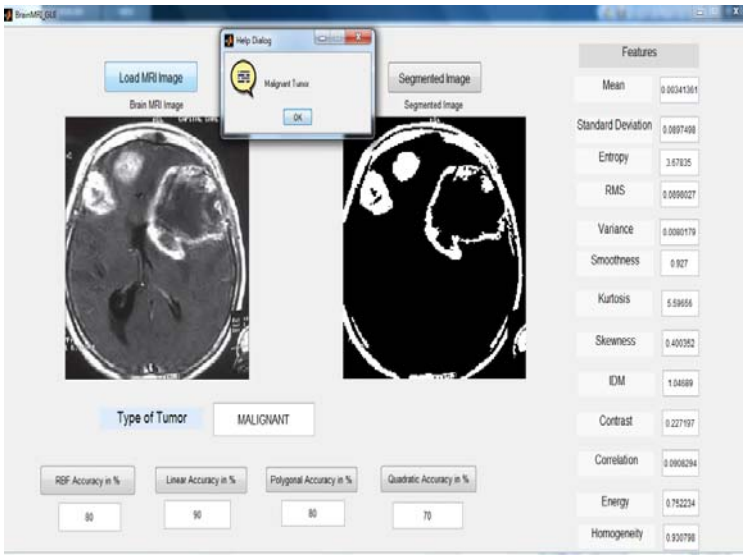

Fig 6 Malignant Tumor

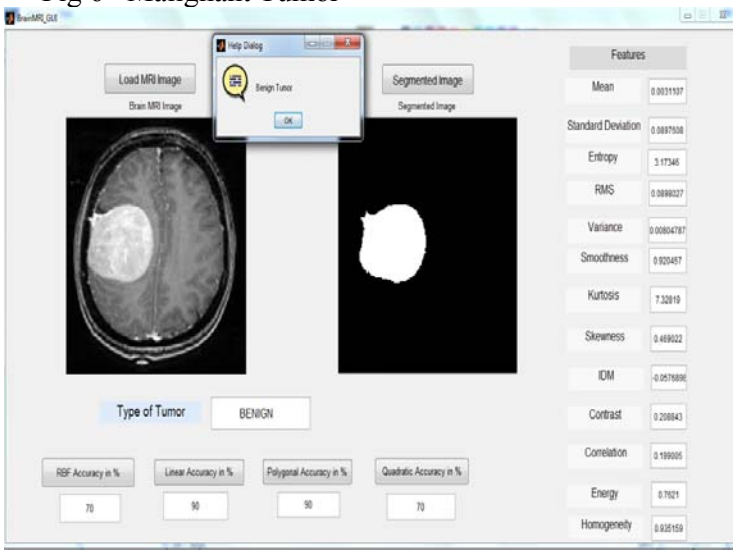

Fig 7 Benign Tumor

VI CONCLUSION

Current prevalent method used by pathologists for diagnosis of brain tumor is to manually observe the morphological changes in the cells by physical examinations, however manual observation is very subjective and poses several problems. The proposed method of automated diagnosis of brain tumor can reduce such discrepancies and workload of pathologists.

Image pre-processing consists of Otsu binarization, K-means clustering and 2D DWT, after which thirteen features (namely Mean, Standard Deviation, Variance, Contrast, Correlation, Energy, Entropy, Homogeneity, RMS, Smothness, Skewness, Kurtosis, Inverse Differnce Method) are extracted for training and classification of MRI images using SVM. Further a GUI is developed to ease the usage. Objective of detection and diagnosis of brain tumor was successfully achieved by classifying the image into Benign and Malignant.

REFERENCES

[1] S D Olabarriaga, A W M Smeulders, " Interaction in the segmentation of medical images: A survey", ELSEVIER Medical image analysis, 5(2001), pp 127- 142.

[2] L P Clarke, R P Velthuizen, S. Phuphanich, J.D. Schellenberg, J.A. Arrington, M. Silbiger, "MRI: Stability of three supervised segmentation techniques", Magnetic Resonance Imaging, Vol 11 (1), 1993, pp 95–106

[3] Y Zhang, L Wu "An MR brain image classifier via support vector machine" progress in electromagnetics research, 2012.

[4] Chaplot, S., L. M. Patnaik, and N. R. Jagannathan, "Classification of magnetic resonance brain images using wavelets as input to support vector machine and neural network" Biomedical Signal Processing and Control, Vol. 1, No. 1, 86-92, 2006.

[5] El-Dahshan, E.-S. A., T. Hosny, and A.-B. M. Salem, Hybrid intelligent techniques for MRI brain images classification'' Digital Signal Processing, Vol. 20, No. 2, 433-441, 2010.

MOTION ANALYSIS OF ARTICULATED ROBOTIC ARM FOR INDUSTRIAL APPLICATION

Pradeep Kumar Dhote[1], J. C. Mohanta[2], Mohd. Nayab Zafar[3]
Department of Mechanical engineering, MNNIT Allahabad
[1]PG Scholar, [2]Assistant Professor, [3]Research Scholar
E-Mail:p.dhote1992@gmail.com[1],jcmohanta@mnnit.ac.in[2], nayab.zafar7@gmail.com[3]

Abstract

This paper presents the analysis of stresses and deformation induced for a particular payload of a robot. An articulated type industrial robotic arm has been considered for motion analysis. The modelling of articulated robotic hand has been created by 3D software SOLIDWORKS and the analysis have been performed by using ANSYS R15 software. In order to compensate the work the kinematic analysis also performed in a 2-D scale through computer simulation. This shows the 2D plot for the different combinations of joint angle within its work envelope. The forward and inverse kinematics analysis has been used to co-relate the desired location and orientation of end effector with joint variables. MATLAB simulation result has been compared with the theoretical analysis for various link positions and it has been found that both the results are in phase and have good agreement with each other.

Index Term*:* Articulated Robot, Forward and Inverse kinematics, Payload, Workspace.

I. INTRODUCTION

Robots that are used in industries having several human like characteristics. This robot includes mechanical arms similar to human hand used for various industry tasks. Such anthropomorphic or human like characteristics include some sensory devices those are used to communicate and interact the machine with other machines to take simple or important decisions to operate efficiently [3].

An industrial robot consists of a mechanical manipulator and a controller to move it and perform other related functions.

- The mechanical manipulator consists of joints and links to position and orient the end of the manipulator relative to its base
- The controller operates the joints based on co-ordinate axis to perform a programmed work cycle
- A robot joint is similar to a human body joint. It provides relative movement between two parts of the body.

Industrial robots work on the same principle like numerical control machine which follows the developed path, and the history is related. Both are assigned with dedicated central computers to operate controlling devices [5]. However, Robots can perform a variety of tasks as compare to numeric control machines.

II. Modelling of Robot

The model of the articulated robotic joint has been created by using software SOLID WORKS. The complete model has been assembled by using the various parts of the robot. The assembly includes parts such as base, body, upper arm, fore arm, end gripper etc. To provide relative motion between these parts a cylindrical type pin has been used. Each and every part of the model having different dimensions. The

model specification has been shown in the table I. For complete modelling used software SOLID WORKS contains four important sections which is manual drawing, part module, assembly module and drawing module shown [1]. First two sections provide the model and design parts of the robot to user. The assembly module enables the parts to be modelled in the assembly which provides the relative motion between the parts by using the revolute joints through cylindrical pin. The final section is drawing module that creates the drawing of the created parts in different formats.

For design analysis the model is being analysed in three different cases. This case study refers to the different joint angle.

I. Specification of Model

II.

Specification	Value
Number of axes	4
Horizontal Reach	300mm
Vertical Reach	450mm
Drives	4 servo motors
Configuration	a)All axes completely Independent b)All axes can be controlled simultaneously
Work envelope	a)Shoulder rotation b)Elbow rotation c)Gripper rotation
Material	Structural steel Density- 7800 kg/m.^{3} Poisson's Ratio – 0.3

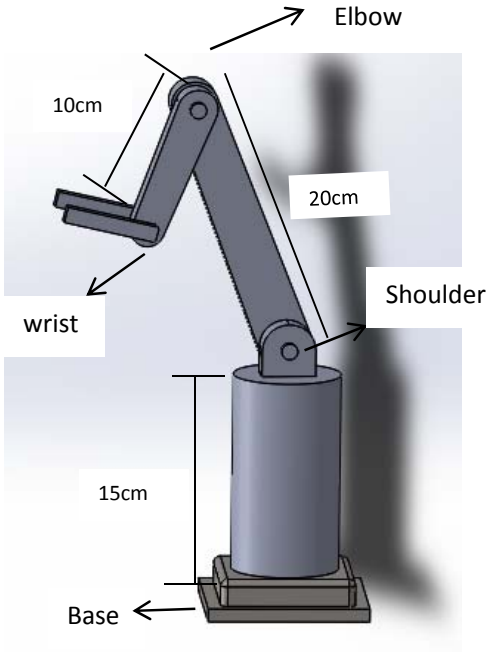

Fig. 2.1: Assembled model

III. Mathematical Calculation

A) Force and Moment calculation

The load which is to be lifted by the robot provide its effect on every part of the model, its effect should be analysed on each joint in terms of moment provided by load lifted and weight of the motor which gives the direct loading on the joints[2]. Direct force and moment calculation gives the result in terms of stress and the deformation of the part. To calculate the parameters under consideration are as follows:

I. weight of each linkage
II. weight of each joint
III. weight of object to lift
IV. length of each linkage

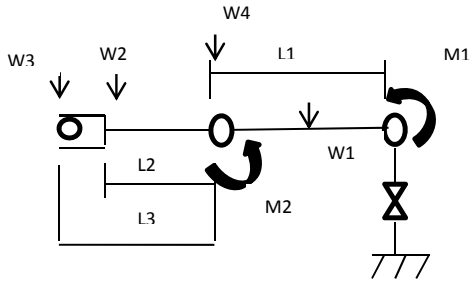

Fig 3.1: Force and moment calculation

Torque About Joint 1:

M1 = L1/2 * W1 + L1 * W4 + (L1 + L2/2) * W2 + (L1 + L3) * W3

Torque About Joint 2:

M2 = L2/2 * W2 + L3 * W3

B) Stress and deformation calculation

To find out the analytical solution the main assumption is that the loading condition makes the arm like a beam is in bending. Hence, by using bending equation

Stress value can be find out by- $\sigma = \frac{My}{I}$

Maximum deformation is given by –

$\delta_{max} = \frac{Pl^3}{3EI}$ and $\delta_{max} = \frac{Ml^2}{2EI}$

C) Kinematic analysis of Robot

Forward Kinematics

It involves the computation of position and orientation of the end effector, while knowing the joint angle and link length. The forward kinematics of the end-effector with respect to the base frame is determined by multiplying all of the ${}^{i-1}_{i}T$ matrices

$${}^{base}_{end\_effector}T = {}^{0}_{1}T\ {}^{1}_{2}T \ldots\ldots\ldots\ldots {}^{n-1}_{n}T$$

An alternative representation of ${}^{base}_{end\_effector}T$ can be written as

$${}^{base}_{end\_effector}T = \begin{bmatrix} r_{11} & r_{12} & r_{13} & p_x \\ r_{21} & r_{22} & r_{23} & p_y \\ r_{31} & r_{32} & r_{33} & p_z \\ 0 & 0 & 0 & 1 \end{bmatrix}$$

Inverse Kinematics

It involves the calculation of joint angle and link parameters for the desired position and orientation of the end effector.

To find the inverse kinematics solution for the first joint (q_1) as a function of the known elements of ${}^{base}_{end\_effector}T$, the link transformation inverses are premultiplied as follows

$[{}^{0}_{1}T(q_1)]^{-1}\ {}^{0}_{6}T = {}^{1}_{2}T(q_2)\ {}^{2}_{3}T(q_3)\ {}^{3}_{4}T(q_4)\ {}^{4}_{5}T(q_5)\ {}^{5}_{6}T(q_6)$

To find the other variables, the following equations are obtained as a similar manner.

$[{}^{0}_{1}T(q_1)\ {}^{1}_{2}T(q_2)\ {}^{2}_{3}T(q_3)\ {}^{3}_{4}T(q_4)\ {}^{4}_{5}T(q_5)]^{-1}\ {}^{0}_{6}T =$

${}^{5}_{6}T(q_6)$

IV. Result and discussion

To analyse the design the structural analysis has been performed by using software ANSYS R15.0. The result shown as snap shot from the ANSYS for every part in all the three different case. The result obtained is then compared with the analytical result that is obtained by using the basic formulas of the strength of material. The result is calculated for lifting a load of say 10N, on comparing the result from both the process is tabulated and the % error obtained is not more than 5% for any part hence it is accepted.

A) To calculate maximum payload of robot

The above result shown is calculated for carrying a load of 10N and for this the robot is safe. Hence to calculate the maximum load for which the robot will not fail gives the maximum load carrying capacity of robot in other terms it is also called as the payload of the robot. By varying the load from 10-60N the robot will not fail for any cases.

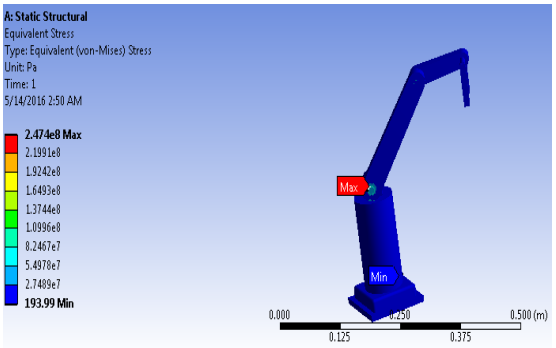

Fig. 4.1 Stress distribution for max. Payload (Case-3)

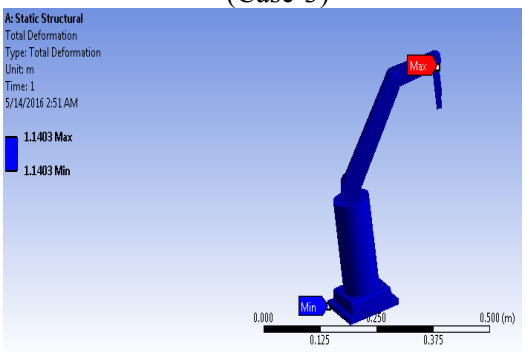

Fig. 4.2 Deformation for maximum payload (Case-3)

- Maximum stress generated for case-3 i.e. approx. 247MPa for the load of 60N
- For structural steel - A36 steel plate

  Yield strength- 250MPa

  Ultimate tensile strength - 400-550MPa

So, while designing the robotic arm the load should be less than 60N calculated at maximum speed based upon yield strength criteria for robot. Hence from the above result the model is best suited for Lifting a load of 50N.

The payload of robot at normal speed calculated as 50N.

B) Results of Kinematic Analysis

Inverse Kinematic modelling of Robotic Arm

Analysis is done for two link, 2 dimensional arm mechanism. For this simple mechanism the angle reducing for each joint will be as per the desired location of the tip of the end arm.

Let θ_1 be the angle between the first arm and the ground. Let θ_2 be the angle between the first and second arm. Let the length of first arm is L_1 and that of second arm is L_2. Assume the limited rotation of arm hence, $0<=\theta_1<=pi/2$ and $0<=\theta_2<=pi$

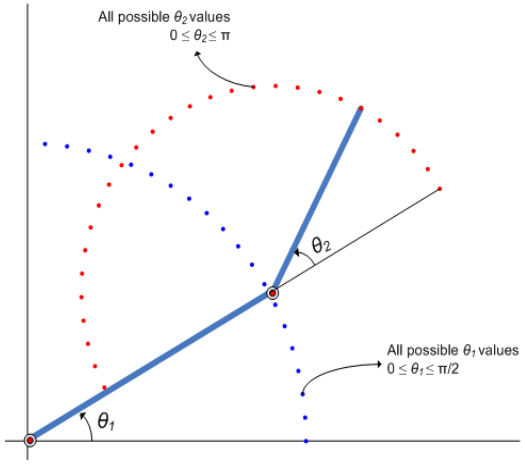

Fig.4.3 All possible joint values of θ_1 and θ_2

The plot shows the generated X-Y data point for different combination of θ_1 and θ_2 and reducing x and y co-ordinate for each joint. The plot has been generated by using the forward kinematics

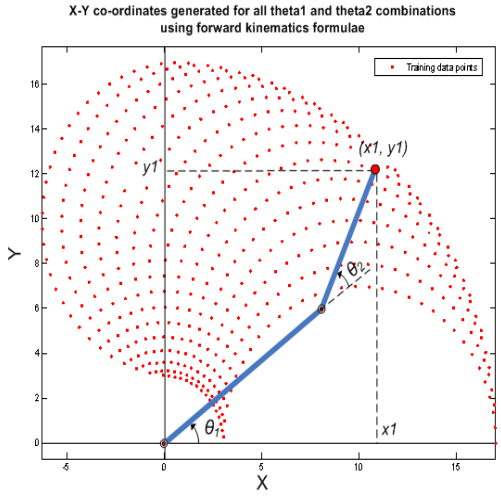

Fig.4.4 X-Y coordinate generated for all θ_1 and θ_2 combinations using forward kinematics formulae

Formula. Since the forward kinematics formulae for two joint robotic arms are known, X and Y co-ordinates of the tip of the arm can be calculated by moving it to desired range of angle rotation.

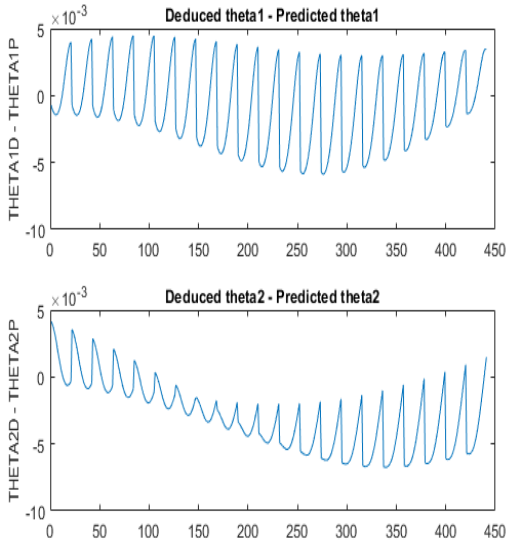

Fig.4.5 Variation between actual and predicted theta values.

THETA1D and THETA2D are the variables that hold the values of θ_1 and θ_2 reduced using the inverse kinematics formulae. The errors are in the range of $1e^{-3}$ which is a fairly good number for the different application.

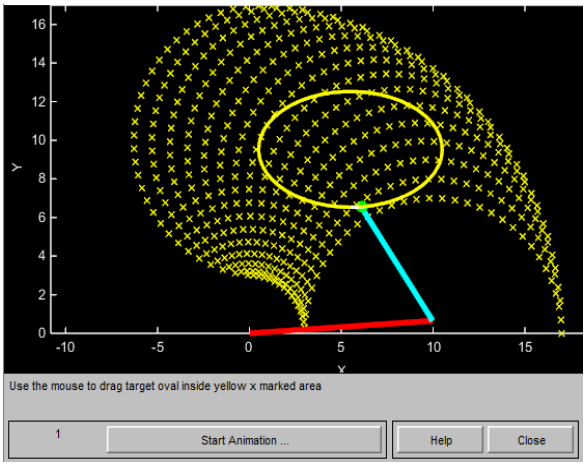

Fig.4.6 GUI for inverse kinematics modelling

GUI shows the inverse kinematic modelling for the mechanism. The command used is *invkine*, this shows the tip is tracing an ellipse. By moving it with in the range of Co-ordinate workspace it will verify the result.

V. Conclusions

After getting results the paper can be concluded to its result in a way that, the work is completely based on theoretical approach to follow certain design criteria. To avoid failure of parts the stress value find should be lower than the yield point limit for the material. Maximum stress (Von Misses Theory) criteria used to define the payload of the robots. On the basis of payload the robots can be used for different applications. At maximum payload the robots will not follow the predefined path hence normal payload is always used for the robots. As from the result obtained the normal payload of the robot is 50N which the model can lift within the yield stress limit of the material.

In the second part, motion planning result containing graph which shows the error between the predicted angle variations with the actual variation of the angle. This type of error is found because of the joint constraints of the robotic manipulator. The estimated errors are in the range of $1e^{-3}$ which is fairly good number and can be used for the applications where the very high accuracy is not desired.

VI. REFERENCES

[1] Rosidah Sam, Kamarul Arrifin, Norlida Buniyamin, "Simulation of pick and place robotics system using solidworks softmotion," International Conference on System Engineering and Technology, September 11-12, 2012.

[2]B.O.Omijeh, R.Uhunmwangho, M.Ehikhamenle ,"Design Analysis of a Remote Controlled Pick and Place Robotic Vehicle," International Journal of Engineering Research and Development Volume 10, Issue 5 (May 2014), PP.57-68 .

[3]Ravikumar Mourya, Amit Shelke, Sourabh Satpute, Sushant Kakade, Manoj Botre, "Design and implementation of pick and place robotic arm," International Journal of recent research in civil and mechanical engineering, Vol. 2, Issue 1 (2015), pp:(232-240).

[4] Songliang Nie, Yuwen Li, Guo Shuai, Song Tao, FengFeng Xi, "Modeling and simulation for fatigue life analysis of robots with flexible joints under percussive impact forces," Robotics and Computer-Integrated Manufacturing 37 (2016) 292–301.

[5] K.Kiran Kumar, Dr. P.R.Thyla, "Singularity and workspace analysis of RRP serial Manipulator," International conference on recent advances in mechanical engineering, ICRAME 2010.

[6] Prashant Badoni, "Direct Kinematic modeling of 6R Robot using Robotics Toolbox," International Journal of Engineering research and application, ISSN: 2248-9622, Vol. 6 Issue 1, part-3(January 2016) pp 151-154.

[7] Serdar Kucuk, Zafer Bingul, "Inverse kinematic solution for industrial Robot manipulator with offset wrists," Applied Mathematical Modelling 38 (2014) 1983–1999.

[8] Nicolae Plitea, Dorin Lese, Doina Pisla, Calin Vaida, "Structural design and kinematics of a new parallel reconfigurable robot," Robotics and Computer-Integrated Manufacturing 29 (2013) 219–235.

[9] Hazim Nasir Ghafil, Ali Hussein Mohammed, Nabil H. Hadi, "A Virtual Reality Environment for 5-DOF Robot Manipulator based on XNA Framework," International Journal of Computer Applications (0975 – 8887) Volume 113 – No. 3, March 2015.

[10] Tahseen Fadhil Abbas, "Kinematics Modeling of 5DOFstationary Articulated Robots ", Eng. &Tech. Journal,Vol.31, No.3, university of Technology, 2013.

DESIGN OF A NEW IMPROVED INTAKE MANIFOLD FOR F-SAE CAR

Abhishek Raj[1], J.C. Mohanta[2], Bireswar Paul[3], Mohd. Nayab Zafar[4]
[1]pg Scholar, [2]assistant Professor, [3]assistant Professor, [4]research Scholar
Department of Mechanical Engineering, MNNIT Allahabad
E-mail:rajabhishek.me@gmail.com[1], jcmohnata@mnnit.ac.in[2], bipaul@mnnit.ac.in[3], nayab.zafar7@gmail.com[4]

Abstract
This paper describes a modified intake manifold for F-SAE (Formula Society of Automotive Engineers) car along with a restrictor. In order to fulfill the criteria of formula SAE competition a restriction device must be placed in order to limit the engine's capability between the throttle and the engine so that all the flow must be take place through the restriction device. To achieve the maximum mass flow rate the output velocity should be high with an even distribution to each cylinder for efficient working of the engine. A series of computer simulation has been performed on the developed model in order to show the efficacy of the model. The simulation results has been compared with the similar results of the previous models, which shows improved performance in terms of even distributions and high velocity at outlet. Which ultimately responsible for greater mass flow rate from the intake manifold to the engine cylinder.
Index Terms-Intake Manifold, Plenum, Restrictor, Runner.

I.INTRODUCTION

The performance of any internal combustion engines are largely depends on its intake systems. For efficient working of an engine it is required that its intake system must be properly designed. All intake system consists of some basic components, such as air restrictor, intake plenum and intake runner etc. together to work as an intake manifold for an F-SAE car. An inlet manifold or intake manifold is a part of engine which supplies fuel/air mixture to the cylinder [3]. The most important function of intake manifold is to evenly distribute the mixture to each cylinder. Even distribution of charge is important to improve efficiency and performance of the engine.

In case of F-SAE air starts flow from air filter which separates abrasive particulates to reduce mechanical wear by cleaning the air which reduces the probability of damage of engine components. After air filter air comes to throttle body which regulates the speed and power of any engine by controlling the amount of air. In case of F-SAE cars restrictor is placed after throttle body and the maximum diameter allowed in F-SAE is 20 mm [1]. There are two types of restrictor devices are available one is orifice meter and other is venturi meter. After restrictor intake plenum is placed this Intake plenum works as a reservoir for air, size and area of Intake Plenum plays a very important role in the performance of a engine. Intake Plenum consists of series of tubes which is known as intake runners, runner length, volume and shape also play a very important role in the efficiency of the engine because if a intake system of a engine

works properly and efficiently it improves the efficiency of a engine also [2].

II. MODELING

A) Design of Restrictor

The main objective in designing the air restrictor is to maintain a constant mass flow rate with optimum flow of air.

- Pressure is the most ideal parameter that can be varied to hold the flow rate constant.
- For the minimum pressure difference mass flow rate is maximum [1].

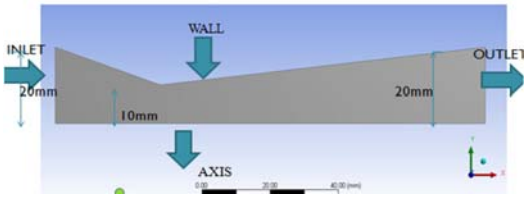

Fig. 2.1 Geometry of restrictor

Inlet Diameter= 40 mm
Outlet Diameter= 40 mm
Throat Diameter= 20 mm

CALCULATIONS

- P_t = 101325 Pa
- T = 300K
- γ = 1.4
- R (air) =0.286 kJ/Kg-K
- A = 0.001256 m^2
- M = 1 (Choking Conditions)

Formula for Calculating Mass flow rate-

$$\dot{m} = \frac{AP_t}{\sqrt{T_t}} \sqrt{\gamma/R} \frac{\gamma+1}{2}^{-\frac{\gamma+1}{(\gamma-1)2}}$$

Result: Mass Flow Rate at Choking = 0.0703 kg/s

B) PRESSURE VARIATION IN RESTRICTOR FOR DIFFERENT CONVERGING AND DIVERGING ANGLES-

I. Pressure drop for 18^0 Converging Angle-

CONVERGING ANGLE(DEGREE)	DIVERGING ANGLE(DEGREE)	PRESSURE DROP(Pa)
18^0	4^0	3447.6001
18^0	5^0	3201.5947
18^0	6^0	3447.6003

II. Pressure drop for 20^0 Converging Angle-

CONVERGING ANGLE(DEGREE)	DIVERGING ANGLE(DEGREE)	PRESSURE DROP(Pa)
20^0	4^0	**3151.9028**
20^0	5^0	3334.8418
20^0	6^0	3590.7903

- As the angle increases, the separation increases however as the angle decreases the pipe becomes longer.
- 4 degree was the optimum angle as it allowed the minimum pressure drop.
- 20 degrees convergent and 4 degrees divergent angle is the optimum angle for this restrictor.

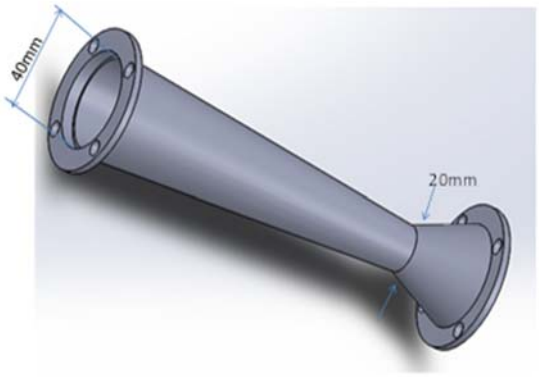

Fig.2.2 Final Design of Restrictor

C) Concept of new design

In order to enhance the flow into all cylinders the plenum must be fed from centre in place of one edge flow.

- If the flow had to turn too much flow rate was significantly diminished, so the concept of equidistant runners from the centerline of plenum suggested.
- Intake ports of cylinder head of the engine are in a line configuration so the runners would need a bend to transform a circular arrangement into inline one.

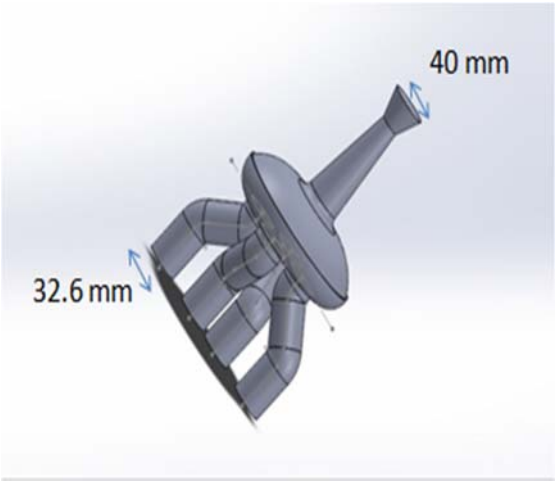

Fig. 2.3 Model of New Manifold

D) Meshing of New Intake Manifold Model
Skewness (cell size/optimal cell size)
Min. skewness = 5.3165E-04
Max. skewness = 0.82426
Aspect Ratio
Minimum=1.1368
Maximum=41.522
Orthogonal quality-
Minimum=2.5035E-02
Maximum=0.998
Nodes=41542
Elements=159350

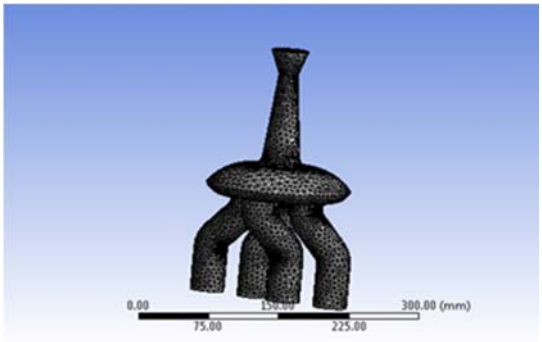

Fig. 2.4 Meshing of New Intake Manifold

III. RESULTS AND DISCUSSION

Flow through Runner 1-

After performing simulation on previous models we come on conclusion that there is need of improvement to enhance the performance of the manifold and for even distribution of air simulation on new model is performed and at outlet we found that design take the advantage of a straight line passage for the air through restrictor and plenum and we get velocity of 69.38 m/sec in runner 1.

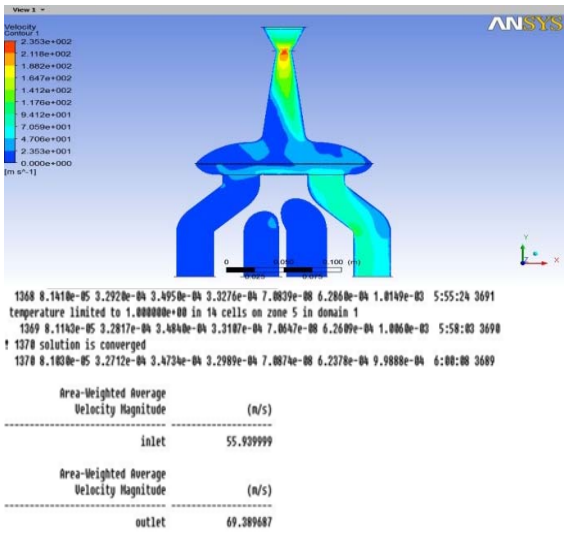

Fig. 3.1 Contour for Runner 1

Flow through Runner 2-

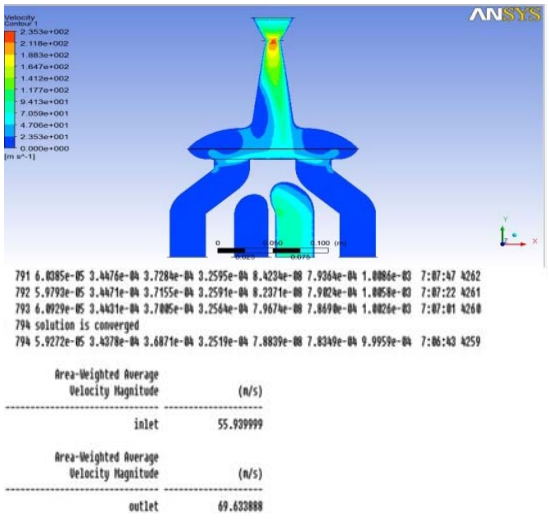

Fig. 3.2 Contour for Runner 2

On performing simulation through runner 2 we get almost same velocity of magnitude 69.6338 m/sec as similar to runner 1 this shows that improvement over previous models of the manifold as this shows even distribution to each runner.

Flow through Runner 3-

The intake runner arrangement is equidistant arrangement from the centerline of the manifold. On observing the flow from runner 3 one of the most important objectives is fulfilling of very less pressure losses due to which equal amount of velocity is observed in runner 3 also of amount 69.36 m/sec.

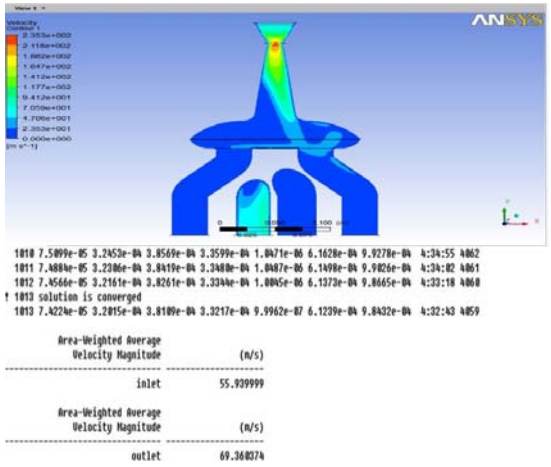

Fig. 3.3 Contour for Runner 3

. **Flow through Runner 4-**

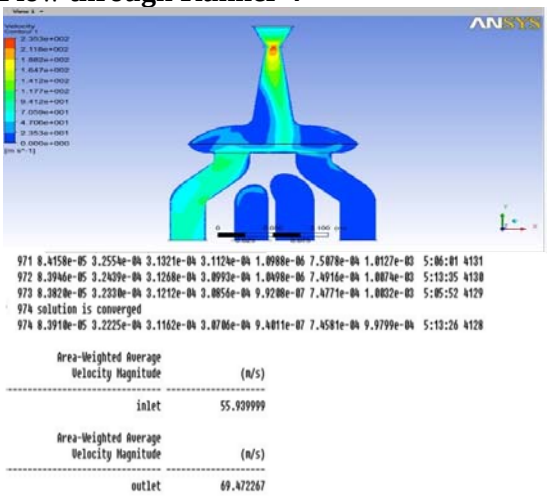

Fig. 3.4 Contour for Runner 4

In the design of the plenum we are using bulbous shape due to which it allows best route for air to reach each runner with large amount of plenum volume and this equals the mass flow rate through each runner. This new design shows clearly modification over previous two models by providing even distribution in each runner in terms of velocity of magnitude 69 m/sec.

A) **Comparison of all the three intake Manifolds-**

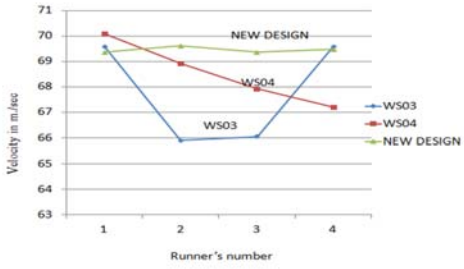

Fig 3.5 Velocity variation in different runners through different manifolds

From the above graph it is clear that WS04 performance is better than the performance of WS03 manifold and at last new design of manifold is performing better in all the intake manifold models.

IV CONCLUSION

From the present work the conclusion can be drawn which are summarized as follows.

- By performing several simulations on different manifold model it has been found that the flow characteristics inside the manifold are greatly depends upon the manifold design.
- The objective of the present work is to improve the design of the manifold by considering the critical areas where the losses are prominent. In the new model the above aspects have been taken into account to achieve higher output velocity as compare to other model with even distribution to each cylinder [7].

In order to improve the performance of internal combustion engine the performance of intake manifold must be improve because efficiency of IC engine is highly depends upon the performance of intake manifold. In order to improve the performance of intake manifold the geometry of runner and plenum must be improve to reduce the pressure losses so that there must be high mass flow rate and even distribution of fuel/air to each runner[4]. If the plenum was fed from centre rather than from one edge flow was enhanced significantly in all cylinders. If the flow had to turn too much after a centre feed like the cases of cylinders at the extremities of the plenum and the flow was diminished new concept of design was incorporated that all the runners must be equidistant from the centerline of the plenum for even distribution.

REFERENCES-

[1] Anshul Singhal, Mallika Parveen, "Air Flow Optimization via a Venturi Type Air Restrictor" Proceedings of the world congress on engineering, Vol 13, 2013.

[2] M.A. Ceviz, M. Akin, "Design of a new SI engine intake manifold with variable length plenum", Energy Conversion and Management, No. 51, pp. 2239-2244, 2010.

[3] M.A. Ceviz, M. Akin, "Intake Plenum Volume and its Influence on the Engine Performance, Cyclic Variability and Emissions",

Energy Conversion and Management, No. 48, pp. 961-966, 2007.

[4] Negin Maftouni , Reza Ebrahimi, "Intake Manifold Optimization by using 3-D CFD Analysis with Observing the Effect of Length of Runners on Volumetric Efficiency", Proceedings of the 3^{rd}BSME-ASME International Conference on Thermal Engineering, 2006.

[5] Hiren R Patel, Prof. V.H.Chaudhari "Optimization of Intake Manifold of Dual Fuel Gasoline Engine", International Journal of Latest Trends in Engineering and Technology ISSN: 2278-621X, Vol. 2, 2013.

[6] Amit Kumar Gupta, Abhishek Mishra, "Design and Development of Inlet Manifold for Six Cylinder Engine for Truck Application", Indian Journal of Research ISSN - 2250-1991, Vol. 3, 2014.

[7] Shrinath Potul, Rohan Nachnolkar, Sagar Bhave, "Analysis Of Change In Intake Manifold Length And Development Of Variable Intake System", International Journal of Scientific & Technology Research ISSN 2277-8616, Vol. 3, 2014.

[8] Margary R, Nino E, Vafidis C, " The effect of intake duct length on the in-cylinder air motion in a motored diesel engine", SAE Paper No: 900057; 1990.

[9] Sachin Singla, Mr. Sumeet Sharma, Dr. D. Gangacharyulu, "Study of Design Improvement of Intake Manifold of Internal Combustion Engine" International Journal of Engineering Technology, Management and Applied Sciences ISSN 2349-4476, Vol. 3, 2015.

[10] Suresh Aadepu,I.S.N.V.R.Prasanth**, "**Design of intake manifold of IC engines with improved volumetric efficiency", International Journal & Magazine of Engineering, Technology, Management and Research ISSN 2348-4845, Vol. 1, No. 6, 2014.

AN IMPROVED PATH PLANNING APPROACH FOR MOBILE ROBOT NAVIGATION BASED ON PARTICLE SWARM OPTIMIZATION

Praveen Kumar Yadav[1], J. C. Mohanta[2], S. R. Mohanty[3]
[1]PG SCHOLAR, [2]ASSISTANT PROFESSOR, [3]ASSISTANT PROFESSOR
[1,2]Department of Mechanical Engineering, MNNIT Allahabad
[3] Department of Electrical Engineering, MNNIT Allahabad
E-mail:praveen.adept.gs@gmail.com[1],jcmohnata@mnnit.ac.in[2],soumaya@mnnit.ac.in[3]

Abstract

This paper describes the motion planning problem of mobile robot based on particle swarm optimisation (PSO). To find a suitable collision free trajectory of a robot is the most important task in path planning problem, which satisfies certain criteria like feasibility, smoothness, safety, minimum path length and so on. Most of the paths developed by the researchers especially for the situation like edge navigation at the turning point, which may be difficult to implement on the real robot in the generated path. Therefore defining a suitable curve to describe a path is become essential for safe navigation. In present work the concept of B-spline curve is used to develop the path of the robot. Various simulations have been carried out and compare the results with the predefined standard benchmark maps problem to prove the effectiveness and efficacy of the developed control scheme.

Index Terms- Path Planning, Particle Swarm Optimization, Bezier Curves, B-spline curve.

I. INTRODUCTION

Mobile robot path planning is one of the most important topic in the field of robotics in last four decades. Path planning is basically the determination of path which will be used by the robot in order to pass over every single point in a given environment with obstacle, the path planning is used to find suitable collision free path, which needs to fulfill certain criteria like minimum path, minimum associated cost, minimum time, feasibility and safety (security), for mobile robot to move from start point to destination point. Researchers are trying to focus on finding the shortest path with minimum time and cost [1-2]. However, the motion of the robot in a sharp edge is still a challenging task for most of the navigation problems.

In order to solve such types of problems, this may be the reason of introducing curve for path planning; also non smooth-motion may have effect on slip [3-6]. In recent year lots of optimization algorithm is introduced which mimics biological behavior of animals and insects found in nature, such as Genetics algorithm, Particle swarm intelligence technique, Ant colony algorithm etc are gradually used in path planning and few of the got better result [7]. Particle swarm intelligence technique is natural heuristic algorithm based on the birds flocking characteristics .In [8] Bezier curve combined with Casteljau algorithm is discussed, particle swarm optimization in [9], genetic algorithm in [10].

Many traditional approaches for mobile robot path planning are artificial potential field method [11], neural network [12], D^* algorithm [13], and so on. With passage of time and development of evolutionary computational algorithm ,many natured inspired optimization algorithm has been proposed to solve path planning problem, Particle swarm optimization (PSO) which was

proposed by Eberhart and Kennedy in 1995 [14-15] is based on swarm foraging behaviour. In this paper a novel path planning method based on PSO is proposed, which is used to optimize the necessary parameter of the curve which will finally achieve the shortest feasible path from start point to destination point, the length of the path is used to compare the optimality of different path planning algorithm. The experimental result shows that the proposed PSO algorithm outperform the algorithm taken for the comparison of the result.

II. METHOD

A. Bezier curve.

An engineer known as P.E. Bezier introduced a new curve representation which was based on the control points in 1962 and is named after him the Bezier curve [16].

Given a set of $N+1$ control point $P_0, P_1, \dots\dots, P_N$,
with degree *n* the corresponding Bezier curve C_v can be represented by :

$$P(t) = \sum_{i=0}^{N} P_i\, B_{i,N}(t) \quad t \in [0,1] \qquad (1)$$

Where, $B_{i,N}(t)$ is the Berstein polynomial represented by $B_{i,N}(t) = C_N^i t^k (1-t)^{N-i}$

$$i = 0, i \dots . n \qquad (2)$$

The parameter equation of every point for three times Bezier curve could be generated by formulas (1) and (2) as follows:

$$p(t) = P_0(1-t)^3 + 3P_1 t(1-t)^2 + 3P_2 t^2(1-t) + P_3 t^3 \qquad (3)$$

Where t,is in the range of [0,1], Bezier curve starts at $t = 0$ and ends at $t = 1$.
Properties of Bezier curve [17]can be defined as follows:

- Bezier curve starts at the start point and ends at the end point.
- First derivative of the start and end points are only related to the nearest control points and in the same direction of line of two points.

The calculation formula

$$P'(0) = 3(P_1 - P_0),$$
$$P'(n) = 3(P_n - P_{n-1}) \qquad (4)$$

A typical first order continuous Bezier curve can be formed by joining many segments of lower order Bezier curve each segment has four control points. In order to meet the property of first order continuity when using n segments of Bezier curves to describe a path, 2 n points are needed. The path can be generated by using the following Equations as follow:

$$P(t) = \begin{cases} P_0(1-t)^3 + 3P_1^i t(1-t)^2 + 3P_2^i t^2(1-t) + P_3^i t^3 & i = 1 \\ P_3^{i-1}(1-t)^3 + 3(P_3^{i-1} - P_2^{i-1})t(1-t)^2 + 3P_2^i t^2(1-t) + P_3^i t^3 & 1 < i < n \\ P_3^{i-1}(1-t) + 3\left(2P_3^{i-1} - P_2^{i-1}\right)t(1-t)^2 + 3P_2^i t^2(1-t) + P_1 t^3 & 1 = n \end{cases}$$

$$p(t) = [x(t), y(t)]^T \qquad (5)$$

where P_0 represents the start point while P_1 stands for the end point. When t changes in the interval (0, 1), we can get a cubic Bezier curve of segment i. These n segments of cubic Bezier curve constitute the entire path of the curve.

B. B-spline curve

As we know that cubic hermit curve is controlled globally i.e. any change in any control point will change the wall curve along its full length, *also it* is not possible to keep the degree of the curve fixed ,while adding additional points any additional points will automatically increase the degree of the curve.

B-Spline curve is the solution of all the problem mentioned above it. B-spline curve is defined by $n+1$ control points P_i is given by

$$P(t) = \sum_{i=0}^{n} P_i\, N_{i,k}(t) \qquad 0 \le t \le t_{max} \qquad (6)$$

Where $N_{i,k}(t)$ are the B-spline functions , parameter k controls the degree $(k-1)$ of the resulting B-spline curve and is independent of the number of control points , ,maximum limit of the parameter t is no longer 1 as was arbitrarily chosen. B-spline curve has the following property:

Partition of unity: $\sum_{i=1}^{n} N_{i,k}(u) = 1$
Positivity: $N_{i,k}(u) \ge 0$
Local support: $N_{i,k}(u) = 0 \quad if\ u \notin [u_i, u_{i+k+1}]$
Continuity: $N_{i,k}(u)\ is\ (k-2)$

$times\ countinously\ \ differentiable.$

Some conclusions can be made on the basis of above properties, the first properties ensures that the relationship between the curve and its defining control points is invariant under affine transformation. The second property guarantees that the curve segment lies completely within the convex hull of P_i . The third property indicates that each segment of B-spline curve is influenced by only k control points or each control point affects only k curve segments.

The B-spline function also has the property of recursion which is given by the equation shown below:

$$N_{i,k}(t) = (t - t_i)\frac{N_{i,k-1}(t)}{t_{i+k-1} - t_i} + (t_{i+k} - t)\frac{N_{i+1,k-1}(t)}{t_{i+k} - t_{i+1}} \quad (7)$$

Where,

$$N_{i,1} = \begin{cases} 1, & t_i \le t \le t_{i+1} \\ 0, & otherwise \end{cases}$$

t_i are called knot values.

C. PSO based path planning

The path planning problem is converted into an optimization problem through using B-spline curve which is used to describe the path, PSO is used to locate the optimal control point in B-spline curve to find the shortest path from start to end point. The basic flow of the algorithm for PSO based path planning is show below:

1) Initialize the particle by randomly assigning each particle an initial velocity and a position within the solution space.
2) Evaluate the desired fitness function which is to be optimized for each particle‘s position.
3) For each particle, update its previously found best position so far, ***Pi,*** if its current position is better than its previous best one.
4) Recognize and update the swarm’s overall globally best particle that has the swarm‘s best fitness value, and set/reset its index as ***g*** and its position at ***Pg***.
5) Update the velocities of all the particles.
6) Move each particle to its new position as per the new velocity.
7) Repeat steps 2–6 until convergence or a stopping criterion is met (e.g., the maximum number of allowed iterations is reached; a sufficiently good fitness value is achieved; or the algorithm has not improved its performance for a number of consecutive iterations).

In PSO velocity and position update equation is given below:

$$v_{id(t+1)}=v_{id}(t)c_1R_1[p_{id}(t)-x_{id}(t)]+c_2R_2[p_{gd}(t)-x_{id}(t)] \quad (8)$$

$$x_{id}(t+1) = x_{id}(t) + v_{id(t+1)} \quad (9)$$

Where,

- v_{id} Tells about the velocity.
- x_{id} Denotes the position of i^{th} particle in d^{th} dimension.
- p_{id} Denotes the previous best position of the i^{th} particle in the d^{th} dimension.
- p_{gd} Denotes the position of swarm’s global best particle in d^{th} dimension.
- R_1 And R_2 are two n-dimensional vector with numbers uniformly selected in the range of [0.0, 1.0].
- c_1 And c_2 are positive constant weighting parameters.

To solve the path planning problem B-spline curve is used to describe the path, first of all model environment is created with start and end points with number of obstacle in it as per the standard map, randomly three points are taken through which path of the robot has to be pass and proposed PSO algorithm is used to optimize the path, length of the path is calculated by dividing the curve into smaller segment and distance of each segment is calculated , summing up the length of all the segment gives the length of the path formula used is as follow:

$$l_1 = (x_1 - x_0)^2 + (y_1 - y_2)^2$$
$$similarly\ l_2, l_3, \dots, l_{n+1}$$
$$L = l_1 + l_2 + l_3 + \cdots + l_{n+1}$$

L gives the length of the path, in order to check the feasibility condition i.e. path is passing or touching the obstacle following equation is used,

$$d = (((xx - x_{obs}(k))^2 + (yy - y_{obs}(k))^2)^{1/2} \quad for\ k = 1,2,3, \dots, \quad (10)$$

Where, x_{obs} , y_{obs} are the x & y coordinate of the obstacles, if it touches the obstacle then it will leads to violation criteria which given by

$$v = (1 - \frac{d}{robs(k)}) \quad (11)$$

$$violation = \frac{v_1 + v_2 + \cdots v_n}{n}$$

Cost function is evaluated as follow:

$$cost = L \times (1 + \beta \times violation) \quad (12)$$

Where, β is a constant taken equal to 100, which is used to balance the proportion of path length.

III. SIMULATION AND RESULT

To compare the result of proposed PSO ,simulation result by J. J. Liang , H. Song, B. Y. Qu, and Z. F. Liu[], is taken with similar environment, the benchmark maps [a,b and c]are employed as the environment, the maps and the path planned by PSO are illustrated in figures . The white areas are negotiable and the coloured areas are impassable, the task is planning a shortest collision free path from starting point (5, 5) to the end point (15, 15).

Environment 1

Table 1.0 Parameter specification map a, b & c

parameter	PSO
Maximum Iterations	100
Number of particles	50
Inertia weight, w	1
Damping ratio (w damp)	.98
Global learning coefficient	1.5
Radius of obstacles	.8

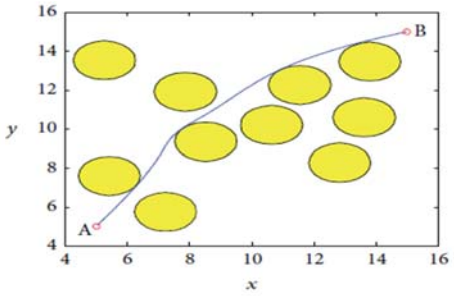

Fig.1.0 Result showing the navigational path of robot by J. J. Liang, et.al.[19]

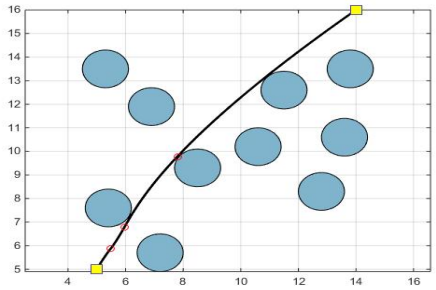

Fig 1.1 Fig. Result showing the navigational path of robot using the proposed algorithm. Environment 1

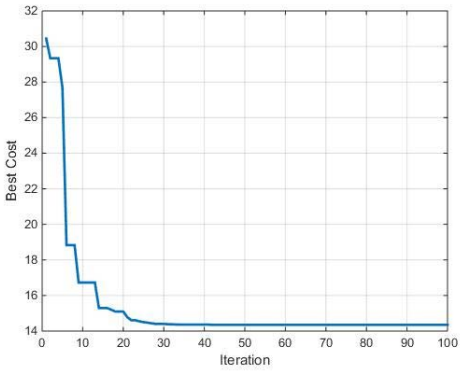

Fig 1.2 cost vs. iteration

The result obtained from the navigational path of robot using the proposed algorithm. is superior and the length obtained is 14.3491 cm, whereas the navigational path length of robot by J. J. Liang, et.al is 18.3684 cm.

Environment 2

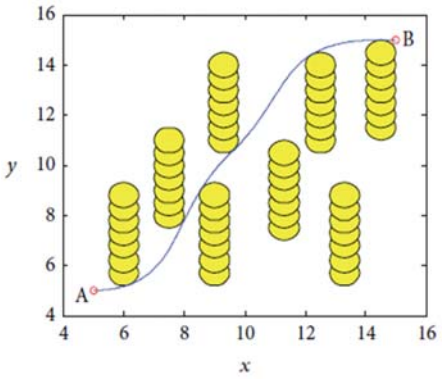

Fig.2.0 Result showing the navigational path of robot by J. J. Liang, et.al.[19]

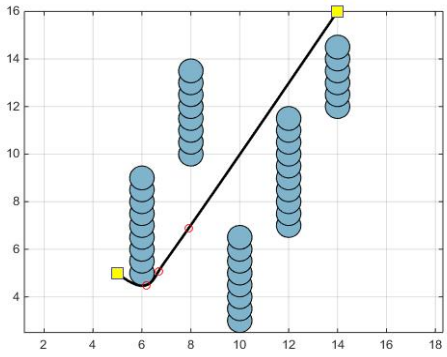

Fig 2.1 Result showing the navigational path of robot using the proposed algorithm Environment 2

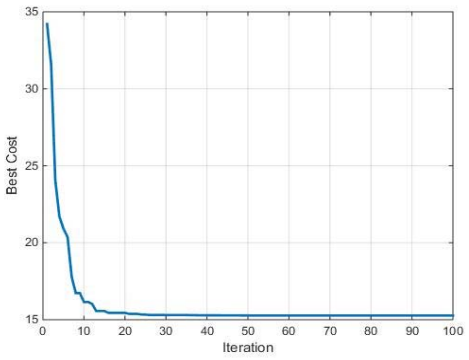

.

Fig 2.2 cost vs. iteration

For this case path length obtained through proposed algorithm is 15.3106 cm, whereas the navigational path length of robot by J. J. Liang, et.al is 16.7417 cm.

Environment 3

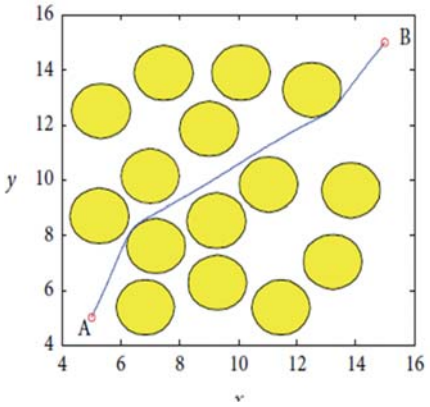

Fig.3.0 Result showing the navigational path of robot by J. J. Liang, et.al.[19]

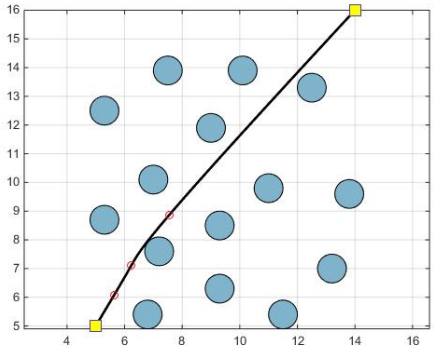

Fig. 3.1Result showing the navigational path of robot using the proposed algorithm. Environment 3.

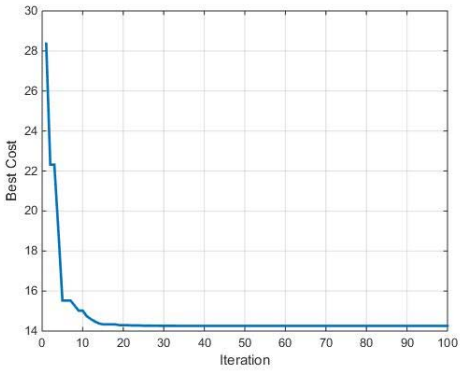

Fig 3.2 cost vs. iteration

For this case total path length is 14.2606 whereas the standard test result is 16.5045 cm.

Table 2.0 Comparison of result

Environment No.	**Results from J. J. Liang, et.al.[19]**	**Proposed method**	
	Distance (cm)	Distance (cm)	Time (sec)
1	18.3684	14.3491	42.368
2	16.7417	15.3106	67.286
3	16.5054	14.2606	44.169

IV. CONCLUSIONS

In this paper, improved PSO is employed to optimize the control points of B-spline curve to solve the path planning problem of mobile robot. Computer Simulations has been performed using MATLAB software for the situation like edge navigation. Results show that during edge navigation a smooth path has been generated by the developed algorithm. In order to validate the proposed control scheme the developed algorithm has been tested in various environments and compared with the results obtained from []. From the comparison it has been found that the proposed algorithm performed better results in terms of path length, smoothness of trajectories, time taken and convergence rate.

REFERENCES

[1] Abiyev, R., Ibrahim, D., & Erin, B. (2010). Navigation of mobile robots in the presence of obstacles. Advances in Engineering Software, 41(10), 1179-1186.

[2] Buniyamin, N., Wan Ngah, W. A. J., Sariff, N., & Mohammad, Z. (2011). A simple local path planning algorithm for autonomous mobile robots. International journal of systems applications, Engineering & development, 5(2), 151-159.

[3]. Zhao, T.: A Transit Path Planning Model Based on The Heterogeneous Road Network. In: International Conference on Geoinformatics, pp. 1–6 (2009).

[4]. Chesi, G.: Designing Image Trajectories in The Presence of Uncertain Data for Robust Visual Serving Path-Planning. In: IEEE International Conference on Robotics and Automation, pp. 1492–1497 (2009)

[5]. Li, G.S.: Study of Technology on Path Planning for Mobile Robots. In: Control and Decision Conference, pp. 3295–3300 (2008)

[6]. Qu, Y.H.: Flight Path Planning of UAV Based on Heuristically Search And Genetic Algorithms. Industrial Electronics Society, 6–10 (2005)

[7] M.J Zhang, Underwater Robot, Beijing: Ocean Press, 2000:Page1-7,123-133.

[9] D. W. Zhu and X. B. Mao, "Path planning algorithm based on improved particle swarm optimization of Bezier curves,"*Application Research of Computers*, vol. 5, pp. 1–6, 2012.

[10] L.Yang, Z. Luo, Z.Tang, and w. Lv, "Path planning algorithm for mobile robot obstacle avoidance adopting Bezier curve based on genetic algorithm," in *Proceedings of the Chinese Control and Decision Conference (CCDC '08)*, pp. 3286–3289, Yantai, China, July 2008.

[11] E. Rimon and D. E. Koditschek, "Exact robot navigation using artificial potential functions," *IEEE Transactions on Robotics and Automation*, vol. 8, no. 5, pp. 501–518, 1992.

[12] N. G. Bourbakis, D. Goldman, R. Fematt, I. Vlachavas, and L. H. Tsoukalas, "Path planning in a 2-D known space using neural networks and skeletonization," in *Proceedings of the IEEE International Conference on Systems,Man, and Cybernetics*, vol. 3, pp. 2001–2005, Orlando, Fla, USA, October 1997.

.[13] S. Koenig and M. Likhachev, "Improved fast replanning for robot navigation in unknown terrain," in *Proceedings of the IEEE International Conference on Robotics and Automation*, pp. 968–975, May 2002.

[14] J. Kennedy and R. Eberhart, "Particle swarm optimization," in *Proceedings of the IEEE International Conference on Neural Networks*, pp. 1942–1948, Piscataway, NJ, USA, December 1995.

[15] Z. A. Bashir andM. E. El-Hawary, "Short-term load forecasting using artificial neural network based on particle swarm optimization algorithm," in *Proceedings of the Canadian Conference on Electrical and Computer Engineering (CCECD '07)*, pp. 272–275, Vancouver, Canada, April 2007.

[16] F. Yamaguchi, F. Yamaguchi, "Curves and surfaces in computer aided geometric design". Berlin: Springer-Verlag, 1988, pp. 23-24.

[17] Z. A. Bashir andM. E. El-Hawary, "Short-term load forecasting using artificial neural network based on particle swarm optimization algorithm," in *Proceedings of the Canadian Conference.*

[18] J. J. Liang, H. Song, B. Y. Qu, et al., "Path planning based on dynamic multi-swarm particle swarm optimizer with crossover", *Intelligent Computing Theories and Applications*. Heidelberg: Springer Berlin, pp.159-166, 2012. *on Electrical and Computer Engineering*

[19] J. J. Liang,1 H. Song,1 B. Y. Qu,2 and Z. F. Liu2," Comparison of Three Different Curves Used in Path Planning Problems Based on Particle Swarm Optimizer", Hindawi Publishing Corporation. Mathematical Problems in Engineering Volume 2014, Article ID 623156, 15 pages

.

A SIMPLE METHOD FOR LOAD FLOW SOLUTION OF RADIAL DISTRIBUTION SYSTEMS

Ujjavala Singla[1], Rajni Bala[2]
[1]M.Tech. (Power Engg.) Student BBSBEC Fatehgarh Sahib (Pb.)
[2]AP (EE dept.) BBSBEC Fatehgarh Sahib (Pb.)
Email: ujjavala.singla@gmail.com[1], rajni.bala@bbsbec.ac.in[2]

Abstract

In this paper a new and efficient method for the reliable load flow solution of radial distribution system is presented wherein an easy and fast load flow solution algorithm is used. It fully exploits the radial structure of the network and employs an effective data structure to identify the nodes beyond a particular branch. Using this concept, load current summations are calculated to obtain the load flow solution. Unlike other traditional methods, the proposed method considers the effective convergence approach which is simple and is capable of reducing execution time of the network.

Index Terms: Constant power load modeling, Load currents, Nodes beyond branch, Radial distribution systems.

I. INTRODUCTION

There are many solution techniques for load flow calculations. However, an acceptable load flow method should meet the requirements [1] such as high speed and low storage requirements, highly reliable, and accepted versatility and simplicity.

The operation and planning studies of a distribution system require a steady-state condition of the system for various load demands. Distribution networks have recently acquired a growing importance because their extension has quite increased and also because their management has become quite complex. Unfortunately the techniques widely known and used at High Voltage level cannot be straightforward applied to distribution systems. This is because the distribution systems are ill-conditioned systems i.e. the systems which show large oscillations in the results by small perturbations. Since Low Voltage lines have a high R/X ratio. This high R/X ratio [2-4] factor of the distribution systems makes them ill conditioned and so the need of new and efficient method for the analysis of distribution system arises. The analysis of distribution systems is an important area of activity as distribution systems is the final link between a bulk power system and consumers.

Kersting and Mendive [5] and Kersting [6] have developed a load-flow technique for solving radial distribution networks using ladder-network theory. They have developed the ladder technique from basic ladder-network theory into a working algorithm, applicable to the solution of radial load-flow problems. Stevens et al. [7] have shown that the ladder technique is found to be fastest but did not converge in five out of 12 cases studied. Shirmohammadi er al. [8] have proposed a method for solving radial distribution networks based on the direct application of Kirchhoff's voltage and current laws. They have developed a branch-numbering scheme to enhance the numerical performance of the solution method. They have also extended their method for solution of weakly meshed networks. Baran and

Wu [9] have obtained the load-flow solution in a distribution system by the iterative solution of three fundamental equations representing real power, reactive power and voltage magnitude. They have computed the system Jacobian matrix using a chain rule. In their method, the mismatches and the Jacobian matrix involve only the evaluation of simple algebraic expressions and no trigonometric functions. They have also proposed decoupled and fast decoupled distribution load-flow algorithms. Chiang [10] has also proposed three different algorithms for solving radial distribution networks based on the method proposed by Baran and Wu [9]. Renato [11] has proposed one method for obtaining a load-flow solution of radial distribution networks. Jasmon and Lee [15, 16] have proposed a new load-flow method for obtaining the solution of radial distribution networks. They have used the three fundamental equations representing real power, reactive power and voltage magnitude derived in [9]. Das et al. [14] have proposed a load-flow technique for solving radial distribution networks by calculating the total real and reactive power fed through any node. They have proposed a unique node, branch and lateral numbering scheme which helps to evaluate exact real- and reactive power loads fed through any node and receiving-end voltages.

The aim of the paper is to propose a simple and fast load flow method for radial distribution systems. Here, a method is presented for identifying the total nodes beyond a particular node, which will improve the speed of the proposed method. Load flow solution is based on simple iterative method of receiving end voltage of radial distribution system. The convergence of the method is accelerated by a judicious choice of the initial voltages and power losses are taken into consideration from the first iteration. The proposed method is tested on standard distribution systems. It is also observed that the proposed method has good and fast convergence characteristics. Loads in the present formulation have been presented as constant power.

II. ASSUMPTIONS

While implementing all the discussed methods it was assumed that:

1. Three-phase radial distribution networks were balanced and represented by their single-line diagrams.
2. Charging capacitances are neglected at the distribution voltage level (medium level).
3. The load flow solution has been computed for constant power load modeling.

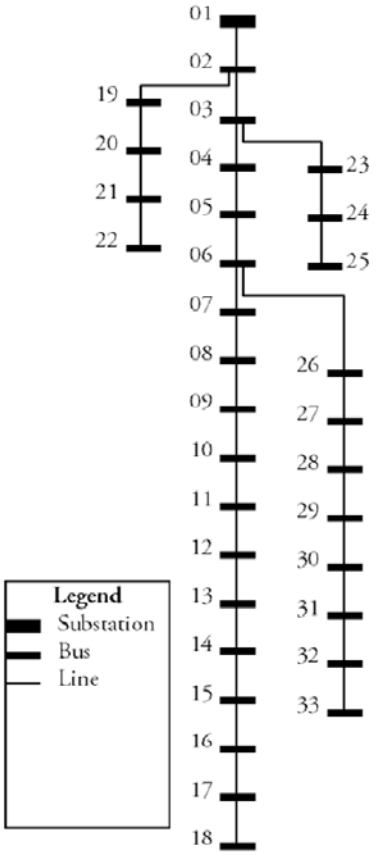

Fig.3. 33-bus radial distribution system

III. SOLUTION METHODOLOGY

A 33-bus radial distribution system Fig.3. was tested using the proposed method [12-13]. The branch number sending-end and receiving-end node of this feeder are given in Table 1. Table 1 also shows the results of nodes beyond a particular node. Consider branch 1. The receiving-end node voltage can be written as

$$V(2) = V(1) - I(1)\ Z(1)$$

Similarly for branch 2,

$$V(3) = V(2) - I(2)\ Z(2)$$

As the substation voltage V(1) is known, so if Z(1) is known, i.e. current of branch 1, it is easy to calculate V(2) from above eqn.

Once V(2) is known, it is easy to calculate V(3), if the current through branch 2 is known. Similarly, voltages of nodes 4, 5, ..., NB can easily be calculated if all the branch currents are

known. Therefore, a generalised equation of receiving-end voltage, sending-end voltage, branch current and branch impedance is

$$V(m2) = V(m1) - I(jj)\,Z(jj) \quad \text{....(i)}$$

where j j is the branch number.

$$m2 = I\,R(jj)$$
$$m1 = I\,S(jj)$$

Eqn. (i) can be evaluated for jj = 1, 2, ..., LN1 (LN1 = NB - 1 = number of branches). Current through branch 1 is equal to the sum of the load currents of all the nodes beyond branch 1.

Therefore, if it is possible to identify the nodes beyond all the branches, it is possible to compute all the branch currents. Identification of the nodes beyond all the branches is realised through an algorithm as explained in Section IV.

The load current of node *i* is

$$IL(i) = \frac{PL(i) - jQL(i)}{V^*(i)} \qquad i = 2, 3, \ldots, NB \quad \text{....(ii)}$$

Load currents are calculated iteratively. Initially, a flat voltage of all the nodes is assumed and load currents of all the nodes are computed. A detailed load flow calculation algorithm is described in Section V.

Table 1: Calculation of Nodes beyond branch jj

jj	m1 = IS(jj)	m2 = IR(jj)	Nodes beyond branch jj	N(jj)
1	1	2	2,3,19,4,23,20,5,24,21,6,25,22,7,26,8,27,9,28,10,29,11,30,12,31,13,32,14,33,15,16,17,18	32
2	2	3	3,4,23,5,24,6,25,7,26,8,27,9,28,10,29,11,30,12,31,13,32,14,33,15,16,17,18	27
3	3	4	4,5,6,7,26,8,27,9,28,10,29,11,30,12,31,13,32,14,33,15,16,17,18	23
4	4	5	5,6,7,26,8,27,9,28,10,29,11,30,12,31,13,32,14,33,15,16,17,18	22
5	5	6	6,7,26,8,27,9,28,10,29,11,30,12,31,13,32,14,33,15,16,17,18	21
6	6	7	7,8,9,10,11,12,13,14,15,16,17,18	12
7	7	8	8,9,10,11,12,13,14,15,16,17,18	11
8	8	9	9,10,11,12,13,14,15,16,17,18	10
9	9	10	10,11,12,13,14,15,16,17,18	9
10	10	11	11,12,13,14,15,16,17,18	8
11	11	12	12,13,14,15,16,17,18	7
12	12	13	13,14,15,16,17,18	6
13	13	14	14,15,16,17,18	5
14	14	15	15,16,17,18	4
15	15	16	16,17,18	3
16	16	17	17,18	2
17	17	18	18	1
18	2	19	19,20,21,22	4
19	19	20	20,21,22	3
20	20	21	21,22	2
21	21	22	22	1
22	3	23	23,24,25	3
23	23	24	24,25	2
24	24	25	25	1
25	6	26	26,27,28,29,30,31,32,33	8
26	26	27	27,28,29,30,31,32,33	7
27	27	28	28,29,30,31,32,33	6
28	28	29	29,30,31,32,33	5
29	29	30	30,31,32,33	4
30	30	31	31,32,33	3
31	31	32	32,33	2
32	32	33	33	1

IV. IDENTIFICATION OF NODES BEYOND ALL THE BRANCHES

For jj = 1 (first branch of Fig. 1 , Table 1, IR(jj) = IR(1) = 2; check whether IR(1) = IS(i) or not for i = 2, 3, 4, ..., LN1. It is seen that IR(1) = IS(2) = 2, IR(1) = IS(18) = 2; the corresponding receiving-end nodes are IR(2) = 3 and IR(6) = 19.

Therefore, IE(1, 1) = 2, IE(1, 2) = 3 and IE(1, 3) = 19. Note that there should not be any repetition of any node while identifying nodes beyond a particular branch [17], and this logic has been incorporated in the proposed algorithm.

From the above discussion, it is seen that node 2 is connected to nodes 3 and 19. Similarly, the proposed logic will identify the nodes which are

connected to nodes 3 and 19. Firstly, it will check whether node 3 appears in the left-hand column of Table 1 . It is seen that node 3 is connected to node 4. Therefore, IE(1, 4) = 4. Then it will check whether node 19 appears in the left-hand column of Table 1 . It is seen that the node 19 is connected to node 20. Therefore, IE(1, 5) = 20.

From the above discussion, it is again seen that node 3 is connected to node 4 and node 19 is connected to node 20. Similarly, the proposed logic will check whether nodes 4 and 20 are connected to any other nodes. This process will continue unless all nodes are identified beyond branch 1. Table 1 shows the result of the coding implemented in MATLAB 7 for the calculation of nodes beyond branch jj. This will help to obtain load flow solution by summation of load currents of all the nodes beyond a particular branch.

The total current flowing through branch 1 is equal to the sum of the load currents of all nodes beyond branch 1.

Note that, if the receiving-end node of any branch in Fig. 1 is an end node of a particular lateral, the total current of this branch is equal to the load current of this node itself.

V. ALGORITHM FOR LOAD FLOW COMPUTATION

The complete algorithm for load-flow computation is shown below:

Step 1 : Start

Step 2 : Read line data and load data of the system.

Step 3 : Read base values.

Step 4 : Set ITMAX = 100.

Step 5 : Set V(i,j) = 1.0 + j0.0 for i = 1,2,3……TFL and j = 1,2,3……..TN(i).

Step 6 : Set IT = 1.

Step 7 : Set PL1(i,j) = PL(i,j) and QL1(i,j) = QL(i,j) for i=1,2,3……TFL and j=1,2,3…..TN.

Step 8 : Using equation (ii) calculate IL(m2) for m2 = 2,3……..TN.

Step 9 : Calculate I(i,jj) for i=1,2,…….TFL and jj = 1,2,……TN-1 where

$$I(i,jj) = \sum_{i=1,jj=1}^{i=TFL,jj=TN-1} IL(i,j)$$

Step 10 : Compute V(i, j+1) = V(i, j) - I(i, jj)Z(i, jj) for i=1,2,3……TFL and j=1,2,3……..TN(i).

Step 11 : Compute $\Delta V^k(i, j) = V^{k-1}(i, j) - V^k(i, j)$.

Step 12 : Arrange ΔVk(i, j) in descending order.

Step 13 : Get the highest value of ΔVk(i, j).

Step 14 : If ΔVk(i, j) < 0.001 go to step 17 else go to step 15.

Step 15 : IT = IT+1.

Step 16 : If IT < ITMAX, go to step 7 else go to step 17.

Step 17 : Display 'SOLUTION CONVERGED'.

Step 18 : Stop.

VI. EXAMPLE

To demonstrate the effectiveness of the proposed method, a 33-node radial distribution system has been selected. Input data for this 33-node system is given in Table 2 [12]. Table 2 also shows the results of votage (p.u.) for each node of this 33-node radial distribution network.

VII. CONCLUSION

A simple and efficient load-flow technique has been proposed for solving radial distribution networks. Herein this work, it is observed that the values of absolute voltage at each node, obtained by the proposed method, are more precise and accurate. In future, the proposed method will be used for the evaluation of voltages for other load models, in a way which will be more convergent.

REFERENCES

[1] B. Scott, "Review of load flow calculation methods," Proc. IEEE, Vol.62, No.7, pp. 916-929, July 1974.

[2] RAJICIC, D., and TAMURA, Y.: 'A modification to fast decoupled power flow for networks with hgh R/X ratios', IEEE Tram., 1988, PWRS-3, pp. 743-746.

[3] IWAMOTO, S., and TAMURA, Y.: 'A load flow calculation method for ill-conditioned power systems', IEEE Trans., 1981, PAS-100, pp.1736-171 3.

[4] TRIPATHY, S.C., DURGAPRASAD, G., MALIK, O.P., and HOPE, G.S.: 'Load flow solutions for ill-conditioned power system by a Newton like method', ZEEE Tram., 1982, PAS-101, pp. 3684-3657.

[5] KERSTING, W.H., and MENDIVE, D.L.: 'An application of ladder network theory to the solution of three phase radial load flow problem'. IEEE PES winter meeting, New York, January 1976

[6] KERSTING, W.H.: 'A method to the design and operation of a distribution system', ZEEE Trans., 1984, PAS-103, pp. 1945-1952

[7] STEVENS, R.A., RIZY, D.T., and PURUCKER, S.L.: 'Performance of conventional power flow routines for real-time distribution automation application'. Proceedings of 18th south eastern symposium on System theory, 1986, (IEEE Computer Society), pp. 196-200

[8] SHIRMOHAMMADI. D.. HONG. H.W.. SEMLYEN. A.. and LUO, G.X.: 'A compensa6on-based power 'flow method for weakly meshed distribution and transmission networks', IEEE Trans., 1988, PWRS-3, pp. 753-743

[9] BARAN, M.E., and WU, F.F.: 'Optimal sling of capacitors placed on a radial distribution system', IEEE Trans., 1989, P-2, pp. 735- 743

[10] CHIANG, H.D.: 'A decoupled load flow method for distribution power network algorithms, analysis and convergence study', Electr. Power Energy Syst., 1991, 13, (3), pp. 130-138

[11] RENATO, C.G.: 'New method for the analysis of distribution networks', IEEE Trans., 1990, PWRD-5, (l), pp. 9-13

[12] A. Arunagiri , Suresh K, B.Venkatesh, R.Ramesh Kumar and Mustajab Ahmed Khan, "Artificial Neural Network Approach: An Application to Harmonic Load Flow for radial systems," Yanbu journal of engineering and science, Vol. 1, October 2010 (1431H).

[13] Vaishali Holkar, Dr. Deepika Masand, "Intelligent System for Radial Distribution Load Flow", International Journal of Engineering Innovation & Research Volume 1, Issue 5, ISSN: 2277 – 5668.

[14] DAS, D., NAGI, H.S., and KOTHARI, D.P.: 'Novel method for solving radial distribution networks', IEE Proc. C, 1994, 141, (4), pp. 291-298.

[15] JASMON, G.B., and LEE, L.H.C.C.: 'Distribution network reduction for voltage stability analysis and load flow calculations', Electr. Power Energy Syst., 1991, 13, (I) , pp. 9-13.

[16] JASMON. G.B.. and LEE. L.H.C.C.: 'Stabilitv of load flow techniques for distribution system voltage stability analysis', IEE Proc. C, 1991, 138, (6), pp. 479484.

[17] S. Ghosh and D. Das, 'Method for load-flow solution of radial distribution networks', IEE Proc.-Gener Transm. Distrib., Vol. 146, No. 6., Nov 1999.

APPENDIX.1. NOMENCLATURE

NB : Total number of the nodes
LN1 : Total number of the branch (LN1 = NB − 1)
jj : Branch number
m1 : Receiving end node
m2 : Sending end node
PL(i) : Real power load of ith node
QL(i) : Reactive power load of ith node
|V(i)| : Voltage magnitude of ith node
R(jj) : Resistance of the branch–jj
X(jj) : Reactance of the branch–jj
Z(jj) : Impedance of the branch–jj
I(jj) : Current flowing through branch–jj
IS(jj) : Sending end node of branch–jj
IR(jj) : Receiving end node of branch–jj
IL(i) : Load current of node-i
kV : Kilovolts
kW : Kilowatts
kVAr : Amount of reactive power

Table 2: 33-BUS RADIAL DISTRIBUTION SYSTEM UNDER STUDY

Branch no. (jj)	Sending End IS(jj)	Receiving End IR(jj)	R(Ω)	X(Ω)	PL(kW)	QL(kVAr)	V(p.u.)
1	1	2	0.0922	0.047	100	60	1
2	2	3	0.493	0.2511	90	40	0.9972
3	3	4	0.366	0.1864	120	80	0.9885
4	4	5	0.3811	0.1941	60	30	0.9923
5	5	6	0.819	0.707	60	20	0.9933
6	6	7	0.1872	0.6188	200	100	0.9866
7	7	8	1.7114	1.2351	200	100	0.9964
8	8	9	1.03	0.74	60	20	0.9852
9	9	10	1.044	0.74	60	20	0.9917
10	10	11	0.1966	0.065	45	30	0.9921
11	11	12	0.3744	0.1238	60	35	0.9988
12	12	13	1.468	1.155	60	35	0.9978
13	13	14	0.5416	0.7129	120	80	0.9906
14	14	15	0.591	0.526	60	10	0.9970
15	15	16	0.7463	0.545	60	20	0.9982
16	16	17	1.289	1.721	60	20	0.9982
17	17	18	0.732	0.574	90	40	0.9970
18	2	19	0.164	0.1565	90	40	0.9994
19	19	20	1.5042	1.3554	90	40	0.9995
20	20	21	0.4095	0.4784	90	40	0.9962
21	21	22	0.7089	0.9373	90	40	0.9991
22	3	23	0.4512	0.3083	90	50	0.9994
23	23	24	0.898	0.7091	420	200	0.9989
24	24	25	0.896	0.7011	420	200	0.9983
25	6	26	0.203	0.1034	60	25	0.9993
26	26	27	0.2842	0.1447	60	25	0.9986
27	27	28	1.059	0.9337	60	20	0.9982
28	28	29	0.8042	0.7006	120	70	0.9930
29	29	30	0.5075	0.2585	500	600	0.9962
30	30	31	0.9744	0.963	150	70	0.9987
31	31	32	0.3105	0.3619	210	100	0.9974
32	32	33	0.341	0.5302	60	40	0.9993

A METHODOLOGY FOR INPUT POWER SHARING AMONG A MULTIPLE-INPUT DC-DC CONVERTER TOPOLOGY

Dr.Sushil Kumar
Principal, Pragati College Of Engineering and Management Raipur (C.G)
Sk1_bit@rediffmail.com

Abstract

Among the power electronic converters, dc-dc converters find applications in key areas such as dc drives, battery charging, electric traction, renewable power generation and so on. The use of multiple input converters topology enables operation at high switching frequency without sacrificing efficiency. High switching frequency of operation reduces the output filter requirement, which in turn helps in reducing the size of the converters.In this research work, a methodology is presented to extract equal powers from multiple (either symmetric or asymmetric) input dc sources of an MIC. In addition, software based simulation results are presented to validate the proposed methodology.

Keywords: Hybrid Energy System (HES), DC/DC converters, Multiple input converters (MICs), Bidirectional power, High switching frequency (HSF).

1. Introduction

As multiple input converters are gaining importance, new topologies are being proposed. Among the power electronic converters, dc-dc converters find applications in key areas such as dc drives, battery charging, electric traction, renewable power generation and so on. While many topologies of dc-dc converters are popular, multiple input converters (MICs) have been emerging as practical and efficient means especially for hybrid energy systems.

Due to wide spread uses of power electronics, a lot of converter topologies have been studied. DC-DC topologies such as Buck, boost, Buck-boost, Cuk and SEPIC provide us with the ability to step up or step down the input DC voltage to the desired voltage precisely. Topologies like Push-pull, forward and Fly-back give us the ability to convert AC to DC while providing isolation. Since power electronic circuits are controllable and relatively small compared with vacuum circuits, they have been widely adopted and further spur the development of a lot of electrical devices. Nowadays, electrical devices, such as laptops and cell phones, have become necessities in our daily life. These portable devices are small which provide us the mobility to learn and communicate.

DC/DC converters/regulators form the Backbone of different portable electronic devices like cellular phones, laptops, MP3 players which are using batteries as their power supply. Portable devices usually comprise of several sub-circuits that should be supplied with different voltage levels, which are not the same as battery's voltage level which is the main supply voltage.

Employing DC/DC converters can be offered as a method to generate multiple voltage levels from a single DC supply voltage to feed the different sub-circuits in the device. This method of generating multiple voltage levels from a single battery source can reduce the device area substantially [26]. On the other hand DC voltage provided by battery or rectifier contains high voltage ripples and it is not constant enough, thus it is not applicable for most devices. DC/DC regulators are employed to attenuate the ripples regardless of change in the load current or input voltage [1].

Figure 2 depicts the block diagram of a general DC/DC regulator which contains two main blocks; power processor and feedback control part. The feedback control part senses the output voltage and adjusts the power transfer by generating corrective control signals to keep the output voltage constant.

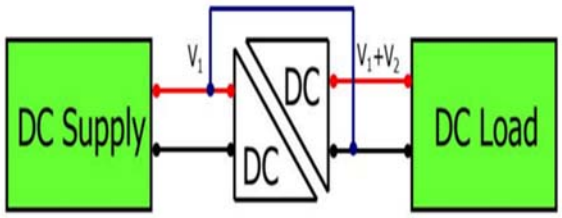

Figure 1: DC-DC Converter

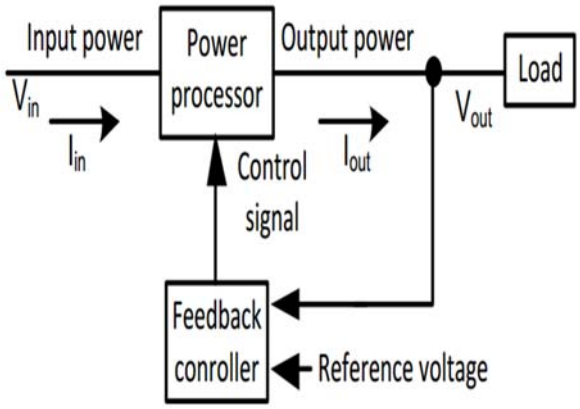

Figure 2: Block diagram of DC/DC regulator

Rest of the paper is organized as follows. The topology is described in section 2. With the help of mathematical formulations, the proposed methodology is described in section 3. In order to validate the proposed methodology, simulation studies and their results are presented in section 4. Concluding remarks are presented in section 5.

2. Description of Topology

The working principle and operation of MIC proposed in [11] is based on the basic dc-dc converter. The passive elements of the converter are charged during a particular period of time and then the stored energy of the passive element is discharged through load during the remaining period of time over a single switching cycle. In MICs, the inductor can be charged by multiple voltage sources instead of single source by adopting an appropriate switching pattern that connects or disconnects multiple sources to the inductor

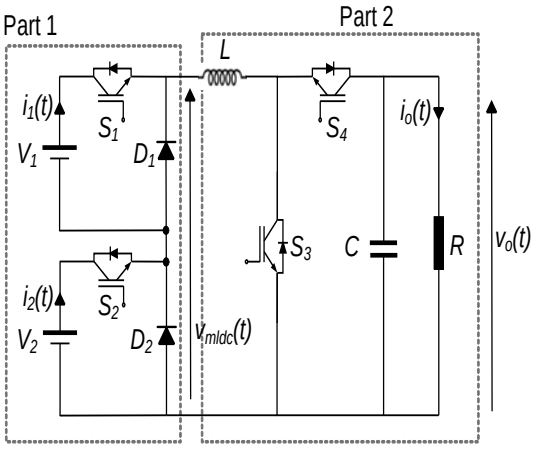

Figure 3: Circuit diagram of proposed MIC topology

individually or simultaneously. The topology as proposed in [11] is shown in Figure 1 with two input sources. It is categorised into two parts: part 1 and part 2. Part 1 is a multilevel dc-link part and it consists of voltage sources V_1 and V_2, switches S_1 and S_2, diodes D_1 and D_2. This part synthesizes a multilevel dc voltage. Part 2 consists of controlled switches S_3 and S_4 and energy storage elements L and C. Operation of this part decides one of the working modes (buck, boost and bidirectional). Complete operation of the structure is described in [11] with different strategies such as : (a) intermediate synchronisation; (b) rising edge synchronisation; and (c) falling edge synchronisation of switching signals. In Figure 1, the source currents of V_1 and V_2 are shown respectively as $i_1(t)$ and $i_2(t)$ while the dc-link voltage is shown as $v_{mldc}(t)$ and instantaneous load voltage and current are respectively shown as $v_o(t)$ and $i_o(t)$.

3. Proposed Methodology

The methodology for even power distribution proposed herewith is with reference to Fig.4.1 with two input sources but it can be extended to any number of input sources with any given asymmetric voltage ratios. It can be observed from Fig.3 that the switch S1 and diode D1 are complementary in nature, that is to say, when the switch S1 is ON, the diode D1 is OFF and vice-versa. Thus, if the ON or OFF position of switch S1 is known, then the position of the diode D1 is automatically known. Similar is the relationship between the switching positions of switch S2 and diode D2.

Thus, let a switching function μ(t) be defined for a given switch S such that,

$$\mu(t) = \begin{cases} 0\,, if\ \ power\ switch\ S\ is\ OFF \\ 1\,, if\ \ power\ switch\ S\ is\ ON \end{cases} \quad (1)$$

Thus, the multilevel dc link voltage can be expressed in terms of switching function and input sources as:

$$v_{mldc}(t) = V_1\mu_1(t) + V_2\mu_2(t) \quad (2)$$

The average multilevel dc link voltage over a switching period 'T' can be accordingly expressed as:

$$V_{mldc} = \frac{1}{T}\int_0^T \{V_1\mu_1(t) + V_2\mu_2(t)\}dt \quad (3)$$

Similarly, the source currents i1(t) and i2(t) can be expressed in terms of switching function and inductor current 'iL(t)'as :

$$i_1(t) = i_L(t)\mu_1(t) \quad (4)$$

$$i_2(t) = i_L(t)\mu_2(t) \quad (5)$$

Thus, for any two given sources (and, for that matter, all the sources), power drawn can be equalized within one switching period, if following condition can be achieved,

$$V_1 * \frac{1}{T}\int_0^T \{i_L(t)\mu_1(t)\}dt = V_2 * \frac{1}{T}\int_0^T \{i_L(t)\mu_2(t)\}dt \quad (6)$$

Equation (19) indicates that, for any given load current (and hence inductor current), with the help of appropriate control of the switching functions, average power drawn from input dc sources can be equalized within one switching cycle. This means that appropriate duty ratios d1 and d2 for S1 and S2 have to be chosen which would satisfy the relationship:

$$d_1V_1 = d_2V_2 \quad (7)$$

Under this condition, however, as per equation (15), the average multilevel dc link voltage will be regulated depending on the ratio of d1 to d2. Accordingly, to obtain a desired voltage at the load, V_{mldc} has to be treated as the input to 'part 2' of the converter topology.

4. Simulation Results

With reference to figure 1, let the magnitudes of voltage sources be binary with values V_1 = 24V and V_2 = 12V. Accordingly, as per equation (7), d_2 should be taken twice of d_1. Hence d_1 is taken to be 0.1 while d_2 is taken as 0.2, with a switching frequency of 10 kHz. Thus, as per equation (3), the average value of multilevel dc link would be $V_1d_1 + V_2d_2$ i.e. 4.8V. Now, let us say that the average output voltage desired at load is 18 V, then it means that the multilevel dc link voltage is needed to be boosted and hence the switch S_3 has to be operated with a duty ratio d_3 , obtained by using the standard expression for boost conversion,

$$V_o = \frac{V_{mldc}}{(1-d_3)} \quad (8)$$

Hence, under the conditions described, d_3 should be chosen to be 0.73.

In order to verify the concepts proposed herewith, a simulation study is performed using MATLAB/Simulink software along with SimPowerSystem toolbox. The parameters are summarized in Table 1.

Table 1: Parameters of MIC for simulation study

Parameter	Unit	Value
Source V_1	[V]	24
Source V_2	[V]	12
Inductance L	[mH]	14.4
Capacitance C	[μF]	216
Frequency f	[kHz]	10
Resistance R	[Ω]	10
Duty ratio d_1	[%]	10
Duty ratio d_2	[%]	20
Duty ratio d_3	[%]	73
Output voltage V_o	[V]	18

Table 2: Power readings

Load	Source V_1	Source V_2
30 W	17W	17 W

The instantaneous output voltage obtained from the simulation model is shown in figure 2. The ripples are seen to be within the range of 5-10% while the average output voltage is 17.25 V. The inductor voltage and currents are shown respectively in figures 3 and 4. In addition, the source currents from sources V_1 and V_2 are shown in figures 5 and 6. The load power and powers drawn from sources V_1 and V_2 are shown in Table 2 and it can be seen that both the sources

impart equal power to the load, while the primary goal of voltage regulation is simultaneously achieved. Hence, it can be safely said that the proposed scheme works satisfactorily.

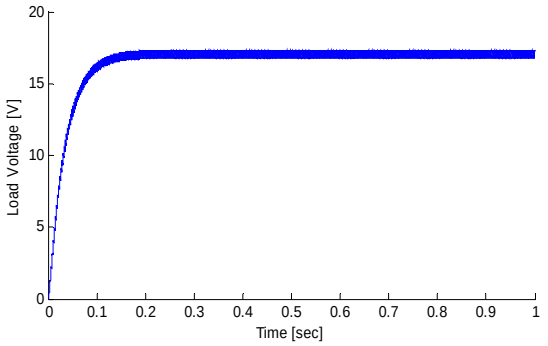

Figure 4: Simulated waveform for the load voltage

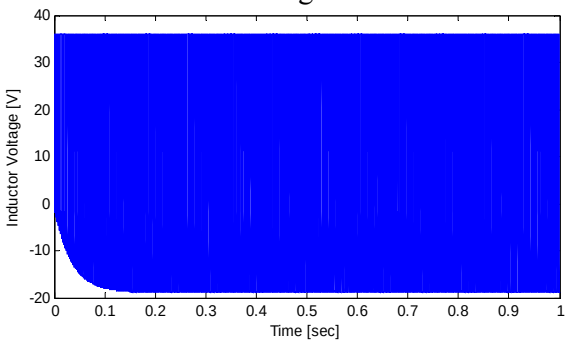

Figure 5: Simulated waveform for the inductor voltage

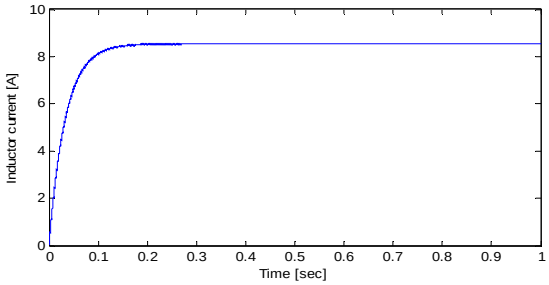

Figure 6: Simulated waveform for the current drawn from source V_1

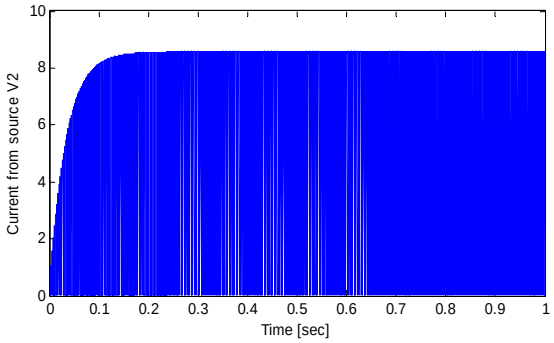

Figure 7: Simulated waveform for the current drawn from source V_2

5. Conclusion

In this research work, a methodology to extract equal average powers from multiple input dc sources in a dc-dc converter topology is presented. The sources voltages may be equal or unequal and accordingly the currents are drawn from the given sources such that the average powers drawn are equated and hence their lifetimes are enhanced. Because of the presence of multiple switching states, both the objectives are obtained: regulation of average output voltage and even power sharing among the input dc sources.

References

[1] P. Gueguen, "How power electronics will reshape to meet the 21st century challenges?," In Power Semiconductor Devices & IC's (ISPSD), 2015 IEEE 27th International Symposium on , vol., no., pp.17-20, 10-14 May 2015.

[2] F. Blaabjerg ; A. Consoli ; J.A. Ferreira ; J.D. van Wyk, "The future of electronic power Processing and conversion," In Power Electronics, IEEE Transactions on , vol.20, no.3, pp.715-720, May 2005.

[3] J. Cao; A. Emadi, "A New Battery/Ultra Capacitor Hybrid Energy Storage System for Electric, Hybrid, and Plug-In Hybrid Electric Vehicles," In Power Electronics, IEEE Transactions on, vol.27, no.1, pp.122-132, Jan. 2012.

[4] F. Valenciaga; P.F. Puleston, "Supervisor control for a stand-alone hybrid generation system using wind and photovoltaic energy," In Energy Conversion, IEEE Transactions on , vol.20, no.2, pp.398-405, June 2005.

[5] S. Kumar; H.P. Ikkurti, "Design and control of novel power electronics interface for battery-ultracapacitor Hybrid Energy Storage System," In Sustainable Energy and Intelligent Systems (SEISCON 2011), International Conference on, vol., no., pp.236-241, 20-22 July 2011.

[6] S.H. Choung; A. Kwasinski, "Multiple-input DC-DC converter topologies comparison," In Industrial Electronics, 2008. IECON 2008. 34th Annual Conference of IEEE, vol., no., pp.2359-2364, 10-13 Nov. 2008.

[7] Wu Hongfei; Xu Peng; Hu Haibing; Zihu Zhou; Yan Xing, "Multiport Converters Based on Integration of Full-Bridge and Bidirectional DC–DC Topologies for Renewable Generation Systems," In Industrial Electronics, IEEE Transactions on , vol.61, no.2, pp.856-869, Feb. 2014.

[8] H. Tao; A. Kotsopoulos; J.L. Duarte; M.A.M. Hendrix, "Family of multiport bidirectional DC-DC converters," In Electric Power Applications, IEEE Proceedings - , vol.153, no.3, pp.451-458, 1 May 2006.

[9] J.T. Hawke; H.S. Krishnamoorthy; P.N. Enjeti, "A multiport power sharing converter topology for renewable-to-grid interface," In Energy Conversion Congress and Exposition (ECCE), 2014 IEEE , vol., no., pp.4992-4999, 14-18 Sept. 2014.

[10] O. Hegazy; M. El Baghdadi; J. Van Mierlo; P. Lataire; T. Coosemans, "Analysis and modeling of a bidirectional multiport DC/DC power converter for battery electric vehicle applications," In Power Electronics and Applications (EPE'14-ECCE Europe), 2014 16th European Conference on , vol., no., pp.1-12, 26-28 Aug. 2014.

[11] L. Kumar; S. Jain, "Multiple-input DC/DC converter topology for hybrid energy system," In Power Electronics, IET, vol.6, no.8, pp.1483-1501, September 2013.

[12] K.K. Gupta; S. Jain, "A Novel Multilevel Inverter Based on Switched DC Sources," In Industrial Electronics, IEEE Transactions on , vol.61, no.7, pp.3269-3278, July 2014.

[13] K.K. Gupta; S. Jain, "Topology for multilevel inverters to attain maximum number of levels from given DC sources," In Power Electronics, IET, vol.5, no.4, pp.435-446, April 2012.

[14] M. Angulo; P. Lezana; S. Kouro; J. Rodriguez; B. Wu, "Level-shifted PWM for cascaded multilevel inverters with even power distribution," In Proceedings of the IEEE Power Electronic. Spec. Conf., pp.2373 -2378.

[15] Shailesh Kumar; Anjanee Kumar; ” A Methodology for Even Power Sharing among Input Sources in a Multiple-Input DC-DC Converter Topology” In International Journal of Science and Research (IJSR) ISSN (Online): pp 1466-1469,Volume5, Issue1, January 2016.

FEATURE LEVEL IMAGE FUSION TECHNIQUE FOR BIOMETRIC PERSON IDENTIFICATION

Namdeo D. Kapale[1] , , Dr. Mrs. M. A. Joshi[2] , Dr M.S.Sutaone[3]
[1]Electronics & Telecommunication Department
SRES's College of Engineering Kopargaon, Maharashtra, India
[2,3]Electronics & Telecommunication Department,
College of Engineering PUNE, Maharashtra, India
Email:[1]ndkapale@gmail.com

Abstract - This paper proposed an innovative contact-less palm print and palm vein recognition system. Palm print is referred to as line textures, which contains principal lines, wrinkles and ridges on the inner surface of the palm. On the other hand palm vein is line texture below the inner surface of palm. These line patterns are unique and stable, and they offer bundle of useful information for personal recognition. The palm prints and palm vein features are extracted using Directional Coding technique. The proposed approach is rigorously evaluated on the CASIA database (100 subjects) and achieves the best FAR 0.2% & FRR 1%.

Finally, we propose a score level combination strategy to combine the multiple palm vein representations. We achieve consistent improvement in the performance, from the recognition experiments, which illustrates the robustness of the proposed schemes.

Keywords: contactless biometrics, palm print recognition, palm vein recognition, region of interest (ROI).

I. INTRODUCTION

Recently, biometrics has emerged as a reliable technology to provide greater level of security to personal authentication system. Among the various biometric characteristics that can be used to recognize a person, the human hand is the oldest, and perhaps the most successful form of biometric technology [1]. The features that can be extracted from the hand include hand geometry, fingerprint, palm print, knuckle print, and vein. These hand properties are stable and reliable. Once a person has reached adulthood, the hand structure and configuration remain relatively stable throughout the person's life [2]. Apart from that, the hand-scan technology is generally perceived as nonintrusive as compared to iris- or retinascan systems [3]. The users do not need to be cognizant of the way in which they interact with the system. These advantages have greatly facilitated the deployment of hand features in biometric applications.

At present, most of the hand acquisition devices are based on touch-based design. The users are required to touch the device or hold on to some peripheral or guidance peg for their hand images to be captured. There are a number of problems associated with this touch-based design. Firstly, people are concerned about the hygiene issue in which they have to place their hands on the same sensor where countless others have also placed theirs. This problem is particularly exacerbated during the outbreak of epidemics or pandemics like SARS and Influenza A (H1N1) which can be spread by touching germs leftover on surfaces. Secondly, latent hand prints which remain on the sensor's surface could be copied for illegitimate use. Researchers have demonstrated systematic methods to use latent fingerprints to create casts and moulds of the spoof fingers [4]. Thirdly, the

device surface will be contaminated easily if not used right, especially in harsh, dirty, and outdoor environments. Lastly, some nations may resist placing their hands after a user of the opposite sex has touched the sensor.

II. Region of Interest(ROI) Extraction

Segmentation of the palm, i.e. the separation of the palm from the background. Since the background is uniformly black, the segmentation can be done using simple thresholding.

Figure1.ImageBinarization (a) Palmvein Image from Casia Multispectral Database (b)Binary image

The Region of Interest in the palm is taken as the central part of the palm because this part contains the most features. For the extraction of the ROI, the tips of the fingers and the valley points between the roots of the fingers are found .Line between little finger valley & middle finger valley is drawn. Line parallel to this line below 25 pixel drawn. Four corner point of square found & square is drawn . This square area is cropped fro original palm image. This procedure is shown in figure 2.

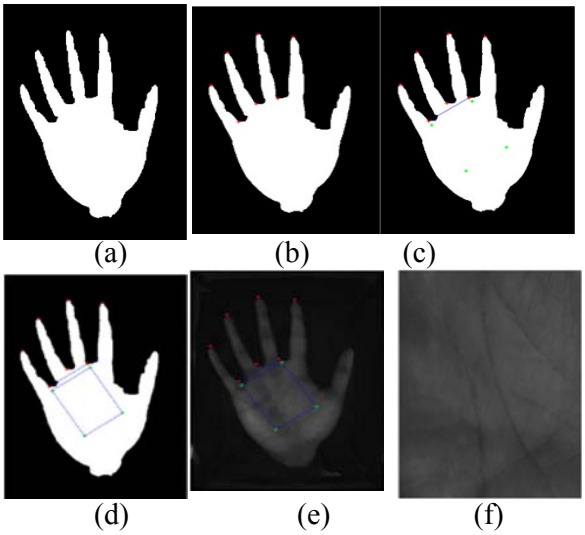

Figure 2. ROI Extraction steps.(a)Binary image(b)Finding tips & valley points. (c) Line from 1st & 3rd Valley point.(d) Rectangle(128x128) (e) Overlapping of rectangle on original palm.(f)Extracted ROI

III. Image Enhancement:

Cropped image is enhanced by using first applying medfilt2 Median filtering is a nonlinear operation often used in image processing to reduce "salt and pepper" noise. A median filter is more effective than convolution when the goal is to simultaneously reduce noise and preserve edges. Then low pass filtering (wiener) an intensity image that has been degraded by constant power additive noise. It uses a pixel-wise adaptive Wiener method based on statistics estimated from a local neighbourhood of each pixel. Contrast enhancement is performed using adaptive histogram equalization. It enhances the contrast of images by transforming the values in the intensity image. It operates on small data regions (tiles), rather than the entire image. Each tile's contrast is enhanced, so that the histogram of the output region approximately matches the specified histogram. The neighbouring tiles are then combined using bilinear interpolation in order to eliminate artificially induced boundaries. The contrast, especially in homogeneous areas, can be limited in order to avoid amplifying the noise which might be present in the image.

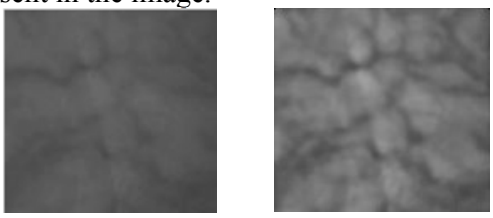

Figure 3. (a)Palm vein image (b) Enhanced image

IV.FEATURE EXTRACTION

We propose a new scheme named Directional Coding method to extract the palm print and palm vein features.These hand features contain similar textures which are primarily made up of line primitives. For example, palm prints are made up of strong principal lines and some thin wrinkles, whilst palm vein contains vascular network which also resembles line-like characteristic. Therefore, we can deploy a single method to extract the discriminative line information from the different hand features. The proposed Directional Coding technique aims to encode the line pattern based on the proximal

orientation of the lines. We first apply Wavelet Transform to decompose the palm print images into lower resolution representation. The Sobel operator is then used to detect the palm print edges in horizontal, vertical, +45o, and -45o orientations. After that, the output sample, Φ(x, y) , is determined using the formula,

$$\Phi(x, y)=\delta(\arg\max_{f}(\omega_R(x, y)))$$

where Rw(x , y) denotes the responses of the Sobel mask in the four directions (horizontal, vertical, +45o, and -45o), and δ ε{1,2,3,4} indicates the index used to code the orientation of Rw(x , y). The index, δ, can be in any form, but we use decimal representation to characterize the four orientations for the sake of simplicity. The output, Φ(x, y), is then converted to the corresponding binary reflected Gray code. The bit string assignment enables more effective matching process as the computation only deals with plain binary bit string rather than real or floating point numbers. Besides, another benefit of converting bit string to Gray code representation is that Gray code exhibits less bit transition. This is a desired property since we require the biometric feature to have high similarity within the data (for the same subject). Thus, Gray code representation provides less bit difference and more similarity in the data pattern.Figure 4. a to 4.d shows the gradient responses of the palm print in the four directions.Figure 5. a to 4.d shows the gradient responses of the palm vein in the four directions.

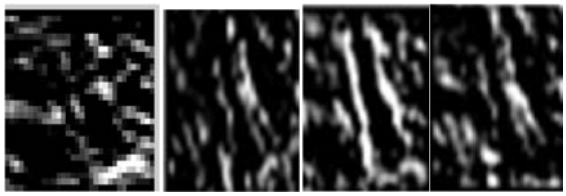

Figure 4. Example of Directional Code applied on palm print image.

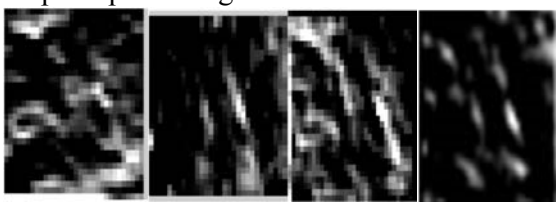

Figure 5. Example of Directional Code applied on palm vein image.

V. Biometric Performance Measurements Criterion: The proposed system can be seen as a two class problems: whether a person should be claimed as a true client or an imposter. In order to evaluate the success of the system, a standard measurement is used to verify the acceptance errors and rejection errors. They are defined as follows: False Reject Rate (FRR) – The percentage of clients or authorized person that the biometric system fails to accept. It will increase proportionally to the security threshold. When the security threshold increases, more users (including the authorized person) will be rejected due to the high security level. FRR is defined as

$$FRR=\frac{\text{Number of rejected clients}}{\text{Total number of client access}}\times 100\%$$

False Acceptance Rate (FAR) – The percentage of imposters or unauthorized person that the biometric system fails to reject. It rises when the security threshold (matching confidence) is lowered. More formally, FAR is defined as

$$FAR=\frac{\text{Number of accepted imposter}}{\text{Total number of imposter accesses}}\times 100\%$$

Equal Error Rate (EER) – is an optimal rate where FAR is equal to FRR. Graphically, EER is recognized as the crossing point between FAR and FRR. It is commonly used to determine the overall accuracy of the system and serve as comparative measure against the other biometric systems. These three performance measures, namely FAR and FRR will be used to testify the proposed algorithms in the subsequent sections.

VI. Identification: After extracting feature vector all feature vectors are stored in database. Test palm sample is processed same as previous. The comparison is done with data base and the decision is made about the person identity. Nearest neighbour search algorithm is used for this. Test feature vector of each individual is compared with all database feature vector & minimum Euclidian distance is found. Based on minimum distance criteria identification result is displayed as test sample is matches with database sample.

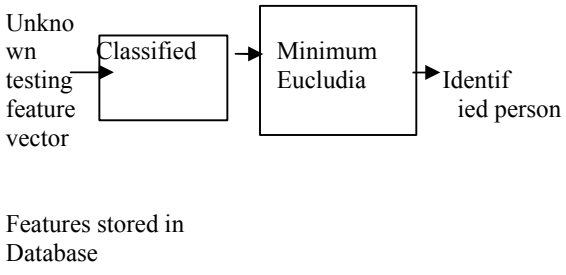

Figure 6. Classifier structure

The matching of unknown person is performed by measuring the dissimilarity between the features of unknown person to the features of database person, The best matching person is vector that minimizes the dissimilarity measure.

$$C._{best} = \arg \min_{1 \le i \le N} \{D E (X , C_i)\}$$

Euclidean Distance metric, D_E between the test features and the database features is found as given below:

$$D_E = \sqrt{\sum_{i=1}^{n} Ts_i^2 - Tr_i^2)}$$

where,
Ts = Testing feature vector
Tr = Database feature vector
n = total number of features

VII. Result

- Training Database-100 Peoples 5 samples of each
- Testing Database-100 Peoples

Figure 7 shows FAR & FRR plotted against different threshold for palmprint alone, figure 8 shows FAR & FRR plotted against different threshold for palm vein alone and Figure 9 shows FAR & FRR plotted against different threshold for fused palmprint & palm vein feature . This figures gives optimum value of threshold to be select for finding values of FAR & FRR.

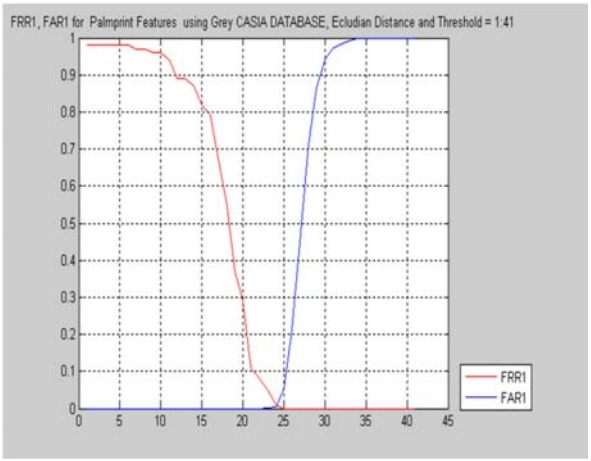

Figure 7. FAR & FRR of Palmprint for different threshold

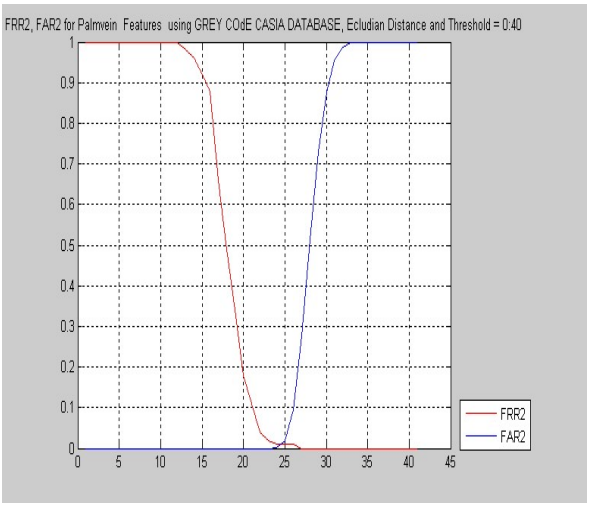

Figure 8. FAR & FRR of Palmvein for different threshold

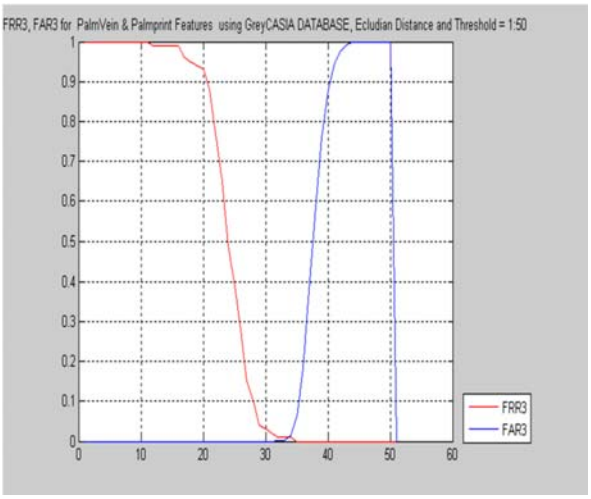

Figure 9. FAR & FRR of Palmprint & Palmvein for different threshold

Palmvein		Palmprint		Decision level Fusion		Feature level Fusion	
FRR	FAR	FRR	FAR	FRR	FAR	FRR	FAR
1%	1.89%	1%	0.56%	1%	0.7%	1%	0.2%

Table 1. Result of palmprint, Palmvein ,Decision & feature level fusion

VIII. Conclusions

Result shown are clearly indicates that performance parameters of individual biometric are improved using fusion techniques. Moreover FAR & FRR of feature level fusion are better than decision level fusion. Proposed feature extraction method i.e. ordinal code gives lower FAR& FRR.

IX. Future work:

It is proposed to design own data acquisition system & create own data base. The system will be make real time by using proposed algorithm.

References

[1] Goh Kah Ong Michael, Tee Connie & Andrew Teoh Beng Jin "Design and Implementation of a contactless Palm Print and Palm Vein Sensor"978-1-4244-7815- 6/10/$26.00 ©2010 IEEE

[2] E. Yörük, H. Dutağaci, & B. Sankur, "Hand biometrics," Image and Vision Computing , vol. 24, no. 5, pp. 483-497, 2006.

[3] D. Huang, W. Jia, & D. Zhang, "Palmprint verification based on principal lines," Pattern Recognition , vol. 41, no. 4, pp.1316–1328, 2008.

[4] X., Wu, K., Wang, & D. Zhang, "A novel approach of palm- line extraction," Proceeding of the Third International Conference on Image and Graphics, pp. 230–233, 2004.

[5] W. Li, D. Zhang, and Z. Xu, "Palmprint Identification by Fourier Transform" *IJPRAI*, 16(4), pp.417-432, 2002

[6] C.C Han, H. L. Chen, C. L. Lin and K. C. Fan, "Personal authentication using palm-line features", *Pattern Recognition*, 36(2), pp. 371-381, 2003.

[7]. Z. Sun, T. Tan, Y. Wang a "Ordinal palmprint Representation For Personal Identification", CVPR, Pp.279- 284, 2005.

[8] Jian-Gang Wang, Wei-Yun Yau And Andy Suwandy "Feature-Level Fusion Of Palmprint And Palm Vein For Person Identification Based On A "Junction Point" Representation" Icip 2008- 978-1-4244-1764-3/08-2008 IEEE

[9] Gayatri U. Bokade , Deepali Sale . Madhuri A. Joshi . A.M. Sapkal "An Efficient And Secure Palmprint Based Authentication A Dct Based Approach" I-Cost Electronics & Communication Conference Proceedings 13-15-Jan 2011

[10] Ying Hao, Zhenan Sun, Tieniu Tan And Chao Ren "Multispectral Palm Image Fusion For Accurate Contact-Free Palmprint Recognition" Icip 2008- 978-1-4244-1764-3/08=2008 IEEE

[11] Yingbo Zhou And Ajay Kumar "Human Identification Using Palm-Vein Images" IEEE Transactions On Information Forensics And Security, Vol. 6, No. 4, December 2011

SMART SAILING ROBOT FOR OCEANOGRAPHIC RESEARCH

[1]Sonali R. Deshpande, [2]Anuradha L. Borkar
Department of E&TC, M.S.S.C.O.E.T., Jalna

Abstract

Over the past decade there has been intense scientific work on autonomous sailing robots. As hardware gets smaller, cheaper and also better performing the possibilities increase for autonomous vessels. Recently there is a lot of research going on with the aim of reducing CO2 emissions. Smart sailing robot fit perfectly into these ambitions.

A robotic sailboat is able to autonomously navigate towards any given target without human control or intervention. The optimal route is calculated dependent on strategic goals and weather parameters. Rudder and sails are autonomously controlled in order to keep course and to execute maneuvers like tack and jibe. As sailboats operate in a highly dynamic, environment an autonomous sailboat has to respond quickly to ever-changing environmental conditions. Incoming data from sensors (GPS, compass, etc.) have to be analyzed permanently by intelligent control mechanisms.

The best routing decision, perfect handling of ever changing wind conditions and perfect timing during tack and jibe are some of the skills an autonomous sailing vessel has to master.

Keywords: Aurdino, Zigbee, Bluetooth module, GPS, Ultrasonic sensor, IR Sensor, Accelerometer, Waterproof dc servomotors, Battery.

I. Introduction

In this paper we will discuss the main developments of the past years in the field of sailing robot. In this paper the main applications for the use of sailing robot will be introduced with Hardware aspects. The most common boats, sails, microcontrollers and sensors that are used for sailing robot will be discussed. Also contains an overview about important software architectures for autonomous sailboats. Since the sailing robot needs a reliable connection for monitoring, debugging and remote control in case of emergency, the sailing robot needs a data link to the shore. To detect and avoid obstacles different mechanisms are used. Regarding to that, the collision avoidance chapter will discuss two approaches. The simulation and testing part of the paper will present common simulation methods and testing approaches. The conclusion will summarize the main aspects of this paper.

This is an embedded hardware/software implementation for the computing system of a small scale unmanned autonomous sailing boat. The system is integrated with aurdino, Zigbee tx and rx, Bluetooth module, GPS, Ultrasonic sensor, Accelerometer, Waterproof DC servomotors,12 V battery supply build in a metallic prototype of boat.

Hardware challenges

Equipping a robotic sailing boat with microcontroller, sensors, actuators and other special hardware needed is very difficult. Waterproofness is a major issue in this context. Sensors have to provide reliable data in an unstable environment. All components have to be small and lightweight enough to be carried by the boat.

Routing algorithms

Routing of autonomous sailing boats is a challenging task since for a sailing boat not every course is directly sailable. There is also a huge difference in the maximum speed a sailboat can reach on a given course. It is also difficult to plan routes because sailboats are operating in an unstable and ever changing environment.

Energy self sufficiency

Autonomous sailing boats used in long term missions on the ocean have to carry all needed energy with them and/or gather energy from the environment.

Collision avoidance

To eliminate the need to monitor robotic sailing boats all the time, they have to be able to avoid collisions with ships and other obstacles in the water.

SAILING MECHANISM

The sailing robot model is made of thin Alluminium Sheet Two brush-less DC motors are fixed to the boat model. Pedals made of MS (Mild Steel) are fixed to the shafts of the DC motors. To move the boat forward, both the motors are operated in clockwise direction by the microcontroller. To move the boat reverse, both the motors are operated in counterclockwise direction by the microcontroller. To turn left / right, one motor is rotated in clockwise and the other is rotated in counter-clockwise directions. The other key factor which must be considered in designing such a vessel is that of the sail type. Traditional fabric sails are typically controlled through a series of ropes known as sheets and halliards, these frequently break or jam (Particularly when swollen by salt water) and require regular attention from the crew. Performing such tasks autonomously would incur significant overheads resulting in excessive power usage, weight and financial cost. A potential alternative is that of a rigid wing shaped sail attached directly to the mast. The sail is manipulated through the rotation of the entire mast via an electric motor. This design eliminates common points of failure found in traditional Sailing and is therefore ideal for use in an autonomous sailing vessel.

II. **Hardware Architecture**

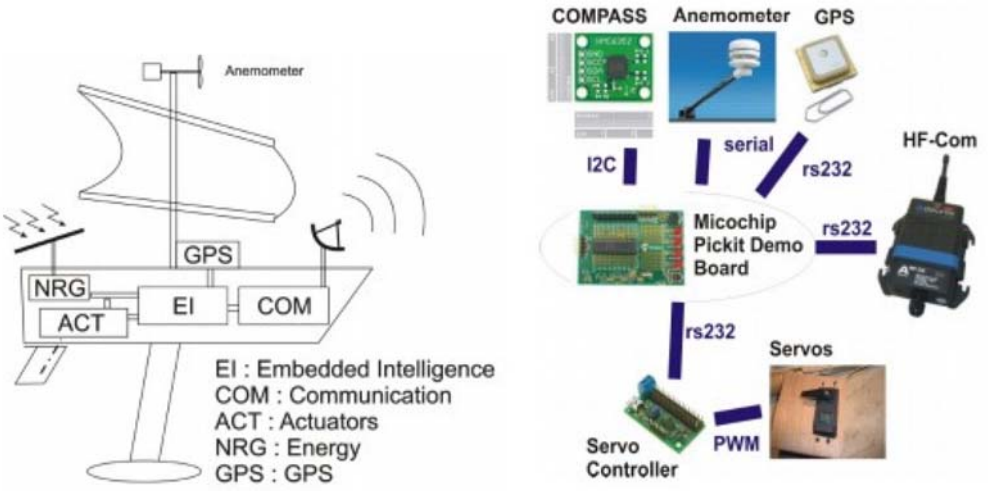

Fig. 1 Hardware Architecture

SAILING ROBOT HARDWARE TOOLS

DC Motors

DC motors are configured in many types and sizes, including brush less, servo, and gear motor types. A motor consists of a rotor and a permanent magnetic field stator. The magnetic field is maintained using either permanent magnets or electromagnetic windings. DC motors are most commonly used in variable speed and torque. Motion and controls cover a wide range of components that in some way are used to generate and/or control motion.

GPS

GPS has been used for navigating purpose. GPS is mainly used to track the location of robot in ocean and help to navigate in right direction.

Features: Environmental surveillance.

III. SYSTEM BLOCK DIAGRAM:

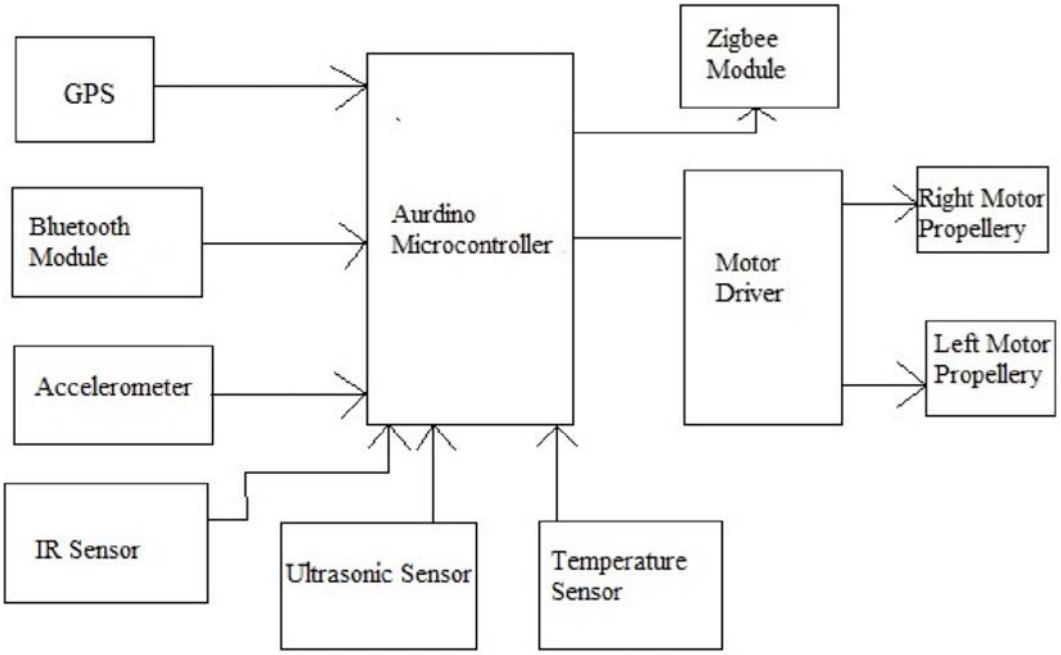

Fig. 2 Block Diagram

This we have the modules of Zigbee, GSM and Sensors which are interfaced with the microcontroller. The sensors used have different activity as per use. Aurdino Microcontroller is the brain of mechanical robot which receives the commands from PC through ZigBee wireless connection and processes these commands to perform pattern motion control. The main part in the robot main board is Aurdino microcontroller which generates two PWM signals for each wheel of DC motor. The two active wheels of the robot are actuated by two independent servo motors modified for continuous rotation. In particular, the robot is powered by 12 V battery. The hardware tools of the robotic system are: ZigBee, Aurdino Microcontroller, DC Motors, Bluetooth Module, Accelerometer, GPS, Ultrasonic Sensor, IR sensor. The hardware components of the robotic system are as shown as above in block diagram.

IV. Related Works

Stelzer et al. also presented a research project where an autonomous sailing boat shall be used for marine mammal research [4]. They use the sailboat for passive acoustic monitoring of marine mammals while reducing the human impact on them. They state that the advantage of using a robot sailing boat is that the area of interest can be sampled with a very high spacial and temporal resolution for comparatively low cost. They also equipped their boat with additional sensors measuring chlorophyll and zooplankton. An acoustic streamer, three hydrophones, a depth sensor and a compass module are towed behind the sailing vessel.

Cruz and Alves also published a paper on the possible applications of autonomous sailboats for ocean sampling and surveillance [10]. For ocean observation they name upper ocean dynamics, chlorophyll concentration, ocean acoustics, calibration of basin-wide ocean models and tracking of pollution plumes as fields of interest for scientists where robotic sailboats can collect required data for low costs. In the field of surveillance the authors state that autonomous sailing boats can be used for the detection and prevention of illegal trading, surveillance of immigration routes and assistance in the detection and disarming of minefields in the ocean.

V. Applications and Advantages of sailing Robot

There are several possible fields of application for autonomous sailing boats.

- Intelligend Sensor Buoys:

Autonomous sailing boats can easily be equipped with several sensors measuring all kinds of data. As they are energy self sufficient their operation time is not limited. Therefore, it is very cost efficient to use them for surveys, mappings and ecological studies of oceans and lakes. Ocean sampling and marine mammal research are two applications where already projects exists to facilitate robotic sailboats.

- CO2-neutral in Transportation of Goods:

Conventional sailboats are unprofitable for the transportation of goods nowadays because they need a very big crew to be operated. Autonomous sailing boats do not suffer from that disadvantage and can therefore be used for the CO2-neutral transportation of goods.

- Reconnaissance and Surveillance:

Sailing robots can also be sent to operate in dangerous regions. For example, they could be used to measure the nuclear radiation in the ocean near Fukushima. Another application would be the surveillance of the borders in the Mediterranean sea.

- Supply Vessel:

Remote islands and regions that are sparsely populated could be supplied using robot sailing boats. For example, they could be used to supply scientists that work on small islands in the arctic ocean.

- Obstacle detection:

Their algorithm uses a map of the coastline that could also be extended to work with other sensed obstacles. The sailboat determines its position on the map using a positioning system (e.g. GPS) and then casts rays from the robots position in every direction (every angle from 0-359 degrees) and senses the distance to the nearest obstacle in that direction.

Once an obstacle is detected a new course is decided that avoids the obstacle. Collision avoidance is a challenging task for autonomous sailboats as they operate in an ever changing, unstable environment. Sailboats can change their route.

- Communication:

A permanent data link between boat and shore is necessary for monitoring, debugging, to control manually in case of emergency, for real-time monitoring. Real-time measurement data are needed for long-term observation tasks. Three communication partners are involved in the communication process.

1) Sailboat: The sailboat transmits sensor values to the visualization.

2)Visualization software: This computer program runs on a computer on the shore and represents the transmitted data. Furthermore, new target coordination, obstacle information or a new desired course can be sent from the visualization to the sailboat.

3) Remote controller: This entity can be used in case of emergency to overrule the autonomous on-board control of the sailboat. It is especially needed during test runs. Desired actuator values like position of the rudder and sails are transmitted in real time to the sailboat.

VI. Conclusion and Future work

The Smart sailing robot for oceanographic research is used to explore all the details on the surface of the water. This robot is used for locating the position of the system using GPS, detects metals present in the ocean and used for surveillance and rescue operation.

In this paper, we introduce a successful working prototype model of manoeuvre sailing mobile robot is designed for oceanographic research. An autonomous sailing robot offers major advantages compared to submerged operated vehicles. It tracks the movement with the help of wireless cam attached to the robot through RF PRO wireless sensor network. The surface environment of ocean i.e., ocean exploration and navigational research can be studied through wireless cam, GPS, Metal detector , IR sensors, Ultrasonic sensors interfaced to the robot. Further development is required to demonstrate the feasibility of a sailing robot for long term use in open sea and helpful for oceanographers and scientists.

REFERENCES

[1] M.P. Khorgade “Application of MEMS in Robotics and Bio MEMS”, Proceedings of the UK sim 13th international conference.

[2] World robot sailing championship, 2011. http://www.wrsc2011.org/.

[3] Mobile Robotic " Navigation and control for large-scale wireless sensor network repair", by Kyle lathy in north Carolina state university on may6, 2009

[4] H. Klinck, Roland Stelzer, K. Jafarmadar, and D.K. Mellinger. Aas endurance: An autonomous acoustic sailboat for marine mammal research. In Proceedings of International Robotic Sailing Conference, pages 43{48, Matosinhos, Portugal, July.2010. Queen's University.

[5] Razavi," RF Transmitter Architectures and circuits", IEEE CICC, pp.197-204, 1999

[6] M.P. Khorgade "Application of MEMS in Robotics and Bio MEMS", Proceedings of the UK sim 13th international conference.

[7] Mobile Robotic " Navigation and control for large-scale wireless sensor network repair", by Kyle lathy in north Carolina state university on may6, 2009

[8] L Giger, S Wismer, S Boehl, G Buesser, H Erckens, J Weber, P Moser, P Schwizer, C Pradalier, and R Siegwart. Design and construction of the autonomous sailing vessel avalon. In Proc. of The World Robotic Sailing Championship and International Robotic Sailing Conference, 2009.

[9] Henly, J. (2006). An Artificial Neuroendocrine Kinematics Model for Legged Robot Obstacle Negotiation. PhD thesis, University of Wales, Aberystwyth

[10] Nuno A. Cruz and Jose C. Alves. Ocean sampling and surveillance using autonomous sailboats. In Proceedings of International Robotic Sailing Conference, pages 30{36, Rua Dr. Roberto Frias, 4200-465, Porto - Portugal, May 2008. Department of Electrical and Computer Engineering Faculty of Engineering of the University of Porto.

ELECTRIC LINEMAN PROTECTION USING USER CHANGEABLE PASSWORD BASED CIRCUIT BREAKER

[1]J.Veena, [2]G.Srivani, [3]Afreen, [4]M.Sunil Kumar, [5]J.Santhosh, [6]K.B.V.S.R.Subrahmanyam
[1,2,3,4,5]BE Students, [6]Associate Professor, SR Engineering College, EEE Department
E-mail:[1]veenajuthi.78@gmail.com,[2]libra_22@rediffmail.com.

Abstract

A circuit breaker is an automatically operated electrical switch designed to protect an electrical circuit from damage caused by overload or short circuit. Its basic function is to detect a fault condition and interrupt current flow. Unlike a fuse, which operates once and then must be replaced, a circuit breaker can be reset (either manually or automatically) to resume normal operation. When operated manually we see fatal electrical accidents to the line man are increasing during the electric line repair due to the lack of communication and co-ordination between the maintenance staff and the electric substation staff.

In order to avoid such accidents, the breaker can be so designed such that only authorized person can operate it with a password. Here, there is also a provision of changing the password. The system is fully controlled by the 8 bit microcontroller of 8051 family. The password is stored in an EEPROM, interfaced to the microcontroller and the password can be changed any time unlike a fixed one burnt permanently on to the microcontroller. A keypad is used to enter the password and a relay to open or close circuit breaker, which is indicated by a lamp. Any wrong attempt to open the breker (by entering the wrong password) an alert will be actuated, indicated by another lamp.

Index terms: Resistors, Capacitors, Diodes, Transistors, Voltage regulator, Rectifier, Microcontroller, EEPROM, Relay, Relay Driver

I.INTRODUCTION

Nowadays, electrical accidents to the line man are increasing, while repairing the electrical lines due to the lack of communication between the electrical substation and maintenance staff. This project gives a solution to this problem to ensure line man safety. In this proposed system the control (ON/OFF) of the electrical lines lies with line man. This project is arranged in such a way that maintenance staff or line man has to enter the password to ON/OFF the electrical line. Now if there is any fault in electrical line then line man will switch off the power supply to the line by entering password and comfortably repair the electrical line, and after coming to the substation line man switch on the supply to the particular line by entering the password.

II.DESCRIPTION

RESISTORS: A resistor is a two-terminal electronic component designed to oppose an electric current by producing a voltage drop between its terminals in proportion to the current, that is, in accordance with Ohm's law: V = IR

Resistors are used as part of electrical networks and electronic circuits. They are extremely common place in most electronic equipment. Practical resistors can be made of various compounds and films, as well as resistance wire.

CAPACITOR: A capacitor or condenser is a passive electronic component consisting of a pair of conductors separated by a dielectric. When a voltage potential difference exists between the conductors, an electric field is present in the dielectric. This field stores energy and produces a mechanical force between the plates. The effect is greatest between wide, flat, parallel, narrowly separated conductors.

DIODES: Diodes are used to convert AC into DC these are used as half wave rectifier or full wave rectifier. When used in its most common application, for conversion of an alternating current (AC) input into a direct current (DC) output, it is known as a bridge rectifier. A bridge rectifier provides full-wave rectification from a two-wire AC input, resulting in lower cost and weight as compared to a rectifier with a 3-wire input from a transformer with a center-tapped secondary winding

TRANSISTORS: A transistor is a semiconductor device used to amplify and switch electronic signals and electric power. It is composed of semiconductor material with at least three terminals for connection to an external circuit. A voltage or current applied to one pair of the transistor's terminals changes the current through another pair of terminals. Because the controlled (output) power can be higher than the controlling (input) power, a transistor can amplify a signal. Today, some transistors are packaged individually, but many more are found embedded in integrated circuits. The transistor is the fundamental building block of modern electronic devices, and is ubiquitous in modern electronic systems.

VOLTAGE REGULATOR: 7805 is a voltage regulator integrated circuit. It is a member of 78xx series of fixed linear voltage regulator ICs. The voltage source in a circuit may have fluctuations and would not give the fixed voltage output. The voltage regulator IC maintains the output voltage at a constant value. The xx in 78xx indicates the fixed output voltage it is designed to provide. 7805 provides +5V regulated power supply. Capacitors of suitable values can be connected at input and output pins depending upon the respective voltage levels.

RECTIFIER: A rectifier is an electrical device that converts alternating current (AC), which periodically reverses direction, to direct current (DC), current that flows in only one direction, a process known as rectification.

MICROCONTROLLER: A microcontroller (sometimes abbreviated µC, uC or MUC) is a small computer on a single integrated circuit containing a processor core, memory, and programmable input/output peripherals. Program memory in the form of Ferroelectric RAM, NOR flash or OTP ROM is also often included on chip, as well as a typically small amount of RAM. Microcontrollers are designed for embedded applications, in contrast to the microprocessors used in personal computers or other general purpose applications

EEPROM: EEPROM (also written E^2PROM and pronounced “e-e-prom”, “double-e prom”, “e-squared”, or simply “e-prom”) stands for Electrically Erasable Programable Read Only Memory and is a type of non-volatile memory used in computers and other electronic devices to store small amounts of data that must be saved when power is removed, e.g., calibration tables or device configuration.
When larger amounts of static data are to be stored (such as in USB flash drives) a specific type of EEPROM such as flash memory is more economical than traditional EEPROM devices. EEPROMs are organized as arrays of floating-gate transistors.

RELAY:A relay isan electrically operated swit ch. Many relays use an electromagnet to mechanically operate a switch, but other operating principles are also used, such as solid-state relays. Relays are used where it is necessary to control a circuit by a low-power signal (with complete electrical isolation between control and controlled circuits), or where several circuits must be controlled by one signal. The first relays were used in long distance telegraph circuits as amplifiers: they repeated the signal coming in from one circuit

and re-transmitted it on another circuit. Relays were used extensively in telephone exchanges and early computers to perform logical operations

RELAY DRIVER: A Relay driver IC is an electro-magnetic switch that will be used whenever we want to use a low voltage circuit to switch a light bulb ON and OFF which is connected to 220V mains supply. The required current to run the relay coil is more than can be supplied by various integrated circuits like Op-Amp, etc. Relays have unique properties and are replaced with solid state switches that are strong than solid-state devices. High current capacities, capability to stand ESD and drive circuit isolation are the unique properties of Relays.

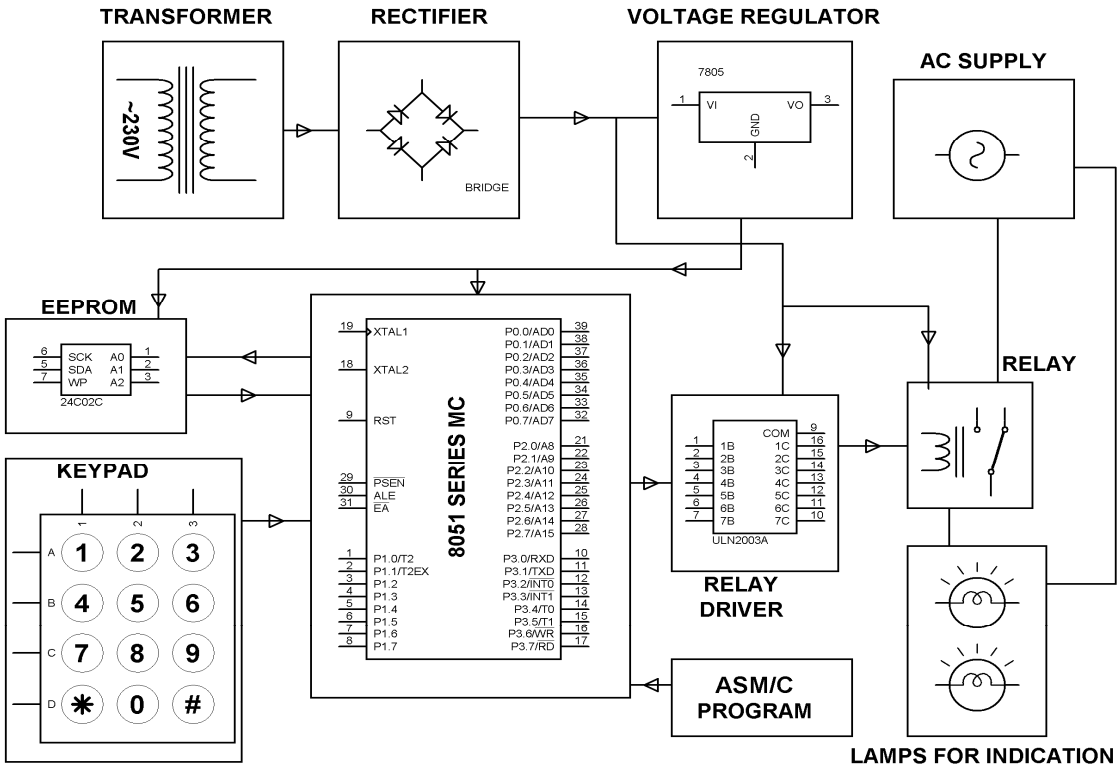

Fig: BLOCK DIAGRAM

III.**PRINCIPLE**

The main component in the circuit is 8051 microcontroller. In this project 4×3 keypad is used to enter the password. The password which is entered is compared with the predefined password. If entered password is correct then the corresponding electrical line is turned ON or OFF. In this project a separate password is provided to each electrical line. Activation and deactivation of the line (circuit breaker) is indicated by the load.

IV.**WORKING**

A) POWER SUPPLY: The circuit uses standard power supply comprising of a step-down transformer from 230Vto 12V and 4 diodes forming a bridge rectifier that delivers pulsating dc which is then filtered by an electrolytic capacitor of about 470µF to 1000µF. The filtered dc being unregulated, IC LM7805 is used to get 5V DC constant at its pin no 3 irrespective of input DC varying from 7V to 15V.

The input dc shall be varying in the event of input ac at 230volts section varies from 160V to 270V in the ratio of the transformer primary voltage V1 to secondary voltage V2 governed by the formula V1/V2=N1/N2. As N1/N2 i.e. no. of turns in the primary to the no. of turns in the secondary remains unchanged V2 is directly proportional to V1.Thus if the transformer delivers 12V at 220V input it will give 8.72V at 160V.Similarly at 270V it will give 14.72V.Thus the dc voltage at the input of the regulator changes from about 8V to 15V because of A.C voltage variation from 160V to 270V the regulator output will remain constant at 5V.

The regulated 5V DC is further filtered by a small electrolytic capacitor of 10μF for any noise so generated by the circuit. One LED is connected of this 5V point in series with a current limiting resistor of 330Ω to the ground i.e., negative voltage to indicate 5V power supply availability. The unregulated 12V point is used for other applications as and when required.

B) MICROCONTOLLER PIN CONFIGURATION: Microcontroller is interfaced with keypad, EEPROM, relay driver, voltage regulator and C program module.

Out of four ports of microcontroller pin configuration, the upper pins of port 1, i.e., pin 1.0 to pin 1.3 of the microcontroller are connected to the row lines of the keypad and lower pins (pin 1.4 to pin 1.6) are connected to the column lines. These are connected in such a way that the column lines acts as input to the microcontroller, and the row line as output lines. The input lines are pulled up internally.

Here 16×2 LCD is connected to the port 0 and port 2 pins. As the port 0 has no internal pull up, it is pulled up externally using a set of resistors which are connected to 8-data lines of the LCD. And control lines of the LCD are connected to the Port 2 pins.

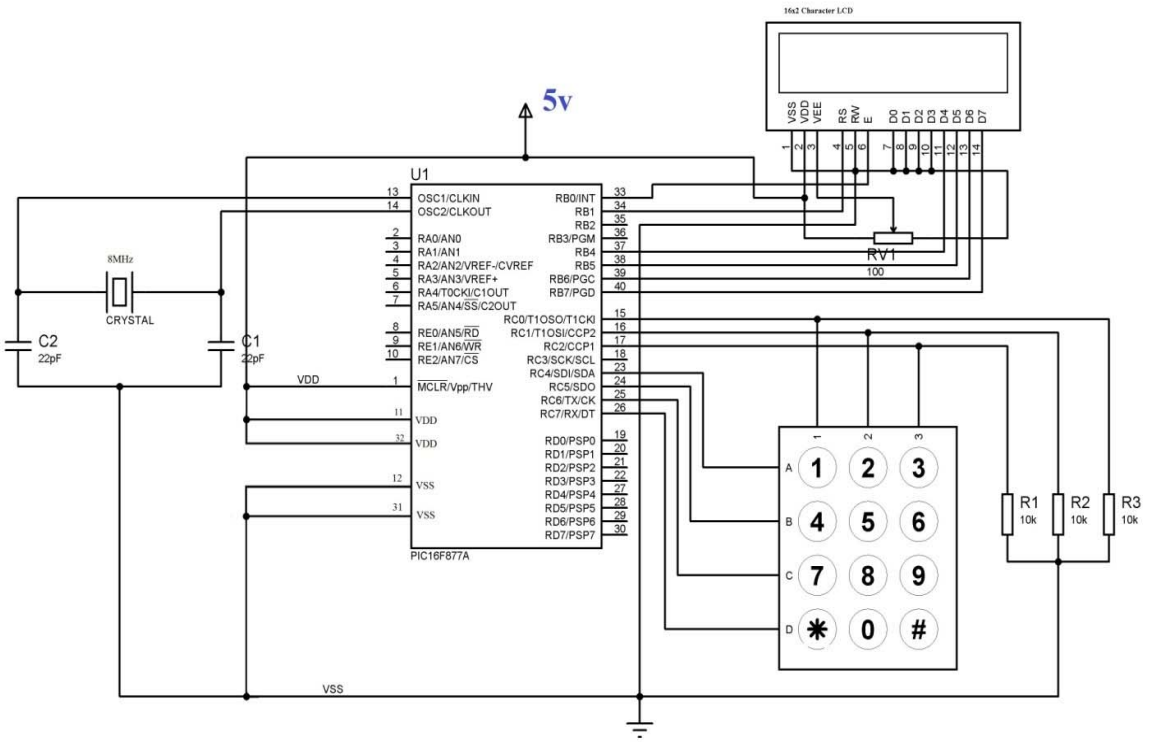

ISBN: 978-93-85225-66-6, 12th June, 2016, Hyderabad

V.OPERATION

For the operation of circuit breaker through a password, program is written in keil software and created into a .hex file that is further burnt onto the controller with the help of flash magic. Connections are given as per the circuit diagram. While giving the connections, it should be made sure that there is no common connection between AC and DC supplies.

5V power supply circuit is to be used to provide regulated 5V DC to the controller. Now both the AC and DC supplies are switched on. Relay output pins gets 230V, so they should not be touched. LCD displays "enter password". Enter the password with the help of keypad, you can see '*' for each digit. Now if the password is correct then the circuit breaker state changes and displays status line on the LCD screen. If the password is wrong then it displays "access denied".

Since this is a user changeable one, to change the password click on '*', '#'. It will display 'enter password'. Here the circuit is provided with a master code that is used to access the circuit by anyone. For changing the password, this master code is to be entered. Then after entering the master code, LCD displays, 'new password'. Now any password of will can be entered. After that it displays 'confirm password' i.e., the new entered password is going to be stored and the person can change the status of circuit breaker only by this new password.

VI.RESULTS AND DISCUSSIONS

This proposed system provides a solution, which can ensure the safety of the maintenance staff e.g. line man. The control to turn ON/OFF the line lies with the line man only. This system has an arrangement such that a password is required to operate the circuit breaker (ON/OFF). Line man can turn off the supply and comfortably repair it, and return to the substation, then turn on the line by entering the correct password. Since it has the provision of changing the password, person can give any password of his will and have his work done safer.

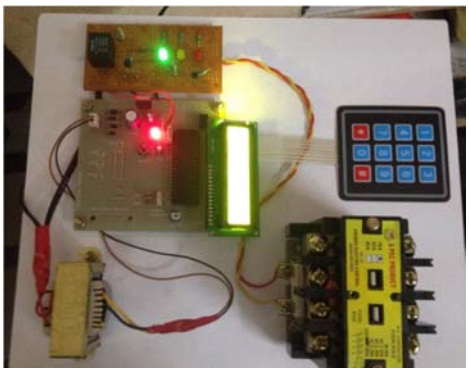

Fig: CB in closed state shown by green LED

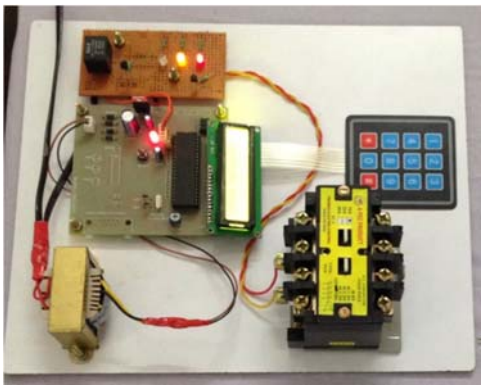

Fig: CB in open state shown by red LED

CONCLUSIONS

The project titled 'ELECTRIC LINEMAN SAFETY BY USER CHANGEABLE PASSWORD BASED CIRCUIT BREAKER' gave the following conclusions.

- It can work on a single given known password
- The password to operate can be changed and system can be operated efficiently with the changed password
- No other person can reclose the breaker once the changed password is given into system other than the person who had changed it.
- It gives no scope of password stealing
- It is effective in providing safety to the working staff

- It is economical
- It can be easily installed

ACKNOWLEDGEMENT

We are thankful to the management of S R Engineering College, Warangal for providing facilities to publish this work.

REFERENCES

1. "The 8051 Microcontroller and Embedded systems" by Muhammad Ali Mazidi and Janice Gillispie Mazidi , Pearson Education.
2. ATMEL 89S52 Data Sheets.
3. Electrical Engineering Fundemantals" by VINCENT DEL TORO.

WEBSITES

- www.atmel.com
- www.beyondlogic.org
- www.wikipedia.org
- www.howstuffworks.com
- www.alldatasheets.com

STUDY AND IMPLEMENTATION OF LEAN MANUFACTURING TOOL - 5S'

[1]Mr. Nikunj S Patel, [2]Mr. Chetan U Patel, [3]Dr. Pragnesh Brahmbhatt
RAI University, Laxmi Institute of Technology, GEC Modasa
Email:[1]mr.nikunjpatel1987@gmail.com, [2]chetan.patel920@gmail.com,
[3]pragneshbrahmbhatt@gmail.com

ABSTRACT- Lean manufacturing is an approach focused on improving quality; reducing variation and eliminating waste in an organization. This research provides a roadmap and implementation of lean manufacturing tools in manufacturing industries. The main objective of this paper is the study, analysis of improvements about different manufacturing industries such as manufacturing of S.G Iron and Alloy Cast Iron ,Nonferrous Aluminum products ,Corrugated boxes Industry, manufacturing heat exchanger and last one is manufacturing of Radiator ,Sealing Gasket etc. where the entire project has been done. Getting these improvements, using the initial resources, it is obtained some benefits, adding more production and easiness to work in general. Also there is an improvement in terms of quality

To make the project, gather data tools have been used. Applying lean Tools and formats, an initial study has been made and then proposal improvements. After analyze the results, it is possible to show positive conclusion using LM as an optimization method, because currently, there is more space less time used and better quality in the final product.

These papers represent the one case study in radiator manufacturing company, where the 5S'tool implemented. The main Objectives are decreasing Inventory, more Utilization of space, Reduce Wastages.

Index term- Lean Manufacturing, 5S' Gap Analysis chart

I. INTRODUCTION

Lean manufacturing is a business philosophy that continuously improved all process involved in manufacturing process irrespective of what type of product being manufactured. India is one of the fastest growing economics of the world. It is provides highest level of customer service through systematic and continuing searching non-value-added activities and wastes and eliminating them. Lean Manufacturing is mainly adopted by organizations in order to reduce wastes and improve the quality of products. In India small and medium scales industry has been very successfully in improving quality of products, because products are tested at each every step in the manufacturing process .The concept of lean production arrived to India in the mid 1980's from Japan and united states of arriving, but it was mostly the larger companies that adopted the techniques now the small and medium companies has started to the Lean manufacturing concept's. This gives the extra edge in today's cost and time competitive in small & medium scale Industry in Indian Markets, they are Price, and Quality and delivery Lean enterprise owners can deliver high quality products with low prices.

II. LITERATURE REVIEW

During the research review, we found that Lean thinking constraints in traditional batch manufacturing environments[1], Development of 5s Practice checklist for environment, housekeeping and manufacturing organization Manufacturing Industry[2]. Lean methodologies

for economically and environmentally sustainable foundries[3] is often seen as a set of tools that reduce the total cost and improve the quality of manufactured products the lean management is philosophy is one which targets waste reduction in every facet of the manufacturing business. Metal casting industries are actively involved to reduce the scrap rejection and rework during the manufacturing process of the components. To achieve these production concerns must follow the quality control procedures correctly and timely implementation of the lean manufacturing [4]. The lean manufacturing of small industry could Implementation the philosophy in own contend lean production concept successfully, an investigation in two middles sizes industries, India[10]. Value stream mapping technique involves flowcharting the steps, activities material flows, communications and other process elements that are involved with a process or transformation. In this respect, value stream mapping helps an organization to identify the non –value –adding elements in a targeted process. Different flow layouts are selected that reduces the transport time [6], production lead-time and lower –in-process inventory [8]. The proposed framework for lean sigma implementation need to be validated in different scenarios for establishing its validity[5] and the ultimate goal of this system is to focus on achieving total communication efficiency that uses Green and lean TQM system[7]. Lean manufacturing philosophy asks for elimination of wastes widen in the manufacturing system by focusing on products value stream and eliminating non value adding activities through continuous improvement [9]. An equipment replacement decision problem within the context of lean manufacturing implementation. In particular, we demonstrate how the value stream mapping suite of tools can be used to map the current state map the current state of a production line and design a desired future state. We provide a roadmap for how VSM can provide necessary information for analysis of equipment replacement Decision problem encountered in lean manufacturing [11].

III. CONCLUSION FROM LITERATURE REVIEWS

From the literature review, we conclude that in the different direction, the various researches done on the lean manufacturing tools and techniques but there are less number of company aware about the LM tools and implementation of the same. So we implemented the 5s' concept in the company.

IV. LEAN MANUFACTURING TOOLS AND TECHNIQUES

The core of Lean is based on the continuous pursuit of improving the processes, a philosophy of eliminating all non-value adding activities and reducing waste within an organization. The Value adding activities are simply only those things the customer is willing to pay for, everything else is waste, and should be eliminated, simplified, reduced, or integrated.

There are a number of Lean techniques available such as, Value Stream Mapping, Visual Workplace, Setup Reduction, Cellular/Flow Manufacturing, Pull Systems and Total Productive Maintenance just to name a few; however, it is absolutely essential that Lean is viewed from a total system perspective. Otherwise, either a company risks putting all of its efforts into the wrong areas, and/or the improvement process will come to a grinding halt after the initial project.

V. CASE STUDY

1. COMPANY PROFILE:

- **Name and Address:**
  Banco Products(India) limited
  BIL padara road
  Near bhaili railway station
  Vadodara
- **Product:** Gasket, Oil Seal & Radiators
- **Turn Over:** 20 cr.
- **Working people:** 40 per 2 shift
-

2. REASON FOR IMPLEMENTATION

Gap analysis of the company, so we can get the clear idea about scope of work (Refer Table no.1). It is found that many area scopes of 5s in this company.

3. IMPLEMENTATION OF 5S

Step 1 –Sort Out –Remove all items from the workplace that workplace that are not needed for current operations.

Figure 1: Improper arrangement of the parts (Jigs / Tooling)mm

5S GAP ANALYSIS SHEET

DATE: 1/12/2012

COMPANY NAME: BANCO Products (India) LTD.

SR NO	ITEM	0	1	2	3	4	COMMENTS
1	Are all notices and other information available in the Work area upto Date			2			in testing and store area not identified
2	Is unused equipment and machinery eliminated from the plant			2			unused equipment parts are store in store area
3	Is obsolete inventory and raw material eliminated from the plant			2			
4	Are doorways free from material and blockages			2			
5	Are safety instructions and guide line display				3		safety instructions are given by Supervisor but not Display
6	Are all work area boundries clearly marked			2			
7	Are storage places for all work in progress designated and marked			2			
8	Are storage places for all tools and equipment properly maintain record			2			only machinary record found and properly storage of tools but not keep record
9	Are all machinary, storage euipment and colunms identified and labled	0					
10	Are all pipes, controls, and gauges identified and labled				3		identification on finish goods are found but semifinished and raw material are not found
11	Is the plant free from trash and dirt				3		at certain interval cleaning is done
12	Is the floor free from all foreign material				3		in production area increase freqency of cleaning
13	Are machines clean and good repair				3		
14	Are sources of dust, dirt and foreigh material under control		1				
15	Are oil analysis and other techniques used to gauge machine condition		1				
16	Are cleaning and checking schedule available and in documented use		1				cleaning schedule prapared but not followed regularly
17	Are up to date work instructions, including quality checks available and in use at all work station		1				work instruction are found but not displayed at all work station
18	Are all bins and parts properly identified and tagged		1				
19	Are gauages and indicator labled to clearly show the normal operating range		1				
20	Are all start up safety checks carried out and documented			2			
21	Is everyone wearing proper safety shoes, glowes, safety glass			2			
22	Are all unused tools and equipment properly stored				3		in store area some parts of unused equipment
23	Are all raw materials and work in progress properly stored			2			properly stored but not identified area
24	Are all personnel fully trained in the tasks they are responsible for, and regularly tested			2			
25	Is there a regular auditing process to verify compliance with all elements of the production and safety system			2			by external consultants ISO internal audit carried out
	TOTAL		**45**		**45/100**		**45%**

Scoring Method

0='NO', where the only choise is '0' or'4', otherwise it means 'not at all'.
1=some evidence of a plan but very little conformance
2=about half the instances noted were in conformance
3=instances note were mostly in conformance, but one or more problems were
4='yes'.where the only choise is '0',or'4',otherwise complete conformance with

Implementation Criteria

Score	Target of implementation days
if<20	365-500
if 20-40	250-300
if 40-70	150-250
if more than 70	if more than 70

Table 1: Gap Analysis Sheet of BANCO Products India LTD.

Step-2 – Set In Order – Arrange needed items so that they are easy to find, use and put away.


Before implementation **After implementation**

Figure 2: Shows the status before and after implementation of 5S

Figure 3: Right thing is in right place

Spatter removing after welding


Before **After**

Figure 4: Implementation status before & after of 5S within 2 months

Step 3: (Clean Lines) shine every things, everything is dust free (clean and safe work plan)

Neat & clean gang ways painted floor

No leakage of oil on the material &shop floor

Figure 5: Shows the Status after 5 Month Implementation of the Shop Floor

Shop floors shine everything Dust free environment

Figure 6: Shows the Status after 5 Month Implementation of the Shop Floor

Step 4- Standardization

Work station layout, work Area layout, and work in process

Air Line

Liquid/ Lubrication Line

Figure 7: Implementation of the color coding

In sustains the benefits achieved by implementing 1s, 2s & 3s.avoids Re-

occurrence, in all the process continuity of work and also provides guidelines for the new people

STEP 5–SELF–DISCIPLINE (follow the standards)

Figure 8: Whatever has been decided must be followed exactly as per standard

Sr. No	Indentified waste	Before 5S	target	Actual after 4 month	Target after 7 month	Actual	Target after 12 month
1	Space utilization	10%	30%	10%	40%	20%	60%
2	Break down hours	6 Hrs	1 Hrs	2 Hrs	1 Hrs	1.5 Hrs	0.5 Hrs
3	Search time of goods	45 Min	15 Min	20 Min	10 Min	15 Min	6 Min

Table 2: 5S Result of case study

VI. CONCLUSION

According to case study, we conclude that lean tools can be used effectively in any kind of sectors as it is a world class manufacturing tool. The prime objective is to carry out process activity mapping for waste reduction. In this study bottleneck product was identified. Further value stream analysis tool was employed for identification of wastes in a process. The significance of each type of the error was studied and waste ranking was carried out. Current state map is plotted to assess current status, waste elimination techniques are presented and future state map is also preferred for improvement. The result of study shows 20% waste reduction in the area of unnecessary inventory, transportation and waiting. A 5S and Value stream mapping tools can be effectively employed to reduce wastes and ultimately improve the process.

IV. FUTURE *RESEARCH*

There is an infinite number of ways of implement Lean Manufacturing in these Industries. In this project Value Stream Mapping is done theoretically but in actual practice it can be useful. Many industries are not aware of these tools. Regarding Implementation of 5s it is popular at higher management level, but by referring this project it will be popular in a worker also. By using 5s and Value Stream Mapping moral of workers can be increased. But this is possible in future by conducting training program of such type.

V. ACKNOWLEDGEMENT

Authors of this paper thankfully acknowledge the generous and continuous support of **BANCO PRODUCTS (INDIA) LTD. BARODA, Gujarat** for giving an opportunity to do the work with them and also wishes to apologize for the unintentional exclusion of missing references and would appreciate receiving comments and pointers to other relevant literature for a future update.

VI. REFERENCES

1. Oduoza, C.F. (2008). 'Lean thinking constraints in traditional batch manufacturing environments', Advances in production Engineering & management.
2. N. Khamis, M.N.Ab Rahman, A.R.Ismail (2009). 'Development of 5s Practice checklist for Manufacturing Industry', World congress on Engineering.
3. R.M. Torielli ,R.A.abrahams , R.W. smillie. 'Using lean methodologies for economically and environmentally
4. sustainable foundries', China foundry Vol.8 No.1
5. T.R Vijayaram, S.Sulaiman, A.M.S Hamouda (2005). 'Foundry quality control

aspects and prospect to reduce scarp rework and rejection in metal casting manufacturing industries', Elsevier 2005.
6. M.kumar J. Antony, R.K. Tiwari. 'Implementing the Lean sigma framework in an Indian SME: a case study', Taylor & francis
7. Mr. Irish . C.Pune, Pro. G.R.Naik. 'Application of process activity mapping for waste Reduction A case study in foundry Industry', International journal of modern engineering Research (IJMER) Vol.2 ISSN 2249-6645.
8. Noor Azlina Mohd, Salleh,Salmiah kasolang (2012). 'Green lean Total Quality Information management in Malaysian Automotive companies', Elsevier 2012
9. fawaz A Abdulmalek Jayant Rajgopal.(2007) 'Analyzing the benefits of lean manufacturing and value stream mapping via simulation :A process sector case study', Elsevier 2007
10. R.K.Sigh, S.Kumar(2006) 'Lean tool, selection in a die casting unit : a fuzz –based decision support heuristic', Taylor& Francis Vol:44 No.7 April 2006
11. Mr. Vijayandra Singh, Mr.Lalit Yadav. 'Implementation of lean manufacturing in small company', ISSN 2248-4622
12. William G.Sullivan, Thomas N. Mcdonald , Eileen M.Aken. 'Equipment replacement decisions and lean manufacturing'.

ANALYSIS OF GEAR PAIR CONTACT TO PRIDICT EFFICIENCY

[1]Mr. Ravindra S. Lahane, [2]Dr. H. P. Jawale
[#] Mechanical Engineering Department, D Y Patil College of Engineering Akurdi,
Savitribai Phule Pune University
Mechanical Engineering Department, Visvesvaraya National Institute of Technology
Nagpur University
Email: [1]ravindralahane@gmail.com, [2]hemant_jawale@rediffmail.com

***Abstract*—Gear pair is higher pair point contact is under the stress. Due to that point contact get converted into line contact. Deformation due to contact losses some energy during meshing of gear is generally neglected, but so many researchers calculate efficiency of gear drive by practically and analytically is upto 98% for metal only.if the error due to deformation in transmission in gear box is small no one proposed this kind work is workout in this paper**.

***Keywords*— Gear pair, Contact, Deformation, Efficiency.**

I. INTRODUCTION

Efficiency of spur and helical gear systems has become an increasingly important research topic as the fuel economy requirements for today's passenger vehicles and rotorcraft are more stringent, not only due to fuel cost, but also environmental concerns associated with energy utilization and air pollution. Improved gear system efficiency also results in less frictional heat generation within the gearbox, resulting in improvements in gear failure modes such as scoring and pitting, and lower-capacity lubrication systems. Sliding friction contributes about 98% of the total power loss for gear trains operating at relatively low speeds (less than 2000 rpm input speed). Rolling frictional losses decrease with increased load while windage losses are only significant for gears running at very high speeds (greater than 3000 rpm). The results also showed that the overall efficiency varies over the path of contact of the gear meshes ranging between 94% to 99.5%.

There are other benefits to improving gear efficiency as well. Since the efficiency losses amount to additional heat generation within the gearbox, several gear failure modes including scoring and contact fatigue failures are directly impacted by the efficiency of the gear pair. A more efficient gear pair generates less heat, and therefore, it is likely to perform better in terms of such failures. In the process, demands on the capacity and the size of the lubrication system and the amount and quality of the gearbox lubricant are also eased with improved efficiency. This also reduces the overall weight of the unit contributing to further efficiency improvements.

The total efficiency loss of the gearbox is attributable to sliding and rolling frictional losses between the gear teeth, windage losses due to complex interactions with the air surrounding the gears, and oil splashing and churning losses inside the gearbox, as well as the losses associated with the bearing and seals. While churning and windage losses are mostly geometry and speed related, friction losses are mainly associated with sliding velocities and load. Friction losses of hypoid gears are of primary interest here since they are a major source of losses in a drive train. As a common automotive application, the drive train of a rear-wheel-drive (or all-wheel-drive) car or truck contains one (or two, one rear and one front) axle

gearbox that is formed by a hypoid final drive reduction unit and a differential. Unlike parallel axis gears that may have a mechanical efficiency well over 99 percent, the efficiency of hypoid gears usually falls into the range of 86 to 97 percent depending on the amount of relative sliding induced the gear geometry. This is mainly because sliding velocities in a hypoid gear contact are significantly larger than parallel-axis gears. As a result of this, an axle unit that is formed by a single hypoid gear set has the same levels of (and in May applications more) power loss as a manual or automatic transmission that contains many spur or helical gears. This presents the hypoid gear drive as a prime candidate for any efficiency improvement efforts.

Until now many researchers have worked on static and dynamic contact of contact with

Gosselin etal [1] applied a new methodology based on FEM to analyze the contact stress and displacement of the line contact condition in spur gears.

Braucr Zanzi and Pedrero and Guing and etal [2] on Tooth contact analysis and stress analysis of gear drives.

Umezawa and Ishikawa [3] presented experimental studies for the deflections and moments of a gear tooth.

Chabert et al also presented valuable results using finite element method (FEM) on the stresses and deflection of spur gear teeth induced by a static load.

Litvin etal [1] developed computer programs that integrate computerized design, tooth contact analysis and automatic modeling and finite element simulation of a new type of helical gear drives.

Vedmar and Henriksson introduced a method to use the deformations of the gears to determine the variation of the gear mesh stiffness and the boundary of the action between the gears.Little research has been reported on finite element based methods to investigate the dynamic contact/impact problems of gear drives.

GEARS are the most common power transmission systems in industrial machinery, automobiles, aircrafts, marine vessels et cetera. The efficiency of these power transmission systems is an important design factor due to the following

reasons:

i. Efficient power transmission systems ensure fuel economy of automobiles, marine vessels and aircrafts.

ii. With less fuel consumption, less pollutant gases and particulate are emitted to the environment

As the recent work is on the gear contact, when gear pair is rotated due tensional effect due to that causes the small deformation in the profile causes minor loss in energy that error affects in transmission efficiency.

1. Gear pair is the higher pair with line contact under the stress , line contact get converted into surface contact i.e. lower pair due to that degree of freedom is zero hence motion will not possible, law of gearing is not possible at all point due to series of deformation.
2. The motion will takes place because of the additional deformation with satisfaction of law of gearing.
3. Resistance to the motion is due to :

a. Friction b. Additional deformation

4. Tractive forces causes the deformation at point of contact, hence some Energy is utilized for Local Deformation. Practically, complete Strain Energy is not regained under elastic deformation.

NOMENCLATURE:

Z1	No. of teeth on pinion
Z2	No. of teeth on gear
α	Pressure Angle
m	Module
dp	Pitch circle Diameter of Gear1
dg	Pitch circle Diameter of Gear2
A	Addendum of gear
D	Dedendum of gear
t	Tooth thickness
w	Face width
P	Circular pitch
F	Applied load vector
Pmax	Maximum contact stress
Fi	Load per unit width
σH	Maximum Hertz stress
a	Contact width
h	Working depth
H	Whole depth
Ac	addendum circle diameter
Dc	dedendum circle diameter
CR	Contact Ratio
CL	Contact Length
R1	Radius of Gear1
R2	Radius of Gear2

L	length of cylinder
Ft	Tangential Force
Fr	Radial Force
Fn	Normal Force
Ei	Young's Modulus of elasticity
μ	Poisson's ratio
∂x	in x-direction
∂y	Deformation in y-direction
∂z	Deformation in z-direction
σ	Normal Stress
τ	Shear Stresses
σxx, σyy, σzz	Normal Stress in X, Y and Z Direction
εxx, εyy, εzz	Normal Elastic Strain in X, Y and Z Direction
τxy, τyz, τxz	Shear stress component in XY, YZ and XZ Plane
γxy, γyz, γxz	Shear strain component in XY, YZ and XZ Plane

II.CONTACT ANALYSIS OF TWO CYLINDRICAL

1. Why is the Contact Problem Significantly Difficult

Despite the importance of contact in the mechanics of solids and its engineering applications, contact effects are rarely seriously taken into account in conventional engineering analysis, because of the extreme complexity involved. Mechanical problems

involving contacts are inherently linear elastic behavior.

First, the actual region of contact between deformable bodies in contact is not known until the solution has been obtained. Depending on the loads, materials, and boundary conditions, along with other factors, surfaces can come into and go out of contact with each other in a largely unpredictable manner. Secondly, most contact problems need to account for friction. The modelling of friction is very difficult as the friction depends on the surface smoothness, the physical and chemical properties of the material, the properties of any lubricant that might be present in the motion, and the temperature of the contacting surfaces. There are several friction laws and models to choose from, and all are nonlinear. Frictional response can be chaotic, making solution convergence difficult (ANSYS). In addition to those difficulties, many contact problems must also address multi-field effects, such as the conductance of heat and electrical currents in the areas of contact. Bodies in contact may have complicated geometries and material properties and may deform in a seemingly arbitrary way. With the rapid development of computational mechanics, however, great progress has been made in numerical analysis of the problem. Using the finite element method, many contact problems, ranging from relatively simple ones to quite complicated ones, can be solved with high accuracy. The Finite Element Method can be considered the favourite method to treat contact problems, because of its proven success in treating a wide range of engineering problem in areas of solid mechanics, fluid flow, heat transfer, and for electromagnetic field and coupled field problems. An easy way to comply with the conference paper formatting requirements is to use this document as a template and simply type your text into it.

2 How to Solve the Contact Problem

There are many types of contact problems that may be encountered, including

contact stress, dynamic impacts, metal forming, bolted joints, crash dynamics, and assemblies of components with interference fits, etc. All of these contact problems, as well as other types of contact analysis, can be split into two general classes (ANSYS),

Rigid - to - flexible bodies in contact,

Flexible - to - flexible bodies in contact.

In rigid - to - flexible contact problems, one or more of the contacting surfaces are treated as being rigid material, which has a much higher stiffness relative to the deformable body it contacts. Many metal forming problems fall into this category.

Flexible-to-flexible is where both contacting bodies are deformable.

Examples of a flexible-to-flexible analysis include gears in mesh, bolted joints, and interference fits.

3. Types of Contact Models

In general, there are three basic types of contact modelling application as far as

ANSYS use is concerned. Point-to-point contact: the exact location of contact should be known beforehand. These types of contact problems usually only allow small amounts of relative sliding deformation between contact surfaces. Point-to-surface contact: the exact location of the contacting area may not be known beforehand. These types of contact problems allow large amounts of deformation and relative

sliding. Also, opposing meshes do not have to have the same discretisation or a compatible mesh. Point to surface contact was used in this chapter. Surface-to-surface contact is typically used to model surface-to-surface contact applications of the rigid-to-flexible classification.

3.2.3 Why contact between two cylindrical Surfaces

Contact of two curved surface is represent the gear teeth so two cylindrical surfaces in contact cuases the contact stress and deformation, in machine design,problem frequently occurs when two members with curved surfaces are deformed when press against one another giving rise to an area contact under the compressive stresses. Of particular interest to the gear designer is the case where the curved surfaces are of cylindrical shape because they closely resemble gear tooth surface

Consider two circular cylinder, B1 and B2, with a radius of R1= 5 mm. and R2= 5mm. as shown in Figure 3.2

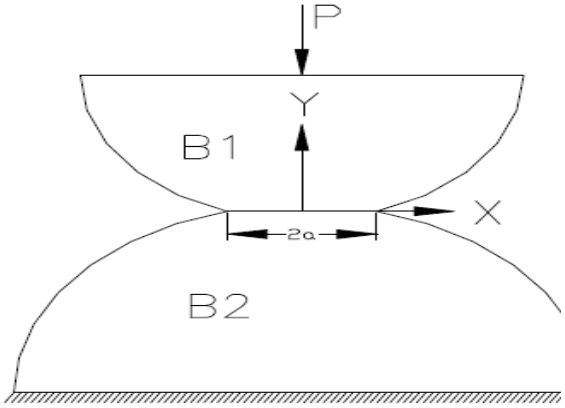

3.2.3.1 Hertz Contact Stress Equations:

Usually, the current methods of calculating contact stresses use Hertz's equations, which were originally derived for contact between two cylinders.

The maximum surface (Hertz) stress:

$$Pmax = \sigma H = 0.564 \frac{\sqrt{F\left(\frac{1}{R1}+\frac{1}{R2}\right)}}{\sqrt{\left(\frac{1-\mu 1^2}{E1}+\frac{1-\mu 2^2}{E2}\right)}} \quad \ldots\ldots\ldots\ldots\ldots\ldots\ldots (1)$$

Where,

F -is load per unit length,
Ri- is radius of the cylinder,
µi- is Poisson ratio,
Ei- is Young's modus of cylinder.

Material properties of the two cylindrical bodies and load data of the contact model are shown in Table 4.1.

TABLE I

MATERIAL PROPERTY AND PARAMETER

Sr. No	Material Property and Parameter		
	Surface Body	**MaterialProperty**	**Dimension**
1	Cylinder 1 (B1)	1.Modulus of Elasticity (E1)=200X10^5Pa 2. Poisson's ratio (µ¹)=0.3	Radius (R1)=5mm, Length (L) = 60mm
2	Cylinder 2 (B2)	1.Modulus of Elasticity (E 2)=200X 10^5Pa 2. Poisson's ratio (µ²)=0.3	Radius (R2)= 5mm, Length (L) = 60mm
3	Load Data:	Load (F) = 2000 N	

Following fig 3.3 (a) and fig 3.3(b) shows the deformation and von misses stress contact zone is near contact surface.

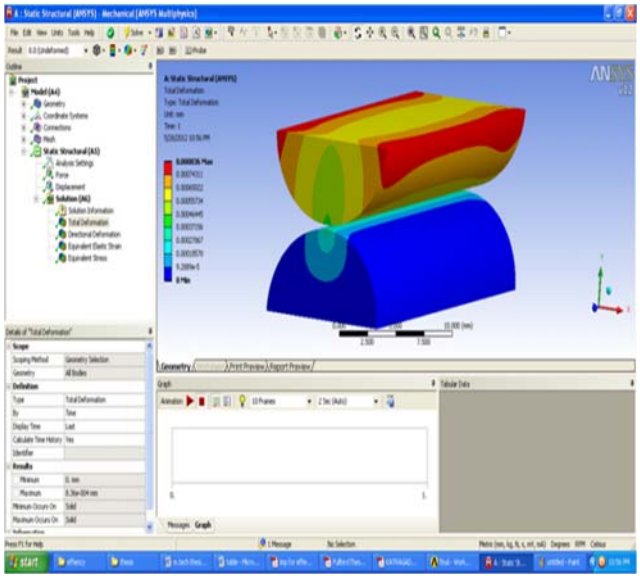

Figure a): Deformed Model two half cylinder surfaces

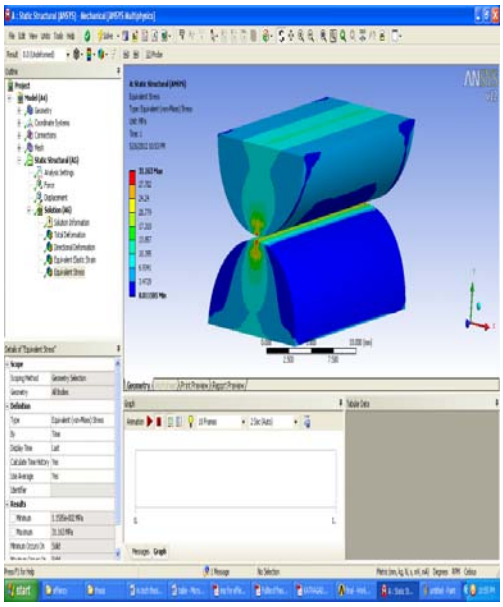

Figure b): Von Mises Stress Model of two half cylinder surfaces

Table 3.1: Comparison of finite element analysis results with analytical results for contact model

REGION	ANSYS	THEORO TICAL	% ERRO R
CONTACT DEFORMATI ON(mm)	0.00 0836	0.00092 8	1.10
CONTACT DEFORMATI ON(mm)	31.6 4	25.467	0.5

Conclusion: Finite element modeling of the contact between two cylinders was examined in detail. The finite element method with special techniques, such as the incremental technique of applying the external load in the input file, the deformation and contact stress and the introduction of the contact element were used. It was found that initial loading using displacements as inputs was helpful in reducing numerical instabilities.

III.Force Analysis for Spur Gear

One of the fundamental parameters to be considered, analyzed and checked for designing a gear system is the load transmitting capability of gear teeth. For this the circumferential force effective on the tooth at the pitch circle of the gear when in mesh, must be known. Irrespective of the value of the contact ratio, for the calculation the total gear forces are taken to be effective on a single pair of teeth in mesh.

Rated Power P_R = 30 KN,

Speed on Pinion = N_P = 1000 RPM

Speed on Gear = N_G = 500 RPM

Z_1 = No. Of Teeth on the Pinion = 18

Z_2 = No. Of Teeth on the Gear = 18

Pressure Angle α = 20 deg for Full Depth

Torque on Pinion & Gear T_P & TG = $\frac{P \times 60}{2\pi NP \text{ or } NG}$ = $\frac{30\,000 \times 60}{2\pi \times 1000}$

= 286.4788 N-mm

Material for Gear and Pinion = Structural Steel

Brinell hardness number (B.H.N) =200

Assuming the steady state condition& 8-10 hrs. service per day

4.1. Design Power (P_d) = (P_R) ×K_1 = 30×10^3 ×1 = 30×10^3 W

Where, P_R = Rated Power, K_1 = Load Factor = 1

4.2. Tooth Load $F_{t,N}$

$$F_t = \frac{(P)d}{Vp}$$

Where Vp = Pitch Line Velocity, m/sec

$$Vp = \frac{\pi Dp\, Np}{60\times1000} = \frac{\pi \times m \times 18 \times 1000}{60\times1000} =$$ 0.9424 m m/sec

$$F_t = \frac{30\times10\text{^}3}{0.9424m} = \frac{31830.9886}{m} \ldots\ldots (1)$$

4.3 Bending Strength by Lewis equation, F_B,N

$F_B = S_o \times Cv \times b \times Y \times m$

Where,

S_o= Basic Strength, MPa= 140MPa

Cv = Velocity Factor = 3 / 3 +Vp = 0.3 (trial value)

b= Face width of gears =10mm (trial value)

Y =Modified Lewis form factor = 0.485 – 2.87 / Tp

=0.485 – 2.87/18

= 0.3256

m= Module, mm

F_B=140×0.3×10m×0.3256×m=138.74 ×m^2..... (2)

Equating Equation (1) & (2), we get

$F_B = Ft$

138.74 ×m^2 = 31830.9886/m

m^3 = 229.4290

m=6.1218 ≈ 8mm

Therefore,

The standard value of module m =8mm

Face width b= 10m = 10×8=80 mm

Diametral Pitch for pinion dp = 8 ×18 =144 mm

Diametral Pitch for gear dg = 8 ×18 = 144 mm

Pitch Line Velocity, Vp= 0.9424 ×m =0.9424 ×8 =7.5392 m/sec

Ft = 31830.9886/m =31830.9886/8 =3,978.8735 N

F_B=138.74×m^2 = 138.74 ×8^2 =8,879.36 N

4.4 Dynamic Load Fd, N Based on Buckingham's Equation

The dynamic force for the gear is given by

$$F_d = F_t + \frac{21Vp\,(Ceb+Ft)}{21Vp+\sqrt{Ceb+Ft}}$$

The permissible error at 7.5392 m/sec i.e. 452.352 m/min is 0.045.

We must use class-2 chain gear for which the permissible error for which the probable error

For 8mm module will be 0.4mm.For deformation factor C for steel with 20^0 full depth teeth

C= 11800

Ceb = 11800×0.04×80 = 37,760

Ceb + Ft = 37,760 + 3,978.36= 41,738.36

21Vp = 158.34

$$F_d = 3{,}978.36 + \frac{158.34\times(41{,}738.36)}{158.34+\sqrt{41{,}738.36}}$$

= 22,203.33 N

4.5. Limiting Wear Strength Fw, N

$F_W = D_P \times b \times K \times Q$

Where, K= Load Stress Factor

Dp= 144mm

b= 80 mm

tg & tp =No. of teeth on gear & pinion respectively = 18

Q = Size Factor = 2tg / tg+tp =1….for internal gear

Fw = 144 ×80×1×k

= 11520 k…….(3)

Equating Fw to Fd, We get kmin;

Kmin = 22203.33/11520=1.9273

Hardness for pinion & gear= 350 B.H.N

4.6. Endurance strength, Fen, N

Fen = Seb×b×Y×m

Seb = Endurance Strength =596 MPa for Steel with 350B.H.N

b= 80mm

Y= 0.1034

Fen= 596×80×0.1034×8

= 39440.8960N

The greater than Fd so O.K.

IV. 3D CONTACT ANALYSIS OF GEAR

5.1 SPUR GEAR PAIR MODEL

This model of spur gear is made in catia V5R20 then this model is import in though IGES format in ANSYS 12.1 Software. It can be seen in fig 2.11 that during the course of action of the teeth engagement along the path of action in a meshing pair of gear teeth, i.e. from beginning of contact to the end of the contact comprising the length of contact ,the load during rest of the time.

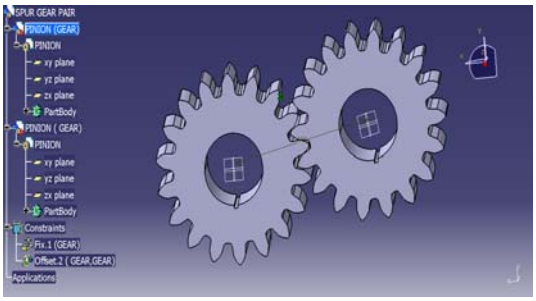

The following parameters are used to design the pair of spur gear.

5.2 Contact Ratio

It can be seen from fig that during the course of action of teeth engagement along the path of action in a meshing pair of gear teeth, i.e. from beginning of contact to the end of contact comprising the length of contact, the load is transmitted by a single tooth of the driving gear for part of the time and by two teeth during rest of the time. For continuous contact, the angle of action must be greater than the angle subtended at the centre by the arc representing the circular pitch (called "pitch angle").the relation between these two angles is termed as the contact ratio.

The physical significance of the contact ratio lies in the fact that it is a measure of average number of teeth in contact during the period in which a tooth comes and goes out of contact with the mating gear. Contact ratio 1 means that only one pair (one tooth from each gear) is engaged at all times during course of action. This is the case when the angle

The zone of action of meshing gear teeth is shown in Figure 4.4. Tooth contact begins and ends at the intersections of the two addendum circles with the pressure line.

In figure, initial contact occurs at a and final contact at b. Tooth profiles drawn through these points intersect the pitch circle at A and B, respectively. As shown, the distance AP is called the arc of approach ua, and the distance P B, the arc of recess ur. The sum of these is the arc of action AB= La.

Now, consider a situation in which the arc of action is exactly equal to the circular pitch= p.This means that one tooth and its space will occupy the entire arc AB. In other words,

When a tooth is just beginning contact at a, the previous tooth is simultaneously ending its contact at b. Therefore, during the tooth action from a to b, there will be exactly one pair of teeth in contact.

According to Machinery's Handbook [8-9], the contact ratio is the ratio of the arc of action in the plane of rotation to the circular pitch.

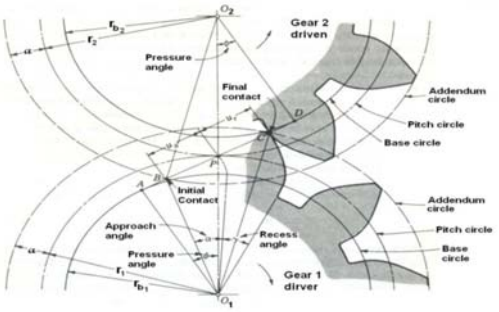

ISBN: 978-93-85225-66-6, 12th June, 2016, Hyderabad

Referring to Fig,

The path of contact La = ua+ ur =Arc of approach (AP) + Arc of recess (PB)

La =√ (〖 (r1+a) 〗 ^2- 〖r1〗 ^2×cos^2 α) + √ (〖 (〖r2〗 ^2+a) 〗 ^2- 〖r2〗 ^2×cos^2 α) - (r1 + r2) sin α

= √ (〖80〗 ^2- 〖72〗 ^2×cos^2 20) + √ (〖 80〗 ^2- 〖72〗 ^2×cos^2 20) - (72+72) sin 20

= 42.6897 + 42.6897 - 49.2509

= 36.1284mm

The contact ratio is given by following formula

Circular pitch = pitch angle = Base pitch

= π×m Cos 20

= π×8 cos20

=23.6170

C.R = (the path of contact)/ (circular pitch)

= La/(π×m Cos 20)

= (36.128)/ (23.6170)

= 1.530..... (1)

Table 5.1 Design Parameter of Spur Gear

Parameter	Formulas	Driving Gear	Driven Gear
Profile		Involute	involute
No. of teeth	Z1/Z2=1	Z1 =18	Z2=18
Pressure angle	α	20 deg	20 deg
Module	m	8 mm	8mm
Circular pitch	P= π m	25.1328 mm	25.1328 mm
Pitch circle diameter	d= m*z	144 mm	144 mm
addendum	a = 1m	8mm	8mm
Dedendum	b = 1.25m	10mm	10mm
Tooth thickness	t =1.57m	12.56 mm	12.56 mm
Face width	b	80 mm	80 mm
Working depth	H =2m	16 mm	16mm
Whole depth	h=2.25m	18mm	18mm
addendum circle diameter	Ac = d+2m	160mm	160mm
dedendum circle diameter	Dc = d- 2m	128 mm	128 mm
Fillet radius	R_f= 0.4m	3.2 mm	3.2 mm
Top land	tp= 0.25m	2mm	2mm
Centre distance	C = (z1+z2)m|2	144mm	144mm
Contact ratio	CR = L_a/Pcosα	1.5297	1.5297
Power (P)	P= 2¶NT/60	30 KN	30 KN
Speed (N)	N	1000 rpm	500rpm
Torque(T)	T	286.32 N-mm	572.95N-mm
Tangential Force	Ft	3978.8748 N	
Normal Force	Fn=Ft/cosα	4234.2301 N	
Radial force	Fr=Ft *tanα	1448.1920 N	

In this session gear teeth in mesh contact causes the deformation in micron over the gear teeth and contact stress at point of contact is maximum. This gear tooth mesh model there is total nodes no 59790 to 61549 and element number 38643 to 39908 on this node in contact, minimum elemental edge length is 0.00984mm.

4 Meshing of spur gear

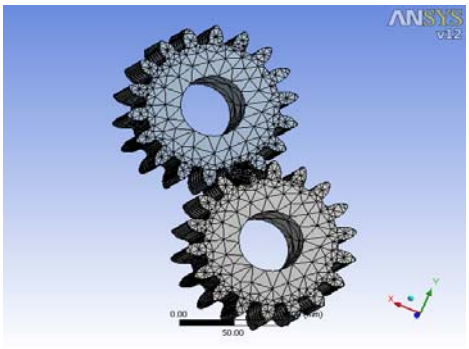

Fig 5.2 Fine Mesh of Spur Gear near Contact

5.2 DEFORMATION, ENERGY AND EFFICIENCY OF GEAR TEETH

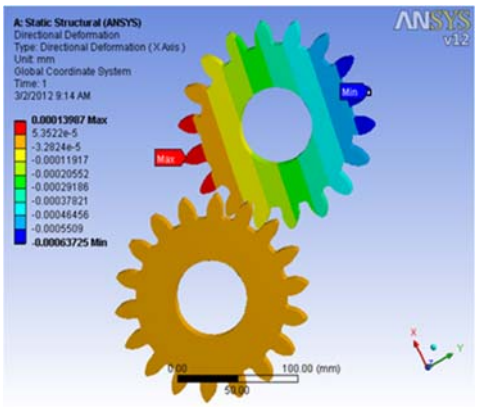

Fig: a) Deformation Model in X- Direction

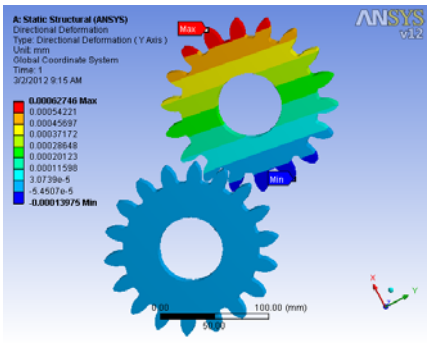

Fig: b) Deformation Model in Y- Direction

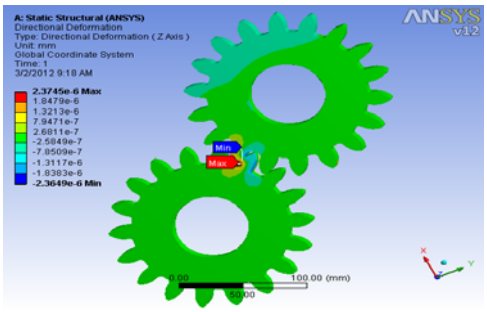

Fig: c) Deformation Model in Z- Direction

Fig 5.3: 3D Deformed Model for gear under contact.

5.2.2 Methods for Energy Estimation under Strain

The following types of energy method used to calculate the gear pair losses

5.2.2.1 Strain Energy Method

The energy stored in body due to deformation is called strain energy. The strain energy stored in an elastic material upon deformation is calculated below for a number of different geometries and loading conditions.

The strain energy stored due to deformation in gear pair contact is calculated as follows:

Strain energy per unit volume.

$$Ue = \tfrac{1}{2} \times \text{Stress} \times \text{Strain} = \tfrac{1}{2} \times \sigma \times \varepsilon$$

$$= \tfrac{1}{2} \times [\sigma xx \times \varepsilon xx + \sigma yy \times \varepsilon yy + \sigma zz \times \varepsilon zz + \tau xy \times \gamma xy + \tau yz \times \gamma yz + \tau xz \times \gamma xz]$$

$$= 1/2 \times [0.46881 \times 1.82E\text{-}06 + 0.2662 \times 7.83E\text{-}07 + 0.19354 \times 4.92E\text{-}07 + 1.59E\text{-}06 \times 1.22E\text{-}01 + 4.62E\text{-}02 \times 6.00E\text{-}07 + 9.28E\text{-}02 \times 1.21E\text{-}06]$$

$$= 7.45E\text{-}07 \text{ Joules}$$

Assumptions for Sample Calculations

Material under consideration is - Cast Steel 0.20 % Carbon, Untreated

Throughout the length of contact, average deformation is assumed to be constant

Assumptions for Energy Estimation

Energy Calculation by considering,

1. Sliding friction and rolling friction is absent No Power losses under friction.
2. Zero Bearing and Churning loss for lubricating oil.
3. The windage losses due to complex interactions with the air surrounding the gears is Zero.

5.2.2.2 Efficiency Calculation of Gear

In gear drive, the efficiency of system is given by

Efficiency (η) = (output power)/(input power)

= (Toutput×ωoutput)/(Tinput ×ωinput)..... (5) There is a power loss in the system due to the sliding action of toothing.

Besides this, there are power losses at the bearing, loss due to the churning of

Lubricating oil and other losses, so that the overall efficiency becomes still lesser

Than the efficiency calculated on the basis of loss due to sliding only.

The following values are typical for the spur gear drive system

η = 92 to 94 % for unmachined teeth

= 96 % for smooth and lubricated teeth

= 98 to 99 % for very carefully machined teeth with hydrodynamic

Lubrication between teeth surfaces With the ideal kind of design, construction and bearing systems coupled with very good Lubrication and gears of high quality, it is not difficult to attain an efficiency as high as 98% to 99%.for automotive drives in general, it is around 97%.

If the sliding velocity is high, it leads to considerable power loss due to friction and the

Efficiency may fall to around 85%. According to Machinery's Handbook [8-9],

Hence efficiency is calculated as follows:

Input Energy = Torque acting on the pinion = 286.4788 Joules

Total loss = Input Energy –Output Energy

Efficiency Estimation is

Efficiency (η) = (Output Energy)/(Input Energy) ×100

= (Input Energy –Total Loss)/(Input energy) ×100

= 286.4788- 7.4544E-7/286.4788×100

= 99. 9997 %

Estimated loss due to strain energy method in transmission is 0.03 %.loss in transmission is minor in due to sliding of the contact of spur gear, hence from that loss we predict to efficiency by reducing the loss.

5.2.2 POSSIBILITIES TO CALCULATE THE AVERAGE DEFORMATION:

The deformation over the gear tooth Profile considering the 100 point on contact surface then each point contact is converted into line contact hence deformation over teeth in nearly equal as the calculated by direct contact in triaxial direction. For that divide gear tooth profile having total length 23.77mm and having dividend distance between points is 0.2377mm is shown in fig 5.1

The first model used is a 2D model. With this model we will find the real points on the tooth profile where the single pair in contact change into a double pair of teeth in contact this way we find with a good approximation the loading diagram for the 100 points on the involute active profile.

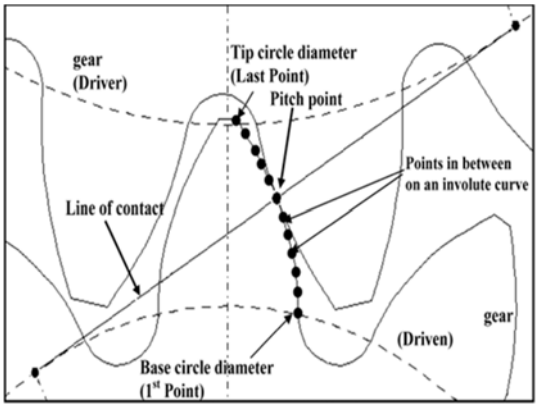

Fig 5-7 2D Meshing point contact of gear teeth model

To keep track of the surface elements the single point observation method was used. Thesingle point observation method was introduced by Andersson and Eriksson [17] and has been successfully used by Hugnell [18], Björklund [19] and others. Andersson and Eriksson studied how a point on a gear tooth moved in relation to another point on the opposing tooth, see figure 5.2. By regarding single points on the teeth, interesting information can be deduced, such as the difference in sliding distance for a local point on the pinion- and gear surfaces, which is discussed below. Local wear and pressure on the flanks can be investigated.

a) Deformed Model in X- Direction

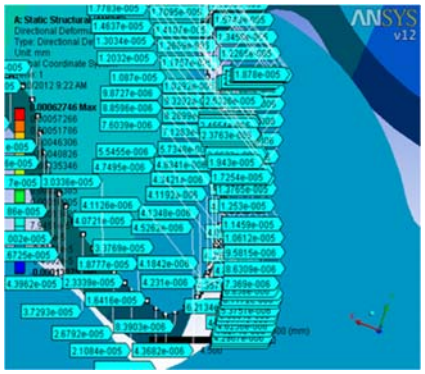

b) Deformed Model in Y- Direction

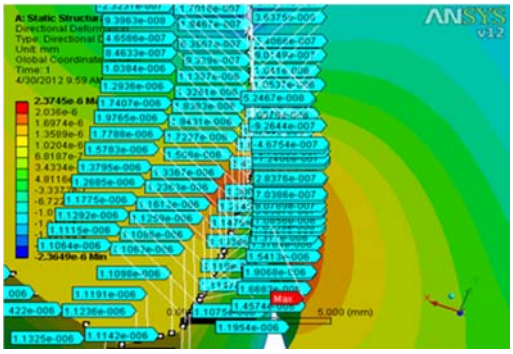

c) Deformed Model in Z- Direction

Figure 5.5 Contact Point along Tooth Face Width

The single point observation method naturally relates the wear, pressure and other relevant quantities, directly to the surface thus facilitating the study of local phenomenon on a tooth face. The surface geometry is also easily changed which is important when researching wear. The change of the surface curvature in contact affects the pressures and contact width as well as the load distribution during the meshing. This is important but often neglected and some works treat the wear as a curve fitting procedure [20], making the wear calculation very specific and not general

Table 5.3 shows the Average Deformation in X, Y & Z Direction over the Profile considering 100 point on face width compare with actual deformation calculated from the ansys.

From Table 5.4 which is shown in Appendix calculate value of normal stress, strain and shear stress and shear strain that value of all around 100 point on tooth edge face along tooth width used to calculated for strain energy.

Strain Energy per Unit Volume

Ue = ½ × Stress × Strain = ½ × σ ×ε

= ½ × [σxx×εxx+ σyy×εyy+ σzz×εzz+ τxy × γxy + τyz × γyz+ τxz × γxz]

= 2.087e-3 joules

Efficiency Estimation is.....

Efficiency (η) = (Output Energy)/ (Input Energy) ×100

= (Input Energy–Total Loss)/(Input energy)×100

= (286.4788- 2.087e-3)/286.4788 ×100

= 99. 9992 %

Estimated loss is

Using Strain Energy Method ignoring cantilever Effect Loss in transmission is estimated to be 0.08%.

Figure 5.5 shows variation of the deformation over point number along the tooth width contact region when complete load acted on contact region it will reached the pick level during contact by considering 50 points on the gear teeth profile.

Figure 5.5 shows variation of the deformation over point number along the tooth width

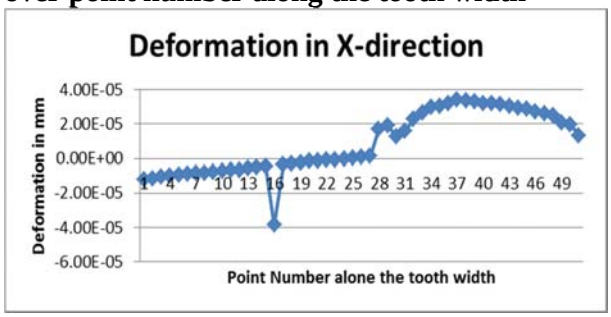

Figure 5.6 also shows variation of the deformation over point number along the tooth

width contact region when complete load acted on contact region it will reached the pick level during contact by considering 50 points on the gear teeth profile.

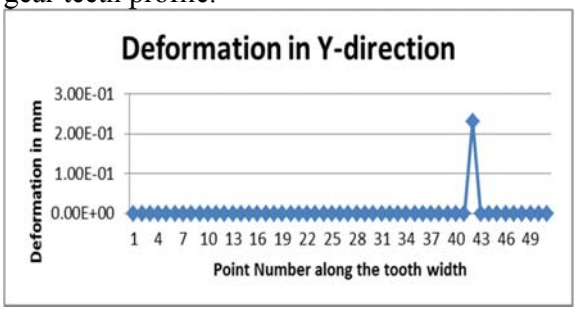

Figure 5.6 shows variation of the deformation over point number along the tooth width

As seen in figure 5.7 shows the deformation is constantly increases in tooth entering the contact and decreases in tooth contact is leaving.

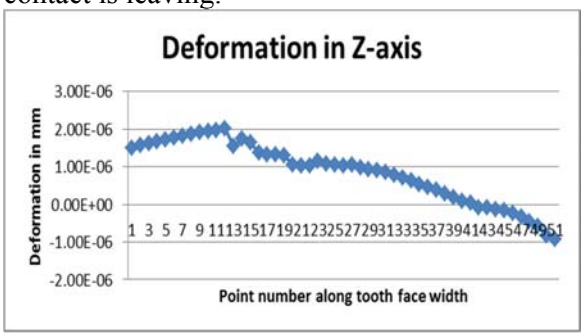

Figure 5.7 shows variation of the deformation over point number along tooth face width

5.4 Energy Required For the Cantilever Effect

Essentially, gear tooth in operation can be considered as a cantilever beam under load. For this reason, the ability of the tooth to resist tooth breakage of the tooth at the root is often reffed to as its beam strength .the basic tooth stresses caused by bending were first investigated by wildfred Lewis and the bending stress equation is still known as the Lewis formula although much modification of the original formula has taken place during the period of nearly 10 years.

Referring to fig5.5 and 5.6, the tooth load F is supposed to act at the tip corner as shown .under this assumption, calculation becomes simplified. Load F acts along the line of action at a grip angle of α1at the tip corner. When referred to pitch point P, angle α is the pressure angle of the system .As explained in earlier section, force F is normal to the tooth profile at pitch point the line of action

If at the intersection of the line of action and the present Centre line of the tooth this force F is resolved, then

We get,

The radial component Fr=F Sin α=1448.1920 N

The tangential component Ft=F Cos α =3978.8748 N

Normal Force Component F= 4234.2301 N

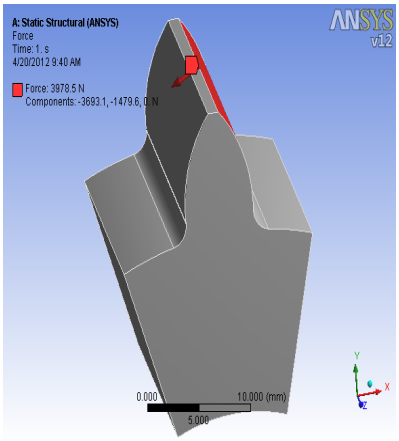

Fig 5.6: Loading and Boundary

Bending Moment at the profile is maximum is given follows:

M = Ft*D = 3978.4788* 18 = 71612.6184N-mm

M1=Ft*D1= 3978.4788*16 = 63655.6608 N-mm

M2= Ft*D2=3978.4788*10 = 39784.7880N-mm

M3= Ft*D3= 3978.4788*8 =31827.8304 N-mm

Bending Moment is Maximum at the top tooth end hence force is applied at the end of gear tip corner. Single tooth is imported into ansysis software and the apply the Boundary Condition the we got Model is discredited into small element by meshing then bottom end of the tooth is fixed and Tangential force is applied at end.

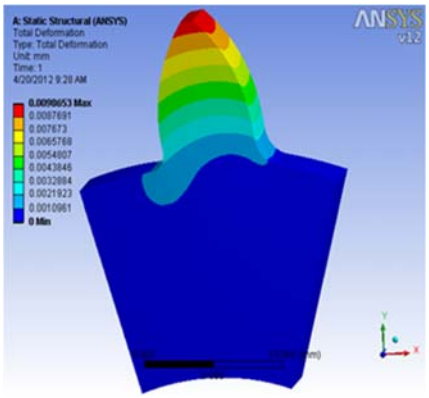

Fig: 5.1 Total Deformations

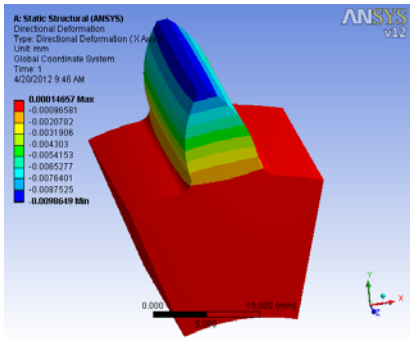

Fig: 5.2 Deformation in x –direction

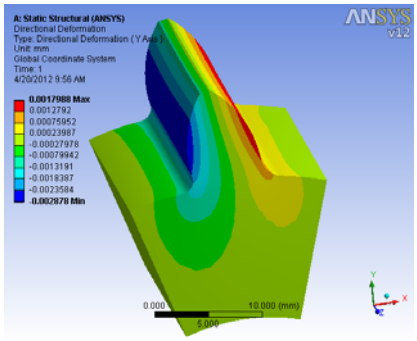

Fig: 5. 3 Deformation in y –direction

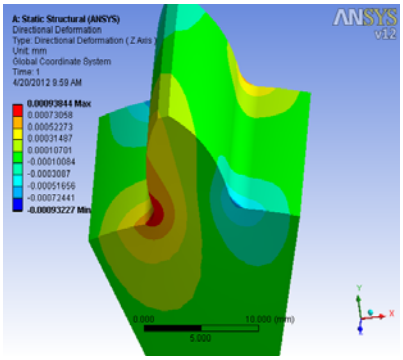

Fig: 5.4 Deformation in z –direction

Strain Energy per Unit Volume is.....

Ue = ½ × Stress × Strain = ½ × σ ×ε

= ½ × [σxx×εxx+ σyy×εyy+ σzz×εzz+ τxy × γxy + τyz × γyz+ τxz × γxz]

= ½ × [105.99×0.0004445 + 147.15 ×0.00066001 + 49.212 × 0.000233 12.731 ×0.00016 + 9.8418 ×0.0001297 + 17.28 × 0.00022465]

= 0.08147 Joules

Efficiency Estimation is.....

Efficiency (η) = (Output Energy)/(Input Energy) ×100

= (Input Energy –Total Loss)/(Input energy)×100

= (286.4788-0.08147)/286.4788 ×100

= 99. 9715%

Estimated loss is.....

Using Strain Energy Method Considering Cantilever Effect, Loss in transmission is estimated to be 2.85%

Energy required for the cantilever effect is large as compared to energy required for the ignoring the cantilever effect so that calculation made by ignoring cantilever effect is correct and also the loss in transmission more than ignoring the cantilever effect

CONCLUSION

A spur gear model was developed to predict the overall efficiency of a gearbox system.The analysis showed that the strain energy losses are highly dependent on the rotational speed of the gear wheels and is insignificant for speeds below 1000 rpm. The rolling friction loss was found to contribute a small percentage of the total power loss in the system. The rolling friction losses depend on the position of contact of the mating gear teeth and reduce with increased load.

The efficiency of gearbox system is varies from 92%,95%,98%,99% by considering contact losses there is 1% loss in transmission contact deformation this big problem in transmission .

The additional energy is required to overcome the deformation of gear pair contact and Force required overcoming the friction.Loss of energy to predict efficiency

Softer gear the material larger is loss in transmission and harder the material Gear material lesser losses in transmission. The Young's modulus of elasticity is more percent loss in energy is less and Youngs modulus of elasticity is less percent loss in energy is more. The speed of rotation of gear is more therefore percent loss of energy is less and Speed is less percent in loss of energy is more.

FUTURE SCOPE

After the successful completion of the current project, the recommendations to improve

the current results and scope for the future work are as follows.

1. Use the full version software to mesh the contact model. Mesh near the contact region using very fine elements, to avoid the high magnitude errors at smaller stick zone sizes.
2. Mesh the contact model as symmetric near the contact region, and solve the model to observe the symmetry in stick zone results.
3. Resistant to motion is due to
4. a. Friction b. Additional deformation
5. Strain energy loss affects efficiency of a gear unit means that it produces the highest possible output power for a given input power. The energy lost in the process manifests itself in the form of heat, for example in bearings, O-ring seals or gear wheels. As gear efficiency increases, its temperature will go down. This has a number of positive effects: a decreasing temperature not only extends the oil life, but the service life of seals as well. This in turn reduces the risk of leakage. Another benefit is that fans or air conditioners in production facilities might be switched off, which is another contributor to lower energy costs and a better CO2 balance.

REFERENCES

[1] Darle W. Dudley, 'Gear Handbook: The design, manufacturing applications of gear', 1965.

[2] Darle W. Dudley, 'Handbook of practical gear design', 1972.

[3] Maitra G.M., "Handbook of Gear Design", Tata McGraw-Hill Company, India, New Delhi, 1997.

[4] Tengjiao Lina, H. Oub, Runfang Lia ," A finite element method for 3D static and dynamic contact/impact analysis of gear drives Comput". Methods Applied. Mech. Engg. 196 (2007) 1716–1728.

[5] T.J.R. Hughes, R.L. Taylor, J.L. Sackman, A. Curnier, W. Kanoknulchai," A finite element method for a class of contact-impact problems", Comput. Methods Appl". Mech. Engg. 8 (1976) 249–276.

[6] K. Umezawa, J. Ishikawa, Deflection due to contact between gear teeth with "finite width, Bull. JSME 16 (97) (1973).

[7] ERRATA, NASA TP–1622 "Spur-Gear-System Efficiency at Part and Full Load"
Neil E. Anderson and Stuart H. Loewenthal February 1980.

[8] Hai Xu, B.S., M.S.E., M.S. By The Ohio State University 2005, "Development of a Generalized Mechanical Efficiency Prediction Methodology for Gear Pairs".

[9] Vaishya, M., Houser, D. R., "Modeling and Analysis of Sliding Friction in Gear Dynamics", Proceedings of DETC'00, ASME 2000 Design Engineering Technical Conferences and Computers and Information in Engineering Conference, Baltimore, Maryland, September 10-13, 2000.

[10] Hochmann, D., Houser, D. R., "Friction Forces as a Dynamic Excitation Source in Involute Spur and Helical Gearing", Proceedings of DETC'00, ASME 2000 Design Engineering Technical Conferences and Computers and Information in Engineering Conference, Baltimore, Maryland, September 10-13, 2000.

[11] Reuleaux, F., "Friction in Tooth Gearing", Transactions of the ASME, Vol. VIII, pp. 45-85, 1886.

[12] Martin, K. F., "A Review of Friction Predictions in Gear Teeth", Wear 49, pp. 201-238, 1978.

[13] Yada, T., "Review of Gear Efficiency Equation and Force Treatment", JSME

International Journal, Series C, Vol. 40, pp. 1- 8, 1997.

[14] H. Xu and A. Kahraman, "Prediction of Mechanical Efficiency of Parallel – Axis Gear Pairs," *Transactions of ASME*, vol. 129, pp. 58–68, 2007.

[15] Fakher Chaari, Manel Ben Romdhane, Walid Baccar,
Taher Fakhfakh, Mohemend haddar "Mechanics Modeling and Production research "Unit National School of Engineers of Sfax BP 1173 - 3038 – Sfax – TUNISIA.

[16] M. Vaishya and R. Singh, "Strategies for Modeling Friction in Gear Dynamics," *Journal of Mechanical Design*, vol. 125, pp. 383–393, 2003.

[17] N. E. Anderson and S. H. Loewenthal, "Efficiency of Non-Standard High
Contact Ratio Involute Spur Gears," Tech Rep., NASA Lewis Research Center, 1984.

[18] P. Heingartner and D. Mba, "Determining Power Losses in the Helical
Gear Mesh," *Gear Technology*, pp. 32–37, 2005.

PROPERTY TESTING OF BIODIESEL DERIVED FROM COCONUT TESTA OIL AND ITS PROPERTY COMPARISON WITH STANDARD VALUES

[1]Swaroop C, [2]Tennison K Jose, [3]A Ramesh
[1,2,3] Mechanical Engineering, Govt. Engineering College, Thrissur
Email: [1]swaroopckz@gmail.com, [2]tengectcr@gmail.com, [3]rameshgec71@gmail.com

Abstract

The fuel obtained from biological sources are termed as biofuel. Biofuel satisfies the physical and chemical standards of the diesel. Hence it can be used as an alternative for diesel in compression ignition engines. As compared to normal diesel, biodiesels are non-exhaustible, causing less pollution and widely available. Biodiesel is being prepared from various feed stocks such as coconut oil, sunflower oil, karanja oil, jetropha oil etc. The use of edible oils for the production of biodiesel may lead to food crisis and there is a need to find out non edible feed stocks for bio diesel production. The primary motive of this experiment is find out the fuel related properties and engine related properties of Coconut Testa biodiesel. Compare the results with standard values and make sure that it can use as an alternate fuel for compression ignition engine.

Keywords: Acid value Biodiesel, Density, Fire point, Flash point, Iodine value, Saponification value, Transesterification, Testa oil, Viscosity

1. Introduction

The fuels currently use in internal combustion engines are nonrenewable in nature. The resources of the fossil fuels will get exhausted. As a result of combustion of fossil fuels, produce harmful emissions which is dangerous to environment and living beings. It is the need of hour to find out alternate sources of energy which has advantages over the conventional fossil fuels. Many experiments are conducted on internal combustion engines using fuel from biological feed stocks.

The oils use for biodiesel production includes edible and non-edible oils. Edible oils include coconut oil, sunflower oil, peanut oil etc. But use of edible oils for biodiesel production can cause food crisis and increase in the price of edible oils. Thus non edible oils are a better option as compared to edible oils for biodiesel production.

The feed stocks can be saturated type and unsaturated type. The biodiesel produced from unsaturated feed stocks cannot be stored for a long time. It will get degraded and fuel quality reduces accordingly and also it produce more emission as compared to fresh biodiesel.

Coconut is a tropical fruit widely available in South India and South East Asian countries. Various experiments have been conducted till date using biodiesel produced from coconut oil. Coconut biodiesel has higher number of saturated content. So long term storage stability biodiesel is higher compared to biodiesel derived from feed stock which has higher amount of unsaturated content. The use of coconut oil as feed stock has a number of disadvantages. Coconut oil is widely used for cooking and other domestic purposes. The use of coconut oil for biodiesel production can cause its scarcity for domestic use.

Coconut testa is a waste removed from coconut during coconut oil production. The industries producing products like coconut milk, virgin oil etc. use only the kernel by peeling out the testa. This work aims the property testing at producing biodiesel from coconut testa. Due to the wide

availability, non-edible nature and high degree of unsaturation of the oil, biodiesel produced from testa has enormous potential in meeting the future fuel demands.

2. Literature survey

Prakruthi Appayya et al [1] studied the composition of coconut testa. The samples had fat as the major component ranging from 34 to 64%. Oils had 90 to 98.2% triglycerols, 1 to 8% diaglycerols and 0.4 to 2 % triglycerols.Oils from testa were richer in monosaturates and polysaturates than other coconut oil samples. These studies indicated that the oil from testa contained more natural anti-oxidants such as tocopherols, tocotrienols and phenolics compared to coconut kernel oil.

Liaquat et al [2] studied the effect of coconut biodiesel blended fuels on engine performance and emission characteristics. As results of investigations, there has been a decrease in torque and brake power, while increase in specific fuel consumption has been observed for biodiesel blended fuels over the entire speed range compared to net diesel fuel. In case of engine exhaust gas emissions, lower HC, CO and, higher CO2 and NOx emissions have been found for biodiesel blended fuels compared to diesel fuel.

Mohankumar Chinnamma et al [3] studied Production of coconut methyl ester (CME) and glycerol from coconut oil and the functional feasibility of CME as biofuel in diesel engine. The test run showed the technical specifications torque (Nm) and power (bhp) similar to the efficiency of diesel fuel. The experiment showed a significant increase in the mileage.

Oguntola J Alamu et al [4] studied the production and testing of coconut oil biodiesel fuel and its blend Test quantities of coconut oil biodiesel were produced through transesterification reaction. The coconut oil biodiesel produced was subsequently blended with petroleum diesel and characterized as alternative diesel fuel through some ASTM standard fuel tests.

Godwin Kafui Ayetor et al [5] studied the Effect of biodiesel production parameters on viscosity and yield of methyl esters. The highest yield was obtained with 1% NaOH concentration for all. The effect of methanol in the range of 4:1–8:1 (molar ratio) was investigated, keeping other process parameters fixed. Optimum ratios of palm kernel oil and coconut oil biodiesels yielded 98% each at methanol: oil molar ratio of 8:1.

Bhuiya et al [6] studied the potential of non-edible oils as an alternative to- edible oil-derived biodiesel. To establish and continue to optimise the procedures for the use of second generation biodiesel, various aspects such as cost effectiveness, necessity of second generation biodiesel, biodiesel conversion technology, improving efficiency of the production process as well as performance and emission characteristics must be scrutinized and studied. The transesterification method is the most suitable method among the several possible methods for biodiesel production.

Istvan Barabas and Ioan-Adrian Todoruţ [7] studied on Biodiesel Quality, Standards and Properties. The paper presented the main standards on commercial biodiesel quality adopted in different regions of the world and the importance and significance of the main properties that are regulated (cetane number, density, viscosity, low-temperature performances, flash point, water content, etc.) and unregulated (elemetal composition, fatty acid methyl and ethyl esters composition, heating value, lubricity etc.) .

Chuepeng [8] studied the use of biodiesel in diesel engines The use of biodiesel blends in diesel engines has affected engine performance as well as combustion characteristics, i.e. ignition delay, injection timing, peak pressure, heat release rate, and so on. The combustion of biodiesel in diesel engines improved and regulated emissions except nitrogen oxides emissions were reduced.

Michael C Madden et al [9] studied the toxicology of biodiesel combustion products. The paper examined human responses to combustion products through an extensive literature exists on nonhuman animal effects.

Bianchi et al [10] studied the use of non-edible oils as raw materials for sustainable biodiesel production .The study gave special consideration to the role played by the development of a sustainable and responsible biofuels production, with no impact on food chain. It was concluded that the use of the oilseed deriving from alternative crops or waste oils as a feedstock for biodiesel production represents a very convenient way in order to lower the production costs of this biofuel.

3. Methodology

3.1 Feed stock

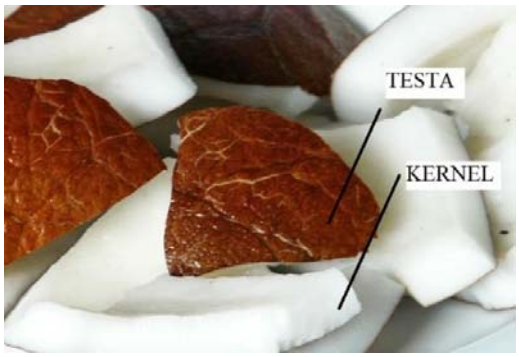

Fig:1 Coconut Kernel and Testa

Fig:2 Coconut Testa

The feed stock used in the production of biodiesel was coconut testa oil. Testa is the outer brown covering of the coconut kernel. In industries that produce coconut milk and virgin coconut oil, the outer brown covering is peeled off and discarded as a waste. The testa oil is produced by pressing the Testa. The properties and composition of the testa oil are similar to that of the coconut oil [1]. As compared to coconut oil, testa oil is advantageous for biodiesel production as it is non-edible and it is being produced out of a waste material.

3.2 Transesterification

Oils can be used directly as fuels in engines. Due to high viscosity of oil the atomization of oil become poor and this produces higher emission. Also long term use of oils lead to the damage of fuel injector. To overcome these barriers, the viscosity of the oil need to be decreased. The method used to decrease the viscosity of the testa oil is transesterification. It is the reaction between triglycerides in the oil and alcohol resulting the formation of esters and glycerol. 1 liter of coconut testa oil was taken in a conical flask. 8 g of KOH was dissolved in 250 ml methanol. The coconut testa oil was heated to 60 ^{0}C with constant stirring. The KOH solution was poured into the testa oil. The solution was stirred continuously for 45 minutes. The resulting mixture was poured into a separating flask and kept for 24 hours. After 24 hours the glycerol settled at the bottom of the flask was separated. The top portion was water washed.
Biodiesel get separated after 4 hours of water washing.

3.3. Properties Testing

1. Viscosity

The viscosity of biodiesel was measured using Brookfield Viscometer which satisfies ASTM standard. Viscosity is defined as the property by which a layer of fluid offers resistance to the motion of the adjacent layer. Viscosity (Engine performance related property) of a fuel determines the easiness by which it can be atomized in injectors. The obtained value is 4.05 centi poise (cP). This value is within ASTM standard value for viscosity (1.9-6.0 cP).

2. Density

Density is defined as the mass per unit volume. It is expressed in kg/ m$^{3.}$ This property (Engine performance related property) of the fuel influences the nozzle opening and injection timing of the fuel into the engine. The value for density was measured by a hydrometer. The obtained value of density for Testa biodiesel was 832.3 kg/m^3, which is within the ASTM standard (575-900 kg/m^3)

3. Flash point

The temperature at which the vapour of a liquid flash when subjected to a naked flame is known as the flash point of the liquid. 50 ml of Testa biodiesel was heated in a flash point measuring apparatus. The temperature was noted continuously with a thermometer. The vapour was exposed to naked flame and the temperature at which a momentarily flash obtained was noted. This temperature is the flash point of the biodiesel. The flash point of the Testa biodiesel was obtained as 124 ^{0}C. This satisfies ASTM standard .ASTM standard value is (minimum 100 ^{0}C)

4. Fire point

Fire point is the temperature of a fuel vapour, if once lit with the flame, will burn steadily at least for 5 seconds. Flash point is a good indication of the relative flammability of a fuel. 50 ml of Testa biodiesel was heated in a fire point measuring apparatus. The temperature was noted by a thermometer. The vapour was exposed to naked flame and the temperature at which the fuel vapour burns continuously for at least 5 seconds was noted. The fire point of the Testa biodiesel was obtained as 132 ^{0}C.Due to the higher fire point of Testa biodiesel, it can be transported and stored safely.

5. Acid value

The acid number is the measure of the amount of carboxylic acid groups in a chemical compound. Acid number determines the degree of degradation of biodiesel when the fuel is used. Acid value of the biodiesel is defined as the number of milligrams of KOH required to neutralize free acid present in one gram of biodiesel. 10 mg of biodiesel was mixed with 100ml neutral alcohol in a conical flask and heated in a water bath for 2 to 5 minutes to dissolve completely. 0.1N KOH solution was taken in a burette. The solution in the conical flask was titrated against 0.1N KOH solution in the burette using phenolphthalein indicator. Titration was continued till the first appearance of a persistent pink colour was obtained. The acid value of the biodiesel was obtained as 0.336 milligram KOH/g, which is within the ASTM standards. ASTM standard value is 0.5 milligram KOH/g.

6. Iodine value

The iodine number is an index of the number of double bonds in the biodiesel. The number of double bonds determines the extent on unsaturation content in the biodiesel. The extent of saturation determines the oxidation stability. Higher the Iodine value, the biodiesel has more unsaturated contents. During long term storage of biodiesel, Iodine value decrease due to degradation of the biodiesel.

0.2 to 0.3 g of Testa biodiesel was taken in a conical flask. 10 ml of carbon tetrachloride was added to the conical flask. 20 ml of Wij's reagent was added to the flask. The stopper of the flask was dipped in Potassium Iodide solution. The mixture was placed in dark for 30 minutes. After taking out from the dark, 20 ml of 15% Potassium Iodide solution and 50 ml of water was added to it. The solution was titrated with 0.1 N Sodium Thiosulphate solution till pale yellow colour appeared. Starch was added as an indicator to the solution. It was again titrated with 0.1 N Sodium Thiosulphate solution. End point was noted when the black colour of the solution just disappeared. The iodine value of the biodiesel was obtained as 23.57 mgI/g.

7. Saponification value

The process of formation of soap is called saponification. Saponification value is defined as the milligrams of KOH required to saponify 1g of fat or oil.

$$\textit{Saponification value} = \frac{56.1 \times (B - S) \times N}{W}$$

B = Titre value for blank, ml
S = Titre value for sample, ml
N = Normality of HCl
(B – S) = Vol. of HCl corresponding to KOH reacted.
W = Weight of sample of oil in g.

0.5 g of testa biodiesel was taken in a conical flask. 25 ml of alcoholic potash was added to it. Alcoholic potash was added to the flask. This served as blank. . Condensers were attached and the flasks were heated in a water bath gently but steadily for about an hour. After one hour of heating, the solutions are allowed to cool and the inside of the condensers were washed down by minimum amount of distilled water. Phenolphthalein indicator was added to both the flask and titrated using 0.1 N HCl. The saponification value of the biodiesel was obtained as 117.81 mgKOH/g, which is within the ASTM standards.

ASTM value is maximum 120 mg KOH/g.

Results and discussion

Biodiesel was prepared out of coconut testa oil and the properties were studied.

1. The value of dynamic viscosity of the Testa biodiesel is 4.05 centipoise. This value meets the ASTM standard.
2. 832.3 kg/m^3 is the value of density of Testa biodiesel obtained during density test which also satisfies ASTM standard.
3. Testa biodiesel has a Flash point of 124 ^{0}C and a fire point of 132 ^{0}C. Both this values satisfies ASTM standard.
4. Acid value of Testa biodiesel is 0.336 mgKOH/g and Iodine value is 23.57 mgI/g.

5. Testa biodiesel has a saponification value of 117.81mgKOH/g.

Biodiesel produced form Testa oil has similar properties as any other biodiesel. The values for engine performance related properties like density and viscosity are within standard value. This shows that it can use in CI engines as an alternate fuel. Fuel stability related properties, Acid value and Iodine value of Testa biodiesel is also within the range. Thus it has good storage stability. Higher flash point and fire point implies that it can be transported and handled safely.

Table: 1 Properties of Testa biodiesel

Sl. No	Property	ASTM standard	Evaluated value
1	Viscosity	1.9 – 6 cP	4.05 cP
2	Density	575 – 900 kg/m ^{3}	832.3 kg/m^3
3	Flash Point	100 ^{0}C, min	124 ^{0}C
4	Fire Point		132 ^{0}C
5	Acid Value	0.5 mg KOH/g, max	0.336 mg KOH/g
6	Iodine Value		23.57 mgI/g
7	Saponification Value	120 mg KOH/g, max	117.81 mg KOH/g

References

[1] Prakruthi Appaiah, L. Sunil , P. K. Prasanth Kumar , A. G. Gopala Krishna Composition of Coconut Testa, Coconut Kernel and its Oil Journal of the American Oil Chemists' Society - 2014

[2] A.M. Liaquat, H.H. Masjuki, M.A. Kalam, I.M. Rizwanul Fattah, M.A. Hazrat, M. Varman, M. Mofijur, M. Shahabuddin Effect of coconut biodiesel blended fuels on engine performance and emission characteristics - 2013

[3] Mohankumar Chinnamma , Salini Bhasker , Harish Madhav , Rajesh Mamkulathil Devasia , Anisha Shashidharan , Balachandran Chandrasekaran Pillai , Pradeep Thevannoor Production of coconut methyl ester (CME) and glycerol from coconut (Cocos nucifera) oil and the functional feasibility of CME as biofuel in diesel engine - 2015

[4] Oguntola J Alamu, Opeoluwa Dehinbo and Adedoyin M Sulaiman Production and Testing Of Coconut Oil Biodiesel Fuel and Its Blend Leonardo Journal Of Sciences – 2010

[5]Godwin Kafui Ayetor , Albert Sunnu , Joseph Parbey Effect of biodiesel production parameters on viscosity and yield of methyl esters: Jatropha curcas, Elaeis guineensis and Cocos nucifera Alexandria Engineering Journal - 2015

[6] M. M. K. Bhuiya , M. G. Rasula, M. M. K. Khana, N. Ashwathb, A. K. Azada, M. A. Hazrata . Second Generation Biodiesel: Potential Alternative to-Edible Oil-Derived Biodiesel,The 6th International Conference on Applied Energy 2014

[7] Istvan Barabas and Ioan Adrian Todorut Biodiesel Quality, Standards and Properties - 2011

[8] S. Chuepeng The Use of Biodiesel in Diesel Engines – 2011

[9] Michael C. Madden, Laya Bhavaraju and Urmila P. Kodavanti,Toxicology of Biodiesel Combustion Products – 2011

[10] C.L. BianchiNon Edible Oils: Raw Materials for Sustainable Biodiesel 2011

FRACTURE ANALYSIS OF MACHINE COMPONENTS USING FRACTOGRAPHY

[1]Omkar M Kaulgud, [2]Bajirao H NangarePatil
[1,2]Assistant Professor, Mechanical Engg Dept
RIT, Islampur
Email: [1] Omkar.kaulgud@gmail.com, [2] bajiraonp1@gmail.com

ABSTRACT

This paper provides an extensive study into the different types of material and component failures observed in industrial enterprises. Fractography is critical to failure analysis of metals and plastics. Fractography of plastics is a relatively new field with many similarities to metals. Failure modes common to both metals and plastics include ductile overload, brittle fracture, impact, and fatigue. Analogies can also be drawn between stress-corrosion cracking (SCC) of metals and stress cracking of polymers. Other metal/plastic failure analogies include corrosion/chemical aging, dealloying/ residual stress/frozen-in stress, and welds/knit lines. Stress raisers, microstructure, material defects, and thermomechanical history play important roles in both types of materials. The key fractographic features for metals and plastics.

INTRODUCTION

Fractography is critical to failure analysis of metals and plastics. Fractography of plastics is a relatively new field with many similarities to metals.Failure modes common to both metals and plastics include ductile overload, brittle fracture,impact, and fatigue. Analogies can also be drawn between stress-corrosion cracking (SCC) of metals and stress cracking of polymers. Other metal/plastic failure analogies include corrosion/chemical aging, dealloying/ residual stress/frozen-in stress, and welds/knit lines. Stress raisers, microstructure, material defects, and thermo mechanical history play important roles in both types of materials. The key fractographic features for metals and plastics.

HISTORICAL PERSPECTIVE

Plastics have been in existence for approximately 130 years. [1] John Hyatt patented nitrocellulose, the first commercial plastic, in 1869. However, full-scale development and use of plastics is only approximately 50 years old. In contrast, metals have been in use for hundreds of years. The application of engineering materials is unavoidably accompanied by the occurrence of failures, many of which have been catastrophic. The consequences of material failures, including deaths, financial losses, and legal ramifications, have encouraged the development of effective failure analysis methods. Although the cost of failure analysis may exceed the value of the part, the cost of service failures usually far exceeds the cost of failure analysis. Many of the techniques used over the years for the valuation of metals have been successfully applied to plastics, with only minor modifications. Fractography is arguably the most valuable tool available to the failure analyst. Fractography, a term coined in 1944 to describe the science of examining fracture surfaces, has actually been used for centuries as part of the field of metallurgy. Even before that, however, Stone Age man possessed a working knowledge of fracture. Archeological findings of lithic implements, weapons, and tools shaped from stone by controlled fracture indicate that prehistoric man knew how to select rocks with favorable fracture behavior, use thermal spalling to detach bedrock from the working core, and shape stone by pressure flaking. Fractography, as we know it today, developed in the 16th century as a quality-control practice employed for ferrous and nonferrous metalworking.

[2]De La Pirotechnia, published by Vannoccio Biringuccio in 1540, is one of the first documents to detail fractographic techniques. Invention of the optical microscope in 1600 provided a significant new tool for fractography, yet it was not used extensively by metallurgists until the eighteenth century.[3] In 1722, R.A.de Réaumur published a book with engravings that depicted macroscopic and microscopic fracture surfaces of iron and steel. Interestingly, the categories of macroscopic features developed by de Réaumur have remained essentially unchanged through the centuries.Partly due to the development of metallographic techniques for examining cross sections of metals, interesting microfractography waned during the nineteenth century. Metalworkers continued to use fractographic techniques for quality-assurance purposes,but, for the most part, researchers and publications ignored fractography. Several technological developments in the twentieth century revitalized interest in fractography.[4] Carl A. Zapffe developed and extensively used fractographic techniques to study the hydrogen embrittlement of steels. His work led to the discovery of techniques for photographing fracture surfaces at high magnifications. The first fractographs were published by Zapffe in 1943.An even more revolutionary development was the invention of the scanning electron microscope SEM).The first SEM appeared in 1943 .Unlike the transmission electron microscope, which was developed a few years earlier, it could be used for fracture surface examination. An SEM with a guaranteed resolution of approximately 500 Å became commercially available in 1965. Compared with the optical microscope, the SEM expands resolution by more than one order of magnitude and increases the depth of focus by more than two orders of magnitude. The tools for modern fractography were essentially in place before plastics achieved widespread use.

FAILURE ANALYSIS OVERVEIW:-

The general procedure for conducting a sound failure analysis is similar for metallic and nonmetallic materials. The steps include:

(1) information gathering;

(2) preliminary, visual examination;

(3) nondestructive testing;

(4) characterization of material properties through mechanical,

Chemical and thermal testing;

(5) selection, preservation, and cleaning of fracture surfaces;

(6) macroscopic examination of fracture surfaces, secondary cracking, and surface condition;

(7) microscopic examination;

(8) selection, preparation, and examination of cross sections;

(9) identification of failure mechanisms;

(10) stress/fracture mechanics analysis;

(11) testing to simulate failure; and

(12) data review, formulation of conclusions, and reporting. Although the basic steps of failure analysis are nearly identical, some differences exist between metals and plastics. Nondestructive testing of metals includes magnetic-particle, eddy-current, and radiographic inspection methods that are not generally applicable to plastics, for obvious reasons. However, ultrasonic and acoustic emission techniques find applications for both materials. Similarly, different chemical test methods are necessary. Typical test methods for metals are optical emission spectrometry, inductively coupled plasma, and combustion. Fourier transform infrared spectroscopy is used extensively to identify plastics by molecular bonding, and thermal testing, differential scanning calorimetry, and thermo gravimetric analysis are also very important for polymer characterization. Energy-dispersive x-ray spectroscopy, used in conjunction with the SEM, is a very practical tool for elemental chemical analysis of both metals and plastics. Also noteworthy is that different chemical solutions are required for metals and plastics to clean and/or protect fracture surfaces and to etch cross sections to reveal microstructure.

CAUSES OF FAILURE:-

Of course, the primary objective of a materials failure analysis is to determine the root cause of failure. Whether dealing with metallic or nonmetallic materials, normally, the root cause can be assigned to one of four categories: design, manufacturing, service, or material. Often, several adverse conditions contribute to the part failure. Many of the potential root causes of failure are common to metallic and nonmetallic materials. Improper materials selection, overly high stresses, and stress concentrations are examples of design-related problems that can lead to premature failure. Materials selection

must take into account environmental sensitivity- ties as well as requisite mechanical properties and welding/joining characteristics. Stress raisers are frequently a preferred site for fracture origin, particularly in fatigue. Stress raisers include thread roots (Fig.1), sharp radii of curvature, through holes, and surface discontinuities (e.g., gate marks in molded plastic parts).Similarly, many manufacturing and material problems found in metals also are observed or have a corollary in plastics. Weldments are a trouble-prone area for metals, as are weld lines or knit lines in molded plastics (Fig. 2) High residual stresses can result from metal forming, heat treatment, welding, and machining. Similarly, high frozen-in stresses in injection-molded plastic parts often contribute to failure. Porosity and voids are common to metal castings and plastic molded parts (Fig. 3).Pores and voids serve as stress raisers and reduce load-carrying capability. Other manufacturing- and material-related problems that may lead to failure include adverse thermo mechanical history, poor microstructure, material defects and contamination.

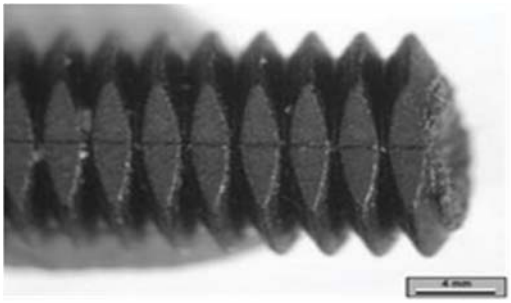

Fig. 1 Fracture of a glass-filled polyamide Cross section showing fracture along the threaded part due to stress concentration at the thread root. [1]

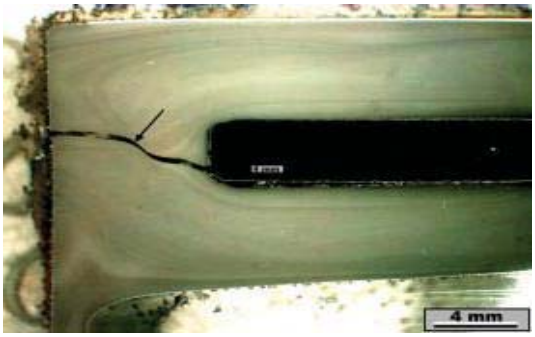

Fig.2 Cross section showing fracture along the knit line of a perfluoralkoxyethylene-lined impeller. [1]

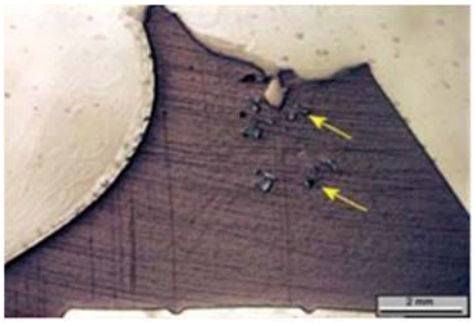

Fig. 3 Cross section of a polyacetal hinge that fractured (arrow) through an area of porosity. [I]

Environmental degradation is one of the most important service-related causes of failure for metals and plastics. Other degradation processes include excessive wear, impact, overloading, and electrical discharge.

FAILURE MECHANISM:-

Another key objective of failure analysis is to identify the failure mechanism(s). Once again, some failure modes are identical for metals and plastics. These modes include ductile overload, brittle fracture, impact, fatigue, wear, and erosion. Analogies also can be drawn between metals and plastics with regard to environmental degradation. Whereas metals corrode by an electrochemical process, plastics are vulnerable to chemical changes from aging or weathering. Stress-corrosion cracking (SCC), a specific form of metallic corrosion, is similar in many ways to stress cracking of plastics. Both result in brittle fracture due to the combined effects of tensile stress and a material-specific aggressive environment. Similarly, dealloying or selective leaching in metals (Fig. 4),the preferential removal of one element from an alloy by corrosion, is somewhat similar to scission of polymers (Fig. 5), a form of aging that can cause chemical changes by selectively cutting molecular bonds. Analogies can also be drawn between metals and another type of polymer: rubber. Internal hydrogen in steels can precipitate and cause hydrogen damage, which is frequently characterized by localized brittle areas of high reflectivity, known as flakes or fisheyes, on otherwise ductile fracture surfaces (Fig. 6). Similarly, explosive decompression in rubber O-rings produces fisheye-like ovular patterns on the fracture surfaces (Fig.7). Explosive decompression is the formation of small ruptures or embolisms when an elastomeric seal, saturated with high pressure

gas, experiences an abrupt pressure reduction. This failure mechanism is analogous to the "bends" that afflict divers who surface too quickly.

FRACTOGRAPHY:-

When material failure involves actual breakage, fractography can be employed to identify the fracture origin , direction of crack propagation, failure mechanism, material defects, environmental interaction, and the nature of stresses. Some of the macroscopic and microscopic features employed by the failure analyst to evaluate fracture surfaces of metals and plastics are described subsequently. Note, however, that many of the fractographic features described forplastics are not observable for reinforced plastics and plastics containing high filler content.

MACROSCOPICALLY VISIBLE FRACTOGRAPHIC FEATURES:-

On a macroscopic scale, all fractures (metals and plastics) fall into one of two categories: ductile and brittle. Ductile fractures are characterized by material tearing and exhibit gross plastic deformation. Brittle fractures display little or no macroscopically visible plastic deformation and require less energy to form. Ductile fractures occur as the result of applied stresses exceeding the material yield or flow stress. Brittle fractures may occur at stress levels below the material yield stress. In practice, ductile fractures occur due to overloading or under designing and are rarely the subject of a failure analysis. However, the unexpected brittle failure of normally ductile materials is frequently the subject of a failure analysis. Many macroscopically visible fracto graphic features serve to identify the fracture origin(s) and direction of crack propagation. Fractographic features common to metals and plastics are radial marks and chevron patterns. Radial marks (Fig. 8) are lines on a fracture surface that radiate outward from the origin and are formed by the intersection of brittle fractures propagating at different levels. Chevron or herringbone patterns are actually radial marks resembling nested letter V"s and pointing toward the origin. Fatigue failures in metals display beach marks and ratchet marks that serve to identify the origin and the failure mode. Beach marks (Fig. 8) are macroscopically visible semielliptical lines running perpendicular to the overall direction of fatigue crack propagation and marking successive positions of the advancing crack front. Ratchet marks are macroscopically visible lines running parallel to the overall direction of crack propagation and formed by the intersection of fatigue cracks propagating from multiple origins. Brittle fractures in plastics also exhibit characteristic features, several of which are macroscopically visible (Fig. 9). These features may include a mirror zone at the origin, a mist region, and rib marks. The mirror zone is a flat, featureless region surrounding the origin and associated with the slow crack growth phase of fracture. The mist region is located immediately adjacent to the mirror zone and displays a misty appearance. This area is a transition zone from slow to fast crack growth. Rib marks are semielliptical lines resembling beach marks in metallic fatigue fractures.

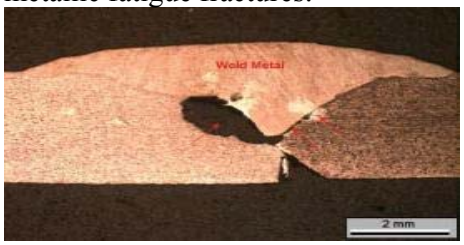

Fig. 4 Microbiologically induced corrosion of a 304 SST vessel weld, characterized by pitting and selective leaching (arrow). [2]

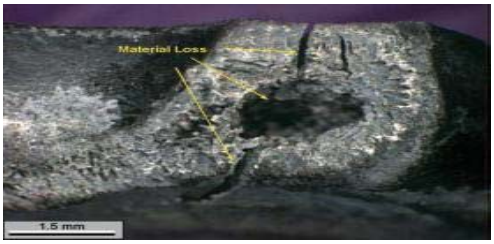

Fig. 5 Hollowing out of a polyacetal hinge due to acidcatalyzed Hydrolysis. [2]

Fig. 6 Hydrogen damage of induction-hardened steel piston rod displaying fisheyes. [2]

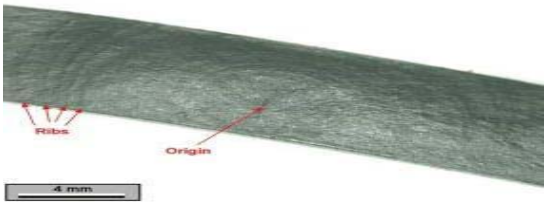

Fig. 7 Explosive decompression fracture of rubber O-ring, characterized by fisheye-like patterns. [2]

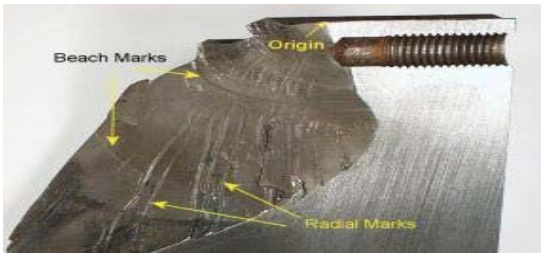

Fig. 8 Beach and radial marks visible on torsional fatigue fracture of a 6 in. Diameter shaft.. [2]

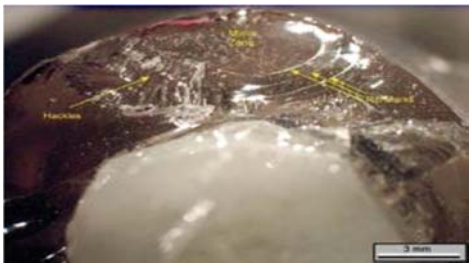

Fig. 9 Brittle fracture of an epoxy layer displaying a mirror zone, rib marks, and hackles. [2]

FRACTOGRAPHY OF METALS AND PLASTICS:-

It identifies the origin and the failure mode. Beach marks (Fig. 8) are macroscopically visible semielliptical lines running perpendicular to the overall direction of fatigue crack propagation and marking successive positions of the advancing crack front. Ratchet marks are macroscopically visible lines running parallel to the overall direction of crack propagation and formed by the intersection of fatigue cracks propagating from multiple origins. Brittle fractures in plastics also exhibit characteristic features, several of which are macroscopically visible (Fig 9). These features may include a mirror zone at the origin, a mist region, and rib marks. The mirror zone is a flat, featureless region surrounding the origin and associated with the slow crack growth phase of fracture. The mist region is located immediately adjacent to the mirror zone and displays a misty appearance. This area is a transition zone from slow to fast crack growth. Rib marks are semielliptical lines resembling beach marks in metallic fatigue fractures.

MICROSCOPICALLY VISIBLE FRACTOGRAPHIC FEATURES:-

On a microscopic scale, ductile fracture in metals (Fig. 10) displays a dimpled surface appearance created by microvoid coalescence. Ductile fracture in plastics (Fig. 11) is characterized by material stretching related to the fibrillar nature of the polymer response to stress. Although a part may fail in a brittle manner, ductile fracture morphology is frequently observed away from the origin. For example, the final fast fracture by ductile overload produces the shear lip in many metal failures, even when the crack originated and was propagated by SCC, fatigue, or hydrogen embrittlement processes. The extent of this overload region is an indication of the stress level. Generally, the larger the overload region, the higher the stress level on the failed component.Brittle fracture of metallic materials may result from numerous failure mechanisms, but there are only a few basic microfractographic features that clearly indicate the failure mechanism.These features are cleavage facets (Fig. 12), intergranular facets (Fig.13), and striations (Fig. 14). Cleavage facets form in body-centered cubic (bcc) and hexagonal close-packed metals when the crack path follows a well-defined transgranular crystallographic plane (e.g., the {100} planes in bcc metals). Cleavage is characteristic of transgranular brittle fracture. Intergranular fracture, recognizable by its “rock candy” appearance, occurs when the crack path follows grain boundaries. Intergranular fracture is typical of many forms of SCC, hydrogen embrittlement, and temper embrittled steel. Fatigue failures of many metals exhibit striations at high magnifications. (Normally, magnifications of 500 to 2,500× are required.) Striations are semielliptical lines on a fatigue fracture surface that emanate outward from the origin and mark the crack-front position with each successive stress cycle. The spacing of fatigue striations is usually very uniform and can be used to calculate the crack growth rate, if the cyclic stress frequency is known. Striations are

discriminated from striation-like artifacts on the fracture surface in that true fatigue striations never cross or intersect one another. Plastics do not display cleavage and intergranular fracture. However, similar to metals, striations are found on fatigue fracture surfaces (Fig. 15, 16). Striations in plastics typically are observable at much lower magnifications (50 to 200×). However, local softening and melting due to hysteretic heating can obliterate fatigue striations in less rigid plastics. In addition to mirror zones, mist regions, and rib marks, which are normally visible without the aid of a microscope,

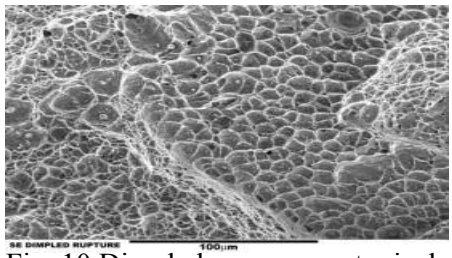

Fig. 10 Dimpled appearance typical of ductile fracture of metallic materials. [3]

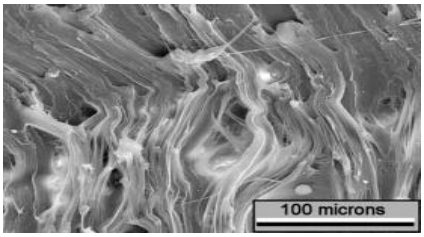

Fig. 11 Fracture of a polyethylene tensile-test specimen exhibiting material stretching. [3]

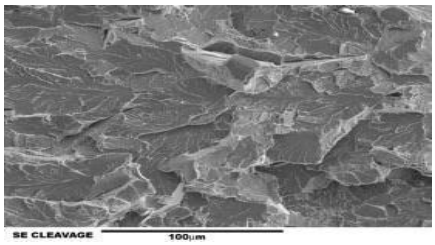

Fig. 12 Brittle fracture of an FC-0205 powder metal control rod displaying cleavage facets. [3]

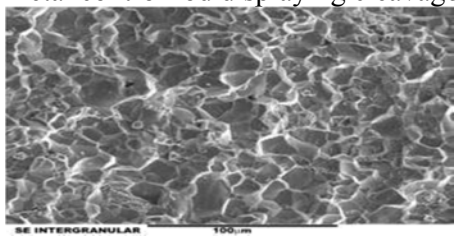

Fig. 13 Intergranular fracture of an embrittled cast steel pneumatic wrench. [3]

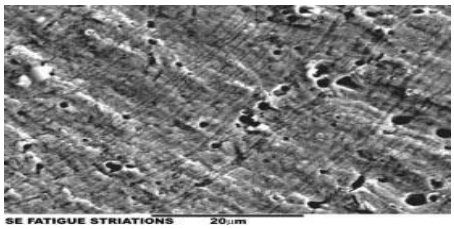

Fig. 14 Fatigue striations visible on type 302 stainless steel spring fracture. [3]

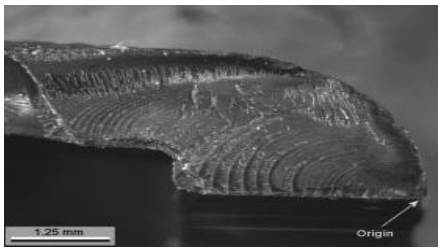

Fig. 15 Fatigue striations emanating from fracture origin of polycarbonate latch handle. [3]

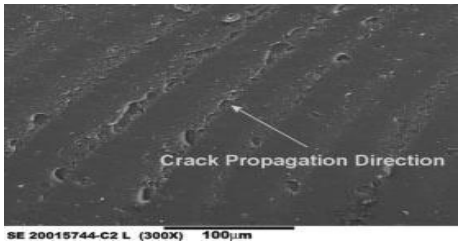

Fig. 16 SEM micrograph of fatigue striations shown in Fig.15. [4]

CONCLUSION

Fractographic techniques, developed and applied to metal failures for centuries, have been readily adapted to the fracture analysis of plastics since their emergence as a key engineering material over the last 50 years. However, more work remains to be done to advance fractography of plastics. One notable area for research is fracture analysis of composites, reinforced plastics, and plastics containing high filler content. Fractures of these materials too often are dismissed as inherently lacking meaningful fractographic features. Also this theory can be applied for the welded components so that the nature of failure can be determined so that their will be input data for the design team to make the necessary changes in the design, manufacturing processes which has to be carried out on the components.

REFERENCES

[1]. V. Biringuccio: De La Pirotechnia, Venice,1540; see translation by C.S. Smith and M.T. Gnudi: The „Pirotechnia‟ of Vannoccio Biringuccio, American Institute of Mining, Metallurgical and Petroleum Engineers, New York, 1942.

[2] R.A. de Réaumur: L‟Art de Convertir le Fer Forgé en Acier, et L‟Art d‟Adocir le Fer Fondu,(in French), Michel Brunet, Paris, 1722; see translation by A.G. Sisco: Réaumur‟s Memoirs on Steel and Iron, University of Chicago Press, 1956.

[3]. C.A. Zapffe and G.A. Moore: Trans. AIME, 1943, 154, pp. 335-59.

[4] W. Brostow and R.D. Corneliussen: Failure of Plastics, Hanser Publishers, Munich, 1986.

COMPARATIVE AND PARAMETRIC STUDY OF EFFECT OF EXHAUST GAS RECIRCULATION ON DIESEL AND BIODIESEL

Somesh Rath[1], Riddhi Joshi[2], Ath S Singhal[3], Vivek Dani[4]
[1,2,3,4]Mechanical Engineering Department, Institute of Technology, Nirma University
Email:13bme119@nirmauni.ac.in[1], 13bme098@nirmauni.ac.in[2], Vivekdani.nit@gmail.com[4]

Abstract

With the enormous increase in number of automobiles, there has been a major demand of alternative sources of fuel and reduction in exhaust emission. One of the novel solution for both is use of biodiesel. Also one of the methods that attracted the researchers to lower down emissions is use of exhaust gas recirculation method. This method is used in many commercial vehicles also.

In the present work a Jatropha Biodiesel (20% v/v) has been used to study the effect of hot exhaust gas recirculation (EGR) method on bsfc and exhaust gas temperature. Various percentages of EGR has been used and optimum EGR percentage was determined that results in least bsfc and exhaust gas temperature. Also a comparative study of effect of EGR has been made on diesel and biodiesel. For the present study an appropriate Test setup with single cylinder diesel engine and hot EGR equipment was made.

I. INTRODUCTION

With the increase in dependence on automobiles around the world, problems like scarcity of petroleum fuels and exhaust emissions are getting more severe. To overcome these problems it is required to enhance fuel properties or use equipment along with the diesel engine to reduce emissions.[1]

Biodiesel is one such solution that reduces the dependence on petroleum fuel on to some extent. Also the motivation by the government policies to use biodiesel has led to researches and manufacturers getting inclined towards making newer and better biodiesels. But at the same time it is necessary to know that how does these biodiesels react with the methods of reducing exhaust emissions. [2]

Exhaust Gas Recirculation (EGR) is an effective method for emission control. The exhaust gases mainly consist of inert carbon dioxide, nitrogen and possess high specific heat. When recirculated to engine inlet, it can reduce oxygen concentration and act as a heat sink. This process reduces oxygen concentration and peak combustion temperature, which results in reduced NOx, Sox and other gases.[3]

Saleh H E [2] used Jojoba methyl ester (JME) as a renewable fuel in numerous studies evaluating its potential use in diesel engines. These studies showed that this fuel is good gas oil substitute but an increase in the nitrogenous oxides emissions was observed at all operating conditions. The comparison of diesel and JME biodesel was made on exhaust emission when EGR technique is used to reduce down emissions. Pradeep and Sharma [3] carried out an experimental work in this field. They have concluded that diesel engines running on JBD are found to emit higher oxides of nitrogen, NOx. HOT EGR, a low cost technique of Exhaust Gas Recirculation, is effectively used in this work to overcome this environmental penalty. NO emissions were reduced when the engine was operated under HOT EGR levels of 5-25 %. However, EGR level was optimized as 15% based on adequate reduction in no missions, minimum possible smoke, CO, HC emissions and reasonable brake thermal efficiency. Abd-Alla [4] G H, reviewed the potential of Exhaust Gas Recirculation (EGR) to reduce the exhaust emissions, particularly NOx emissions, and to delimit the application range

of this technique. A detailed analysis of previous and current results of EGR e_ects on the emissions and performance of Diesel engines, spark ignition engines and duel fuel engines is introduced. From the deep analysis, it was found that adding EGR to the air ow rate to the Diesel engine, rather than displacing some of the inlet air, appears to be a more bene_cial way of utilizing EGR in Diesel
engines. Zheng et al.[5] worked on this topic. According to their work, Exhaust Gas Recirculation (EGR) is effective to reduce nitrogen oxides (NOx) from Diesel engines because it lowers the flame temperature and the oxygen concentration of the working fluid in the combustion chamber. However, as NOx reduces, particulate matter (PM) increases, resulting from the lowered oxygen concentration. Hebbar and Bhat[6] give insight into the effect of EGR level on the development of gaseous emissions as well as mechanisms of its formation. Reductions in NOx amount are found to be remarkable with EGR but combustion quality deteriorates at higher loads and higher percentages of EGR due to a significant decrease of A/F ratio.

II. EXPERIMENTAL SETUP AND METHODOLOGY

The primary point of the experimentation is to figure out practicality of Exhaust Gas Recirculation (EGR) utilizing biodiesel as a halfway substitute of diesel oil in C.I motor to minimize NOx development. The test work under this task comprises of two sections, first to test normal diesel on various parameters by using different loads on various EGR percentages. And secondly the same paramenters to be tested with Jatropha biodesel.

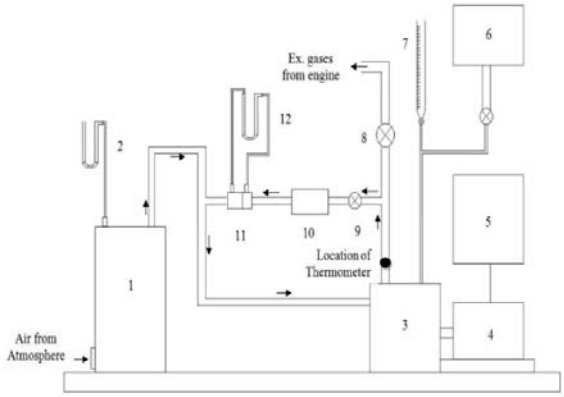

Figure 1 Schematic Line diagram Experimental Setup

(1) Air box with orifice, (2) Manometer for air flow measurement, (3) Engine, (4) A.C. Alternator, (5) Load bank, (6) Fuel tank, (7) Burette, (8) Flow control valve, (9) EGR valve, (10) Filter, (11) Orifice, (12) Manometer for measurement of recirculated gas flow

A solitary chamber 4 - stroke air-cooled diesel motor (4) creating 5.5 kW at 1500 rpm was utilized for test work. The schematic outline of the test set up is appeared in Figure 1. An electrical dynamometer (4) was utilized for stacking the motor. A manometer (2) with water as manometric liquid, associated with a vast tank (1) of 0.2 m^3 which is 275 times the cleared volume of the motor, was connected to the motor to make wind current estimation. Wind current was measured with the assistance of weight contrast created by a round, sharp edge hole of 32 mm width. The fuel stream was measured on a volumetric premise utilizing a 50 ml limit burette (7) and stopwatch. Thermometer with dial marker (reach 0°C to 600°C) was utilized for measuring the fumes gas temperature. An electrical burden bank (5) is readied utilizing globules of 200 watts and 100 watts limit. Electrical associations product made in a manner that 20% burden interim can be accomplished for whole load range. For distribution of fumes gasses, fumes control valve (8) and EGR valve (9) are utilized. Recycled gasses go through a channel (10). Stream of recycled gasses measured with the assistance of opening (11) associated with a manometer (12) with water as manometric liquid.

Figure 2 Actual Experimental Setup

For the experimentation, the load is varied from 0 to 80% at an interval of 20%. The EGR volume percentages are taken as 0, 5, 10 and 15. The biodiesel used is Jatropha Biodiesel with a 20% blend. For each experiment the value of break specific fuel consumption (bsfc) and the exhaust gas temperature is measured. The valves are calibrated and marked to ensure that the required amount of exhaust gas is recirculated inside the engine. For a cross check the orifice meter readings are taken which were inline with the required percentage of exhaust gas recirculated. To insure the repeatability of the experiments, testing of the engine was done as per the Indian standard (IS: 10000 Part IV), which lays down the guidelines for declaring power, efficiency and fuel consumption and specifies relevant correction factors which are required for adjusting the observed readings to the standard reference conditions, as specified in IS: 10000 (Part II).[7] The experiments were conducted three times to increase the confidence level.

III. RESULTS AND DISCUSSIONS

Figure 3 represents the results of variation in temperature of exhaust for various EGR levels with respect to different load conditions when normal diesel is used. It can be inferred from the figure that all EGR levels the temperature of exhaust has reduced. Also among various EGR levels 5% EGR gives minimum exhaust temperature over almost all load conditions. However at 80% load condition 10 % EGR is more effective in reducing exhaust temperature. In general a reduction in 20-30 degrees is seen at all loads when 5% EGR is compared with 0% EGR. At 80% load 13 percent reduction in temperature is observed with 10 percent EGR as compared to no EGR.

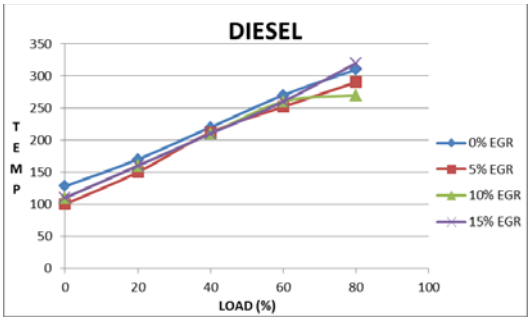

Figure 3 : Variation of temperature for normal Diesel at different EGR levels.

Figure 4 represents the results of variation of bsfc for various EGR levels with respect to different load conditions when normal diesel is used. The result shows that bsfc has increased nominally in all EGR levels with respect to 0% EGR, except for 5% EGR level. The maximum reduction in bsfc is 7.19 percent with use of 5 % EGR as compared with no EGR. Rest for all the EGR there is an increment in bsfc with 15% EGR being the maximum.

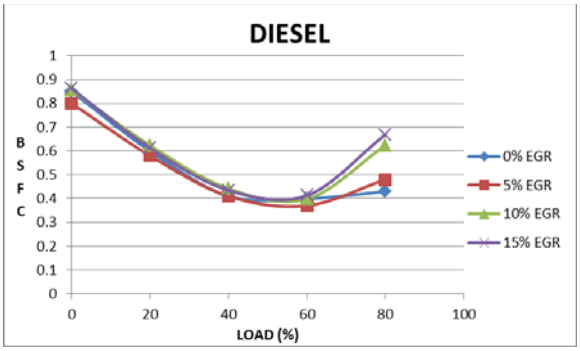

Figure 4 : Variation of bsfc for normal Diesel at different EGR levels.

So from the above graphs use of 5% EGR with normal diesel proves to be the best option in the current diesel engine.

For the biodiesel, there is a shift in trend of results. Here in figure 5, it can be seen that the temperature of the exhaust is minimum in case of 10% EGR. The maximum drop in temperature is observed to be 40 degrees with 10% EGR at 80 % loading of engine when compared with no EGR condition. The variation in temperature between 5% and 10 % EGR is not much. It can be seen that as in figure 3, here also at all the EGR's the temperature of exhaust is less than the temperature when no EGR is used.

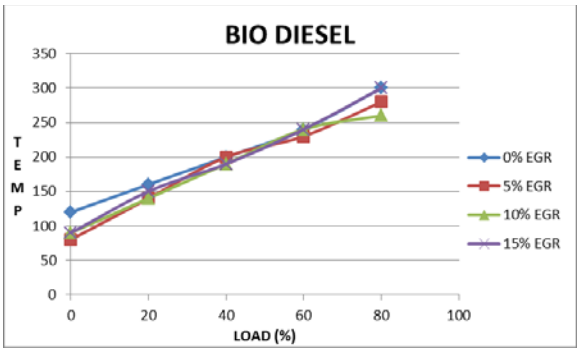

Figure 5 : Variation of temperature for bio-Diesel at different EGR levels.

It can be observed in figure 6 that bsfc has increased in all the EGR levels as compared to no EGR. But the bsfc for 5% and 10% EGR levels is almost same. There is a maximum increase of 13.5 % in bsfc for 5 % and 10 % EGR increase of as compared with no EGR. And an

average increase of 7.53% as compared with no EGR.

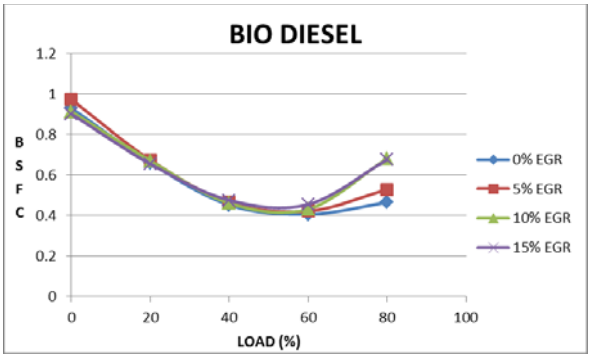

Figure 6 : Variation of bsfc for bio-Diesel at different EGR levels.

The probable reason for reduction in temperature with EGR is due to reduction in oxygen content at the time of combustion of fuel. And the probable reason for increase in bsfc can be improper combustion of fuel inside the engine.

IV. CONCLUSION

It is observed that there is a significant temperature drop in the exhaust temperature with EGR. A further 10 % temperature drop is observed in case of biodiesel and 5% EGR when compared with normal diesel. And the use of biodiesel doesn't have a significant impact of increase in bsfc. So it can be concluded that Jatropha Biodiesel are beneficial in reducing the exhaust temperature which in-turn will reduce NOx and SOx emissions, without much increase in bsfc.

REFERENCES

[1] J. B. Heywood, Internal combustion engine fundamentals. New York: McGraw Hill, 5 ed., 1988.

[2] H. E. Saleh, "Effect of exhaust gas recirculation on diesel engine nitrogen oxide reduction operating with jojoba methyl ester," Renewable Energy, vol. 34, pp. 2178-2186, 2009.

[3] V. Pradeep and R. P. Sharma, "Use of hot EGR for NOx control in a compression ignition engine fuelled with bio-diesel from jatropha oil," Renewable Energy, vol. 32, pp. 1136-1154, 2007.

[4] G. H. Abd-Alla, "Using exhaust gas recirculation in internal combustion engines: a review," Energy Conversion and Management, vol. 43, pp. 1027-1042, 2002.

[5] M. Zheng, G. T. Reader, and J. Gary Hawley, "Diesel engine exhaust gas recirculation a review on advanced and novel concepts," Energy Conversion and Management, vol. 45, pp. 883-900, 2004.

[6] G. S. Hebbar and A. K. Bhat, "Analysis of performance and emission of a naturally aspirated stationary di diesel engine with exhaust gas recirculation," Progress in Energy and combustion science.

[7] J. P. Holman, Experimental methods for engineers. New York: McGraw Hill, 5 ed., 1989.